THE UNIVERSITY OF MICHIGAN

INDUSTRY PROGRAM OF THE COLLEGE OF ENGINEERING

AN INVESTIGATION OF THE ACOUSTIC EMISSION FROM COMMERCIAL FERROUS MATERIALS SUBJECTED TO CYCLIC TENSILE LOADING

Jal N. Kerawalla

A dissertation submitted in partial fulfillment
of the requirements for the degree of
Doctor of Philosophy in the
University of Michigan
Department of Mechanical Engineering
1965

October, 1965

IP-720

ACKNOWLEDGMENT

The author gratefully acknowledges all those who aided in this investigation and those associated with his doctoral studies, in particular the following:

Professor Julian R. Frederick, Chairman of the doctoral committee for his encouragement, counsel, and very useful criticism.

Professors W. C. Bigelow, J. Datsko and F. E. Fisher, for their advice, assistance and co-operation concerning the use of various equipment under their supervision.

Professors D. K. Felbeck and J. H. Enns for their assistance, advice and invaluable suggestions related to the various aspects of this dissertation.

Doctor A. J. McEvily Jr. for his candid comments, invaluable suggestions, and kind co-operation in the use of the microstrain testing facility at the Scientific Laboratories of the Ford Motor Company.

Professor T. A. Despres for his very valuable advice, assistance and discussions on specimen preparation techniques and electron microscopy.

Mr. B. H. Schofield and Mr. L. D. Mitchell for the candid and stimulating discussions relating to the acoustic emission phenomena.

The National Science Foundation and the Department of Mechanical Engineering for providing the equipment and the financial support needed during this investigation.

The staff of the Machine Tool and Electronics Laboratories of the Department of Mechanical Engineering for their co-operation in the fabrication of the test facilities.

Mr. D. Danford and the staff of the Industry Program of the College of Engineering for assistance in the preparation of this manuscript.

TABLE OF CONTENTS

TABLE OF CONTENTS CONT'D

TABLE OF CONTENTS CONT'D

LIST OF TABLES

LIST OF FIGURES

LIST OF FIGURES CONT'D

LIST OF FIGURES CONT'D

NOMENCLATURE

S_u	Ultimate strength
S_y	Yield strength
S_e	Endurance or fatigue limit
S	Stress
S_{max}	Maximum stress attained during a load cycle
S^*	Stress at which $\sum E_u$ is maximum
S_1	Stress at which a specimen was fatigued above the fatigue limit
S_2	Stress at which a specimen was fatigued below the fatigue limit
S_{y_u}	Upper yield point
$S_{e_{max}}$	Maximum value of fatigue limit found in the literature
$S_{e_{min}}$	Minimum value of fatigue limit found in the literature
S_m	Mean stress during fatigue
S_a	Alternating stress during fatigue
ϵ_f	True strain in monotonic tension
ϵ_m	Mean strain
ϵ_a	Variable strain
ϵ_{max}	Maximum strain during a cycle
ϵ_{min}	Minimum strain during a cycle
ϵ_p	Plastic strain in a specimen at the end of a given load cycle from o to S_{max} to o .
$\sum E$	Total number of counted emission pulses
$\sum E_\ell$	Total number of counted emission pulses while loading
$\sum E_u$	Total number of counted emission pulses while unloading
H.R.	Hot rolled steel
C.R.	Cold rolled steel

I. INTRODUCTION

A. Review of Literature

1. Fatigue and Fatigue Limit in Steel

(a) Background

The study of fatigue of metals can be traced back to the early part of the 19th century.(33) This was the time in history when reciprocating mechanisms were coming into existence and the masonry and brickwork of bridges was being replaced by wrought iron structures. In 1837 and again in 1843 Hodgkinson reported to the British Association that his experiments on transversely-loaded bars showed that, " . . . when bodies, as the axles of railway carriages, are alternately bent, first one way and then the opposite, at every revolution, we may expect that a total change in the arrangement of their particles will ensue". This in effect was the first formally reported observation of the fatigue phenomenon. This report was soon followed by an interesting but fundamental theorem enunciated by James Thomson in 1848 namely, "There are two elastic limits for any material between which displacements or deflexions, or what may in general be called changes of form must be confined, if we wish to avoid giving the material a set, or in the case of variable strains, if we wish to avoid giving it a succession of sets which would bring about its destruction; . . . " This statement uses the term "elastic limits" which was later redefined as the endurance limit or fatigue limit. Nevertheless this is the first direct statement found in literature which establishes the existence of a fatigue limit. After that time a whole

series of investigations were started by Wöhler in 1870 and he used a rotating cantilever machine to obtain the first notions of an S-N curve (a curve of stress versus number of cycles to failure at the stress). The techniques used and the results obtained by Wöhler[34] are in use even up to the present day. These experiments were later confirmed and continued by Spagenburg (1878) and Bauschinger[35] (1881) who later added a great deal to the store of knowledge in the area of cyclic loading. All these investigations were mainly of a purely experimental character, dictated by engineering requirements of the day and as such were mostly phenomenological in nature. Such studies are still being conducted and will be discussed later.

The second approach to the problem of fatigue was formally begun by Ewing, Humfrey, and Rosenhain who applied the optical metallurgical microscope to the observation of the surface of a metal under fatigue. Their efforts have paved the way for a second approach which will be referred to as a microscopic approach. Such an approach was further aided by Von Laüe's prediction of X-ray diffraction through crystal lattices and Bragg's investigations of structures of various metals. Methods for preparing large crystals were next developed by Carpenter, Czochralski, Gomperez, and Elam. In 1924 de Broglie enunciated the concept of electron wave length and paved the way for a new tool in microscopic observation, the electron microscope. The microscopic observations will be discussed separately.

(b) Phenomenological Studies

In 1910 Basquin[36] analyzed a large number of data obtained from varied sources and found that when the logarithm of stress is plotted versus the logarithm of the number of cycles to failure there existed a straight line relationship between life values of 10^3 to 10^6 or 10^7 cycles. Such a relation is schematically represented by Figure 1.1. The life axis is separated into three regions; the low-cycle region, the finite life region, and the infinite life region. In the low cycle region the fatigue behavior is described by

$$N = \frac{(\epsilon_f - \epsilon_m)}{\epsilon_a}^2$$

where N = number of cycles to failure

ϵ_f = true strain in monotonic tension

ϵ_m = mean strain = $\frac{1}{2}(\epsilon_{max} + \epsilon_{min})$

ϵ_a = variable strain = $(\epsilon_{max} - \epsilon_{min})$.

This relation was proposed by Manson[31] and Coffin[32] and was later modified by Sachs et al.[29] and according to Weiss[27] it seems to be well supported by experimental data.

Most effort in the area of fatigue behavior is concentrated in the finite and infinite life regions. The outcome has been a large amount of information that is quite often conflicting. The region of interest in this investigation lies in the abrupt change in behavior of a ferrous material when it is fatigued above and below the fatigue limit.

Hence a literature survey was also conducted to determine the effect of various factors on the fatigue limit.

In 1874 Gerber[38] analyzed the data of Wöhler and Bauschinger and found that for a given life there was a relationship between the mean stress (S_m) and alternating stress (S_a). This relationship later came to be known as the Gerber Parabola. This was soon followed by a large number of investigations leading to modifications by Goodman[39], Fischer[44], Nishihara[45], Soderberg[46], and others. In 1939 Orowan[40] presented another approach based on his theory of fatigue. In recent times Sines[47] and Little[41] have made substantial contributions to the understanding of the effect of mean stress on fatigue. All these investigators have made recommendations that are useful only in establishing a general trend. Yet the details are different enough to warrant the conclusion that the variations between each of the test specimens used were too high to resolve the effect of mean stress on fatigue in a precise manner.

Besides the mean stress there are several other factors that definitely affect the fatigue limit and these will be discussed briefly:

Carbon content affects the fatigue limit in a direct manner. In case of high hardness steels the fatigue limit increases with the carbon content.

Lead content affects the fatigue limit only under certain conditions and the exact reasons for this effect are not yet established.[48]

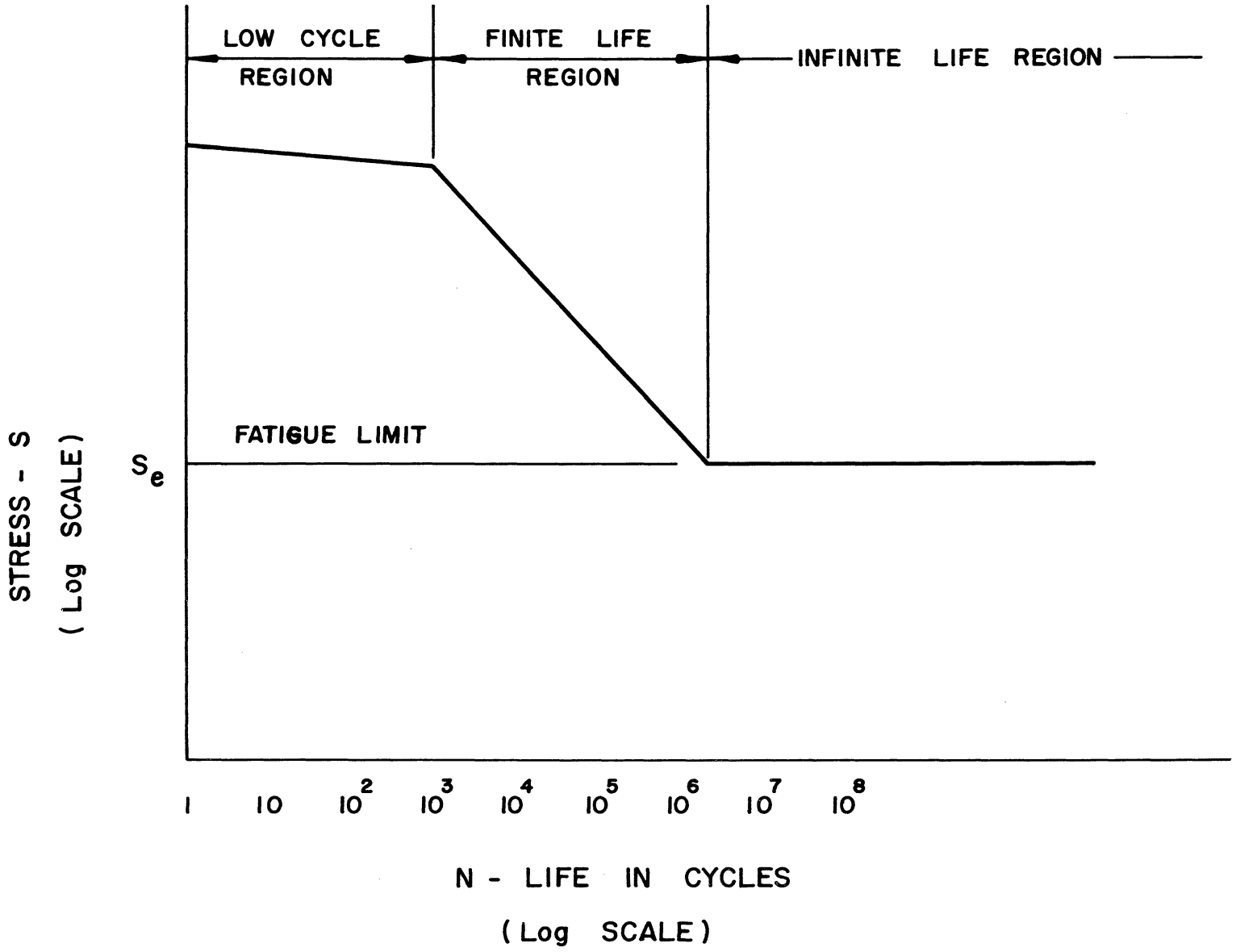

Figure 1.1. Schematic Representation of Stress-Life Relationship (S-N Curve)

The effect of small quantities of austenite have been documented by French,[49] Sachs,[50] and Frankel et al.,[51]. Microstructures containing spheroidite have been shown to have superior over-all fatigue strength when compared with those containing pearlite by Dieter, Mehl and Horne[52] in their studies using high carbon steels.

The effect of size has been discussed in detail by Boegehold[53] and the effect of surface finish, surface treatment, and hardenability, are discussed in references (48, 12, 7).

The size, shape, and orientation of inclusions play an important role in the deterioration of fatigue limit and correlations between fatigue limit and inclusion size have been demonstrated by Cummings et al.[54][48]. Yet certain research conducted by British Iron and Steel Research Association[55] indicates that the inclusions made of silicates and refractory aluminum compounds are the most injurious to fatigue properties. This research also indicates that there is a clear correlation between inclusion size and fatigue life when the inclusions are subsurface. No such correlation was found with surface inclusions.

Fatigue behavior has been studied under thermal stresses by Coffin[56] and Manson.[57] The effect of surface coatings and surface environment on fatigue properties is reported in several studies[48, 58, 59, 60].

Attempts have been made to correlate fatigue limit with other microscopic, static, or dynamic properties. The first attempted correlation is given in Figure 1.2 which is a plot of fatigue limit versus Rockwell hardness. The results show that the scatter in fatigue limit is about

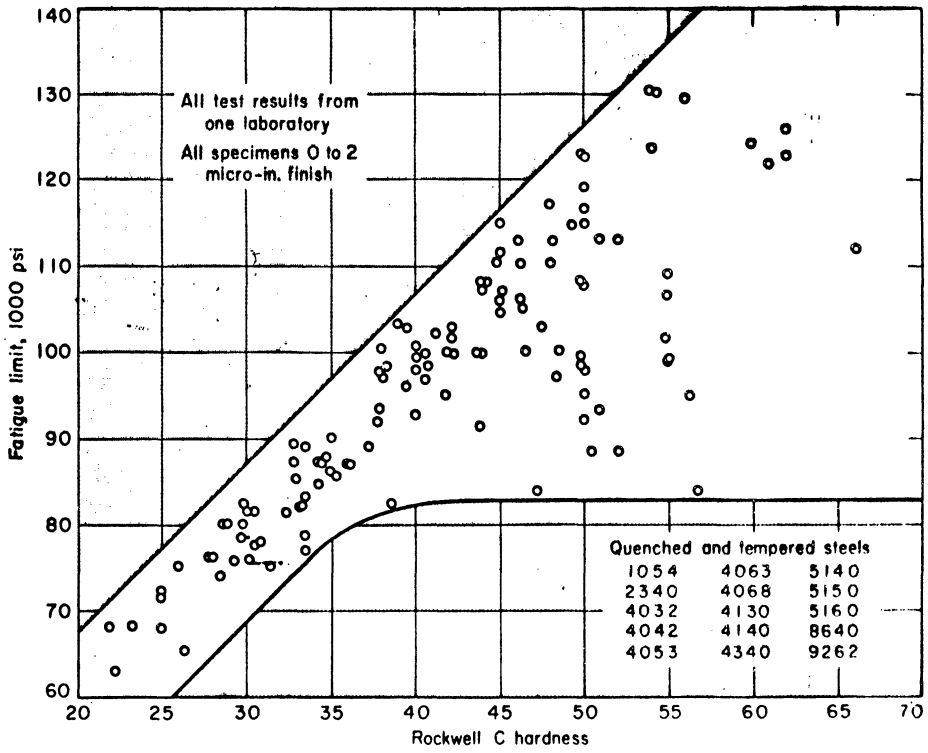

Figure 1.2. Effect of Hardness on Fatigue Limit of Through Hardened and Tempered Steel. Standard .25" Diameter R.R. Moore Specimens were tested in Rotating Beam Fatigue.(48)

± 10,000 psi for hardness values up to $35R_c$. The correlation deteriorates still further as hardness increases and for hardness values greater than $55R_c$ the scatter band is about ± 27,000 psi. The next correlation commonly found in machine design literature[87] is $\frac{S_e}{S_u} = 0.5$, where S_u = ultimate strength. This relationship was compared (by the author) with published data on fatigue strength and ultimate strength from many different sources (for more than 150 polished specimens tested in rotary bending). The ultimate strength (S_u) was plotted versus the ratio S_e/S_u. The specimens were sorted out by the diameters in order to prevent the size effect from creating variations. The results showed that S_e/S_u can vary anywhere from 0.65 to 0.22 and hence the relation $S_e/S_u = 0.5$ is not a satisfactory rule to follow.

Fatigue limit is a dynamic property and as a rule it cannot be predicted closely by any known static property. This belief was quite well known even in the 1800's. Bauschinger[35] was the first to note the difference between the proportional limit of a virgin specimen and the proportional limit of a specimen after cyclic loading. He designated the former as the "primitive elastic limit" and the latter as the "natural elastic limit". In 1932 Gough[65] and others attempted a correlation between a "dynamic proportional limit"and the fatigue limit and found them to be in good correlation. To obtain a dynamic proportional limit a specimen is cyclically loaded and its hysteresis curve is first plotted for each cycle as in Figure 1.3(a). As the cycling progresses the maximum stress σ_y is increased and the dynamic

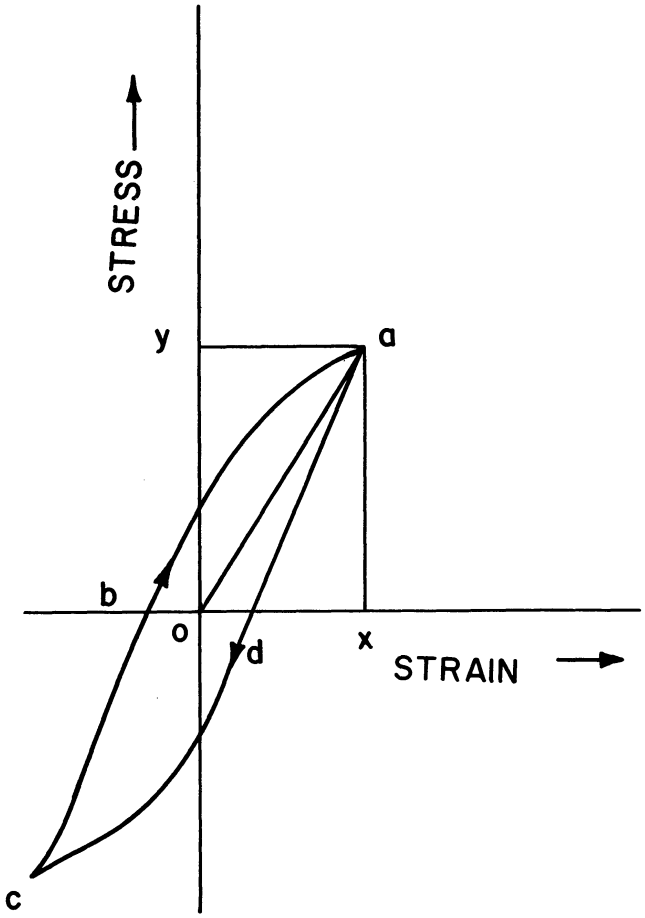

(a) Hysteresis Loop

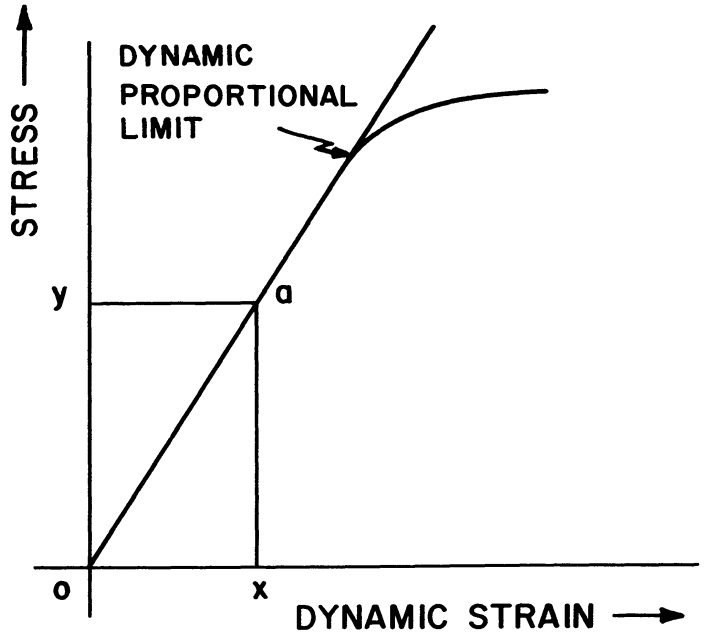

(b) Dynamic Stress-Strain Curve

Figure 1.3. Hysterisis Loop and Its Relation to the Dynamic Stress-Strain Curve.

strain 'o x' is noted. The dynamic stress-strain curve is the locus of the point a . The dynamic proportional limit is the point at which the dynamic stress-strain curve deviates substantially from a straight line. Gough[63], Lazan[93, 94], Wu[92], Blatherwick[91], and Olsen[90] conducted experiments which have shown that the dynamic proportional limit is a good indication of fatigue limit during cyclic stressing (see Figure 1.4). Note also that in Figure 1.3(a) 'o d' is the plastic strain for each cycle and as such gives a good measure of the area inside the hysteresis loop, which is also a good measure of the damping present at that particular value of maximum stress 'o y'. Lazan and Wu[92] found that the damping increased quite rapidly as the cyclic stress was raised above the fatigue limit. Figure 1.4, shows a plot of the plastic strain 'o d' (indicated in Figure 1.3) as well as the dynamic strain 'o x' at each level of cyclic stress.

There are many theories which suggest models explaining the phenomena of internal damping[97, 98, 99, 100, 102, 113]. Most of these theories deal with damping phenomena at very low strain amplitudes and as such fall quite short of explaining the abrupt increase in damping beyond the fatigue limit.

(c) Microscopic studies

The extensive use of the metallurgical microscope, the electron microscope, and x-rays, has resulted in a great deal of information regarding the microscopic behavior exhibited by materials during the progress of fatigue. The principal observations that have been made are described below. Most of these investigations seem to indicate that

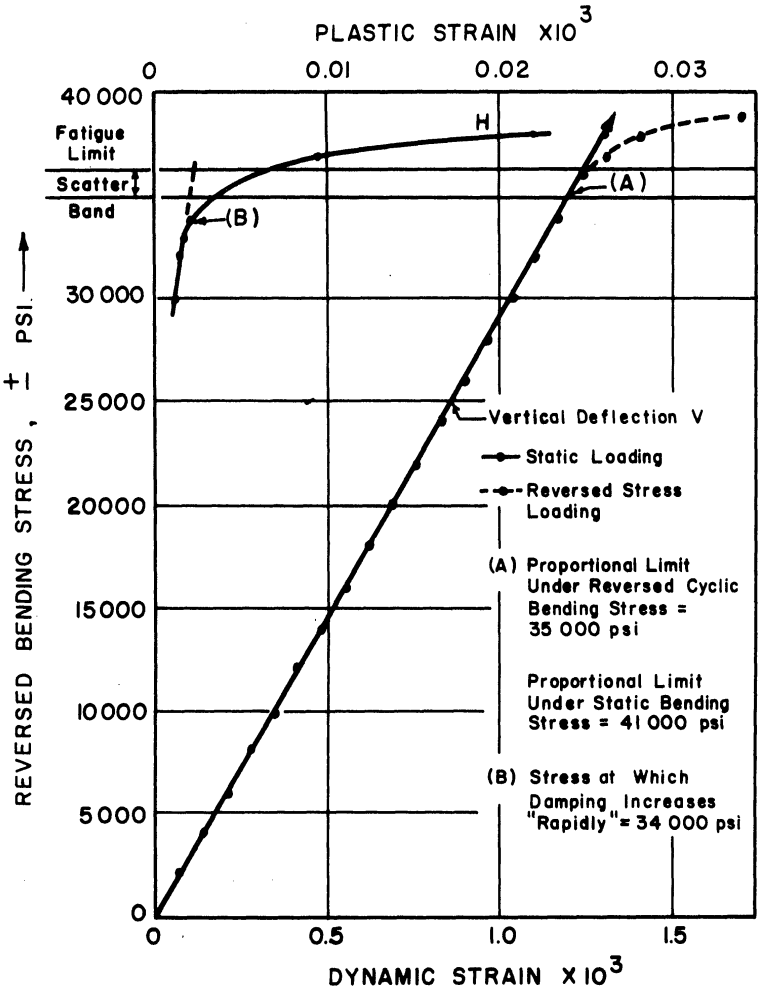

Figure 1.4. Relationship Between Fatigue Limit, Dynamic Proportional Limit and Damping Properties for Mild Steel(92)

a fatigue specimen undergoes three stages; work hardening and the formation of slipbands, the nucleation of cracks, and the growth and propogation of cracks.

The formation of slipbands was observed as early as 1903 by Ewing and Humfrey. This lead to the attrition theory of fatigue which was based on the observations of slipbands, extrusions and intrusions. Then in 1924 Gough[62-67] and his co-workers began their series of very important investigations and found that even during fatigue at considerably low stresses slip did occur on well defined planes. They also showed that environment does not affect crack initiation but it does affect crack propogation.[65, 66, 67] Then came the very important enunciation of the dislocation theory by Taylor[68], Orowan[40] and Polanyi[120] in 1934 who worked independently of each other. Since then many mechanisms have been suggested which can explain work hardening, formation of slipbands, and extrusions and intrusions. The most prominent mechanisms for work hardening have been proposed by Taylor[68], Seeger[69], Baisinski[70], Mott[71], Hirsch and Warrington,[72] and Kuhlmann-Wilsdorf[73]. The theories of extrusion, intrusion, and slipband formation have been advanced by Mott[75], Cottrell-Hull[74], and Fisher[76]. Fleischer[77], Thomson[78] and McEvily and Machlin[79] have made further suggestions regarding the formation of extrusions and intrusions. Many observations have been made on extrusions, intrusions and slipband formation. Hempel[80, 81, 82] has conducted extensive studies in steels and has found that there is a change in the slip behavior above and below the fatigue limit. He found that just below the fatigue limit the number of slipbands appearing even after a few

million cycles of stress was much lower than that observed in the finite life region. There are other observations made by Wood[84, 85, 86] who, working with x-rays as well as taper sections, concluded that there are two mechanisms of fatigue. One of these operates above S_e (fatigue limit) and causes slipbands of high localized distortion which give rise to asterisms in x-ray defraction spots. The other mechanism seems to operate below S_e and gives rise to fine slip lines.

Despres[88] using electron transmission microscopy in 304 stainless steel found that at stresses corresponding to lives below 10^5 cycles there is very strong evidence of cellular structure formation, while lower stresses give a band structure that increases in width and density of imperfections with increasing number of cycles.

Once these slipbands are formed cracks appear to be initiated inside the slipbands. Yet there is only one mechanism[79] proposed so far that can explain to some degree the initiation of a crack following the formation of slipbands. These cracks grow and propagate within the slipbands until they meet the cracks in neighboring grains, and thus give rise to large scale fracture. This process was first photographed and reported by Gough[69] in 1924 yet the explanations of micromechanisms and processes involved in crack growth and propagation are still being developed.

2. Acoustic Emission Phenomena

Historically the evidence of stress-induced sounds was first observed as the "cry of tin". Czochralski[103] traced the cry of tin back to the spontaneous reversal of atomic structure at twin locations. The existence of the emission of acoustical pulses from most other materials when they are subjected to applied stress was relatively unknown until recent times. In 1950 Dr. J. Kaiser[104, 111, 112] reported the existence of stress induced sounds from other materials such as zinc, steel, aluminum, copper, lead, and even wood. This work has been followed by Schofield[15-24], Cusick[105], Tatro and Liptai[13, 25, 26], J. R. Frederick at the University of Michigan, and more recently by Hartbauer[106], Bainbridge and Baker[106], and Dunagan and Harris[107].

Kaiser observed that the emitted sounds have an intensity in the range of 10^{-18} to 10^{-20} watts/in.^{2} and a frequency range of 5,000-25,000 cycles per second. Using an electronic detection system with a background noise of 15 microvolts, he reported that emission starts and stops with load. He concluded that the acoustic phenomena were irreversible in the entire stress range. He also noted that on re-stressing a previously stressed material the emission did not begin until the previous stress was reached. This was later called the Kaiser effect. On the basis of his observations he concluded that the grains shifted owing to the stress and gave rise to the noise. Hence he thought that this noise was a "thermofrictative phenomenon" at the grain boundaries. In his observations the amplitude reached maximum

values thrice as the load increased from zero to failure. This was explained by assuming that these peaks were emitted by the outer zone, the core zone, and the recrystallized zone respectively. He was able to observe that there were two types of pulses, the burst type and the continuous or the high frequency type.

Tatro and Liptai[13] have observed that in the case of aluminum there is no marked difference between the emission from single crystals and polycrystals. They believed that the appearance of emission corresponded to the oxide cracking induced by the formation of surface slip markings.

Schofield[15-24][108-110] has conducted some of the most extensive studies in this area. Working with single crystals of different orientations he concluded that there is a marked difference in emission with orientation. In order to isolate the effect of surface oxide layer, tests were conducted on aluminum crystals with .5 orientation in an etchant solution and on gold crystals of .5 orientation. The results showed conclusively that the emission is not solely a surface phenomenon but the surface affects emission by altering dislocation mobility on the periphery of the specimen. These experiments on gold are of further interest because for the first time some emission was also observed on the unload in a virgin specimen as well as in specimens with two or four cold worked edges as shown by Figures 1.5, 1.6, 1.7.

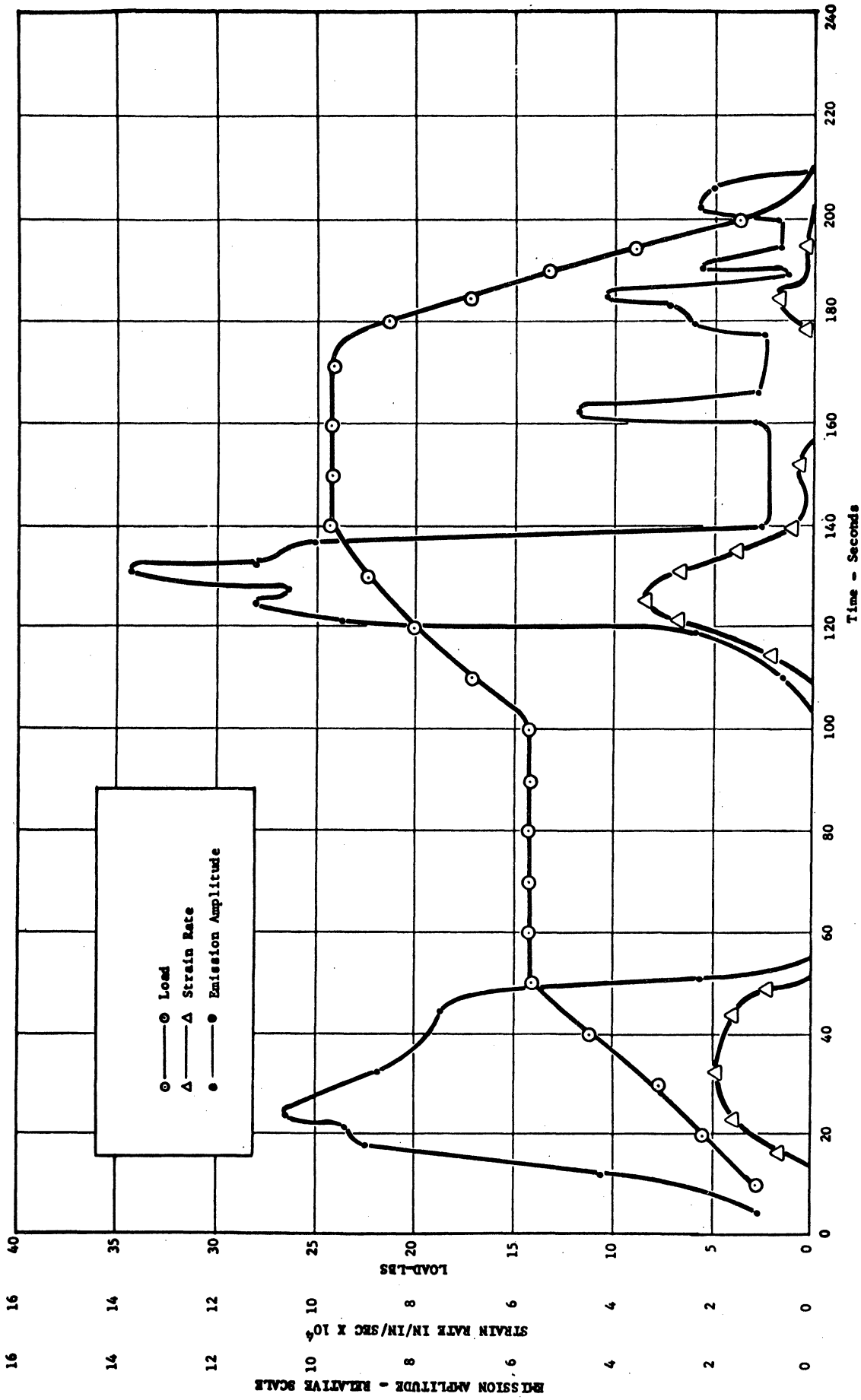

Figure 1.5. Emission Behavior of Gold .5 Orientation(109).

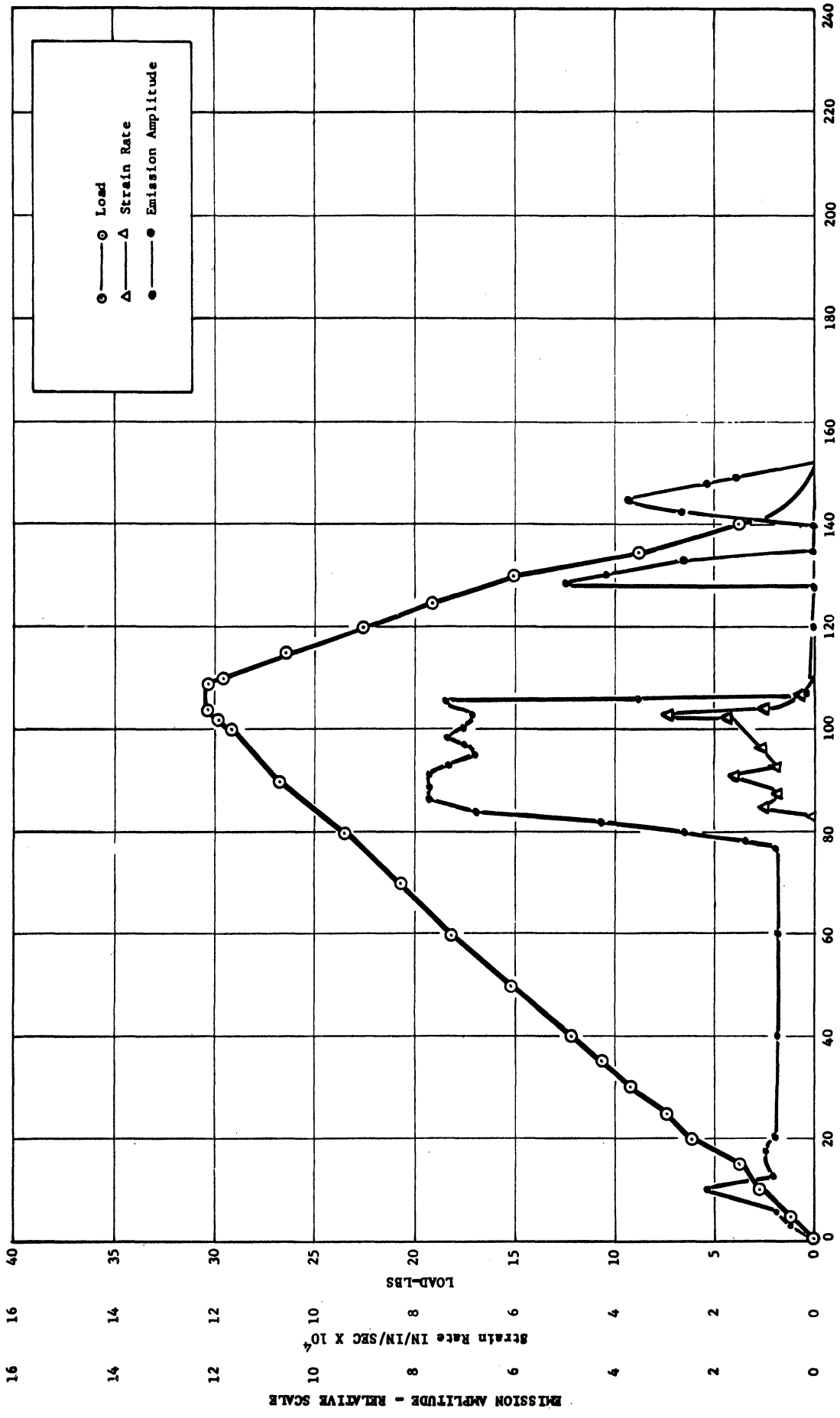

Figure 1.6. Emission Behavior of Gold .5 Orientation Following Cold Working of Screw Edges. (109).

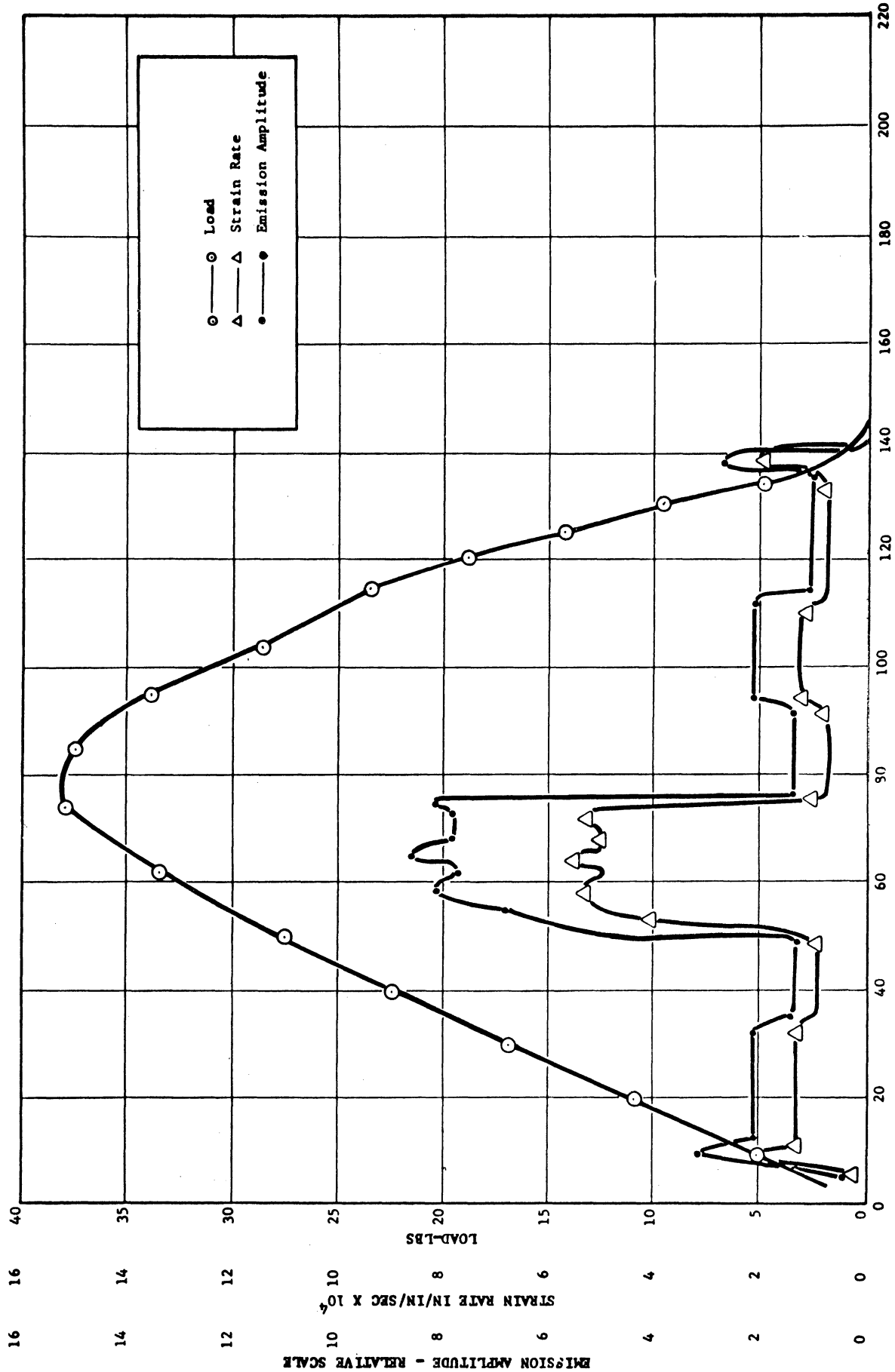

Figure 1.7. Emission Behavior of Gold .5 Orientation Following Cold Work of all Edges(107).

3. Summary of the Literature Survey

The literature survey thus indicates that during cyclic loading the behavior of a ferrous material when stressed above the fatigue limit (endurance limit) is remarkably different from the behavior of the same material below the fatigue limit. This is borne out by the observations arising from surface observations, electron transmission studies, damping studies, and dynamic stress-strain studies.

B. Statement of Problem

The purpose of this investigation was to observe the difference in the acoustic emission as well as surface behavior of commercial ferrous materials when they are subjected to cyclic tensile loading above and below the fatigue limit.

II. EXPERIMENTAL PROCEDURES

A. Test Specimens

1. Materials

In order to add to the practical value of this research program, it was decided to test the most commonly used ferrous materials. In order to observe the effect of carbon content on acoustic behavior, steels with two different ranges of carbon content were investigated namely 0.18 to 0.20% and 0.42 to 0.45%. Two markedly different forms of prior deformations are available commercially: the hot rolled and cold rolled conditions. During cold rolling the grains are deformed and elongated while during hot rolling the temperature is high enough to allow recrystallization. The materials used were low and medium carbon steels in hot rolled and cold drawn conditions. All the steels used in this investigation had a microstructure of ferrite and medium to fine pearlite.

There were many long and elongated inclusions in each of the materials and quite often these were visible at magnifications as low as 10X.

Each material was obtained in the form of a single 20 ft. long 1-1/8 inch diameter bar. In order to minimize the effect of inherent variations of properties within each bar on the test results, specimens were machined from adjacent sections of the bar.

A great deal of prior information is available regarding the microscopic properties and fatigue behavior of these materials. Table 2.1 gives the nominal compositions (as reported by the manufacturer). The engineering stress-strain diagrams for each of the materials are given in Figure 2.1

Table 2.1

CHEMICAL COMPOSITIONS OF THE STEELS USED FOR THIS INVESTIGATION*

AISI No	Condition (Prior deformation)	Carbon %	Manganese %	Phosphorus Max %	Sulphur Max %
C1018	Cold Rolled	0.15 - 0.20	0.60 - 0.90	.04	.05
C1020	Hot "	0.18 - 0.23	0.30 - 0.60	.04	.05
C1042	Cold "	0.40 - 0.47	0.60 - 0.90	.04	.05
C1045	Hot "	0.43 - 0.50	0.60 - 0.90	.04	.05

*Ryerson Steel

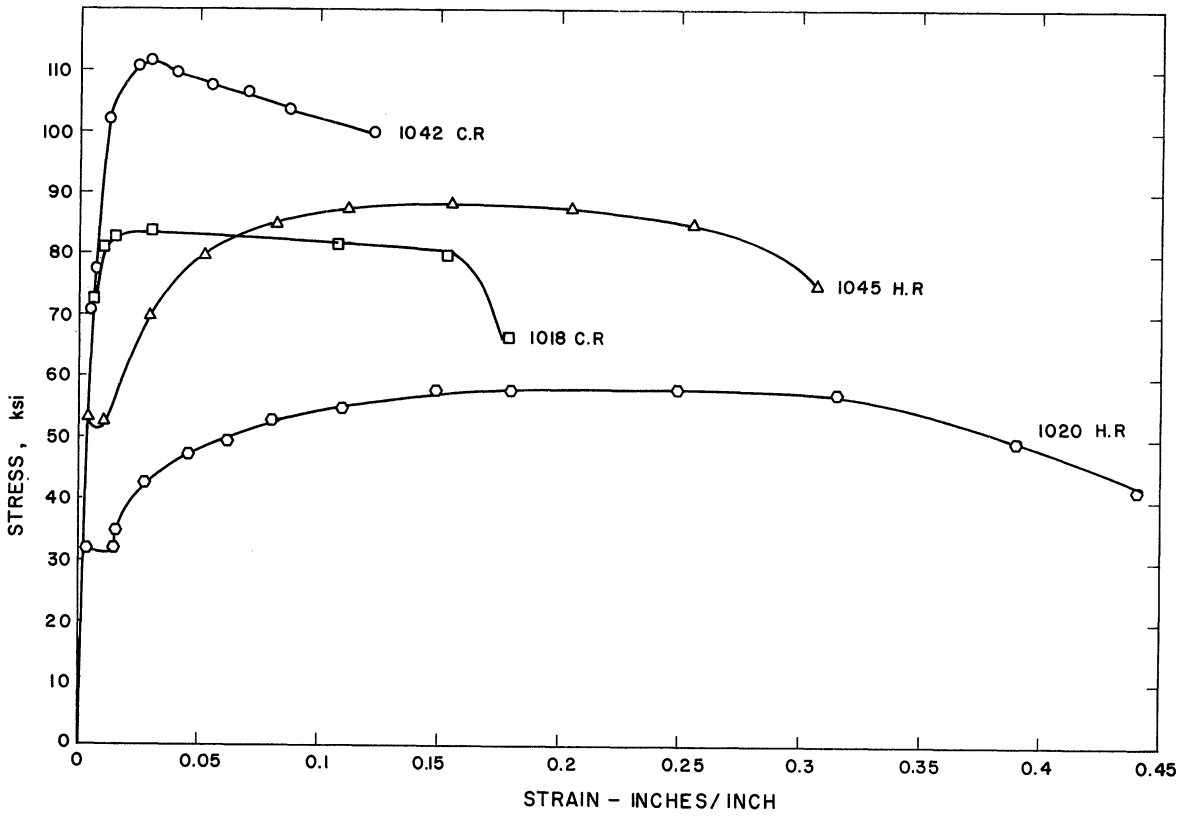

Figure 2.1. Engineering Stress-Strain Curves for Materials Used

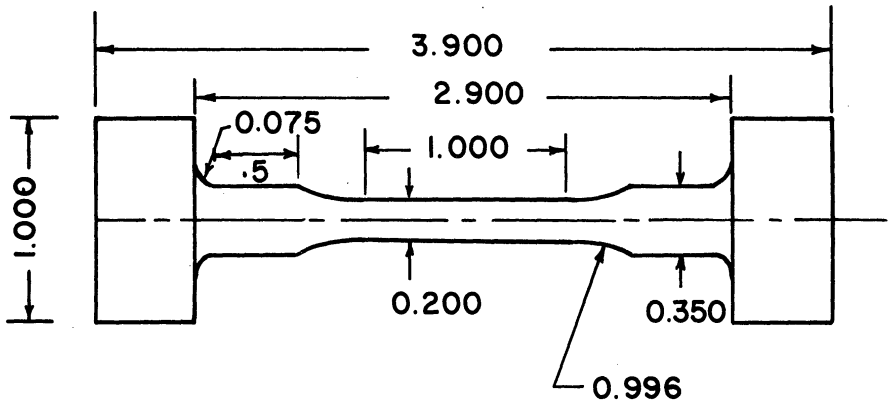

(a) Schematic

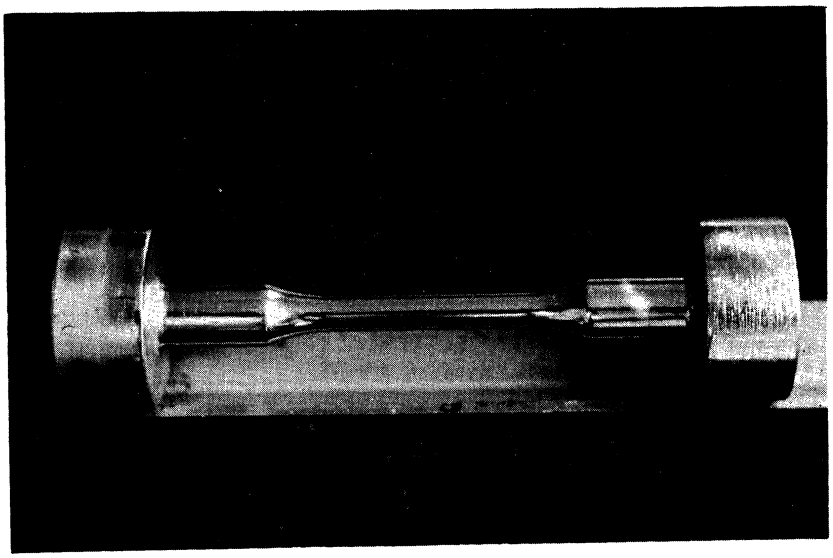

(b) Photograph

Figure 2.2. Fatigue Specimen

2. Specimen Preparation

The specimen shape and size are indicated in Figure 2.2. This shape is quite similar to that proposed by Kroll[11] and is considered highly favorable for acoustic emission studies. These specimens were machined on a lathe out of the steels in their as-received condition and then finished with 500 grit emery paper. They were next electropolished to a very high surface finish (.4 microinches R.M.S.) with the help of an electrolyte containing 25 grams chromium trioxide, 125ml glacial acetic acid and 5ml distilled water. The polishing was done in the cell shown in Figure 2.3, using a stabilized and filtered d-c power supply at a current density of 40 milliamperes per square centimeter. The cathode used was made of copper and the cell was constantly stirred and cooled to 27°C. The specimens were stored in mineral oil. During the acoustic or fatigue tests these specimens were removed from the oil but precautions were taken to make sure that there was enough oil adhering to the surface. During surface observations and replication these specimens were removed from the mineral oil, cleansed with chloroform and then immersed in acetone for a very short period. Care was taken to avoid exposing the bare metal to the atmosphere over extended periods in order to minimize oxidation.

A specimen in its machined and electropolished state prior to any external loading will be referred to as a virgin specimen.

B. Test Plan

From each of the four materials selected, namely 1018 and 1042 cold rolled and 1020 and 1045 hot rolled steels, four specimens were prepared. The first specimen was used for a static tensile test, the second specimen was used to obtain microstrain data, while the last two specimens were fatigue specimens. One of the fatigue specimens was cyclically loaded above the fatigue limit while the other fatigue specimen was cyclically loaded below the fatigue limit.

The following observations were made on each fatigue specimen in its virgin state and after 10^3, 10^4, 10^5, 10^6, and 10^7 cycles of cyclic loading:

1. Observations of acoustic emission behaviour using a specially designed testing facility.
2. Observation of surface changes with a light microscope and with an electron microscope by replication.

The cyclic loading on a fatigue specimen was discontinued after 10^7 cycles of loading. Specimens that survived 10^7 cycles of loading were etched (partially) with Fry's reagent* and the surface observations were repeated on the etched as well as unetched portions.

---

*Composition:

5g	Cupric Chloride
40ml	Hydrochloric Acid
30ml	Water
25ml	Ethyl Alcohol

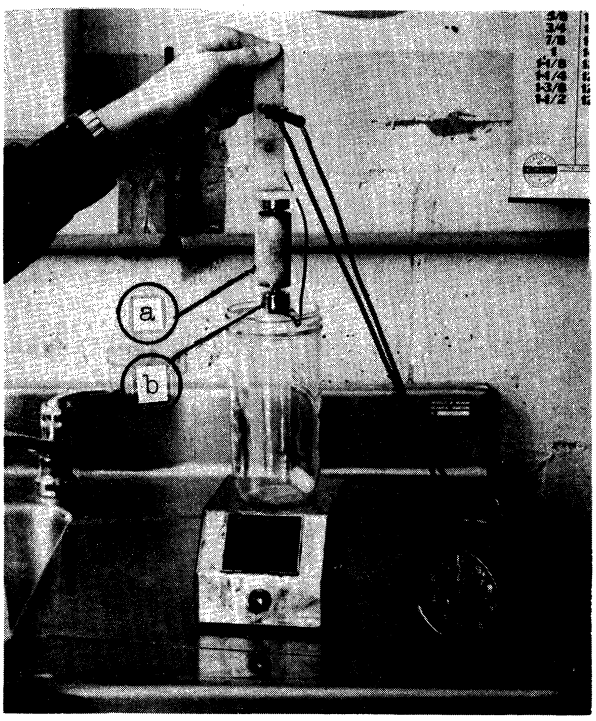

(a) Copper Cathode

(b) Specimen

Figure 2.3. Electro Polishing Cell (cooling coils not shown)

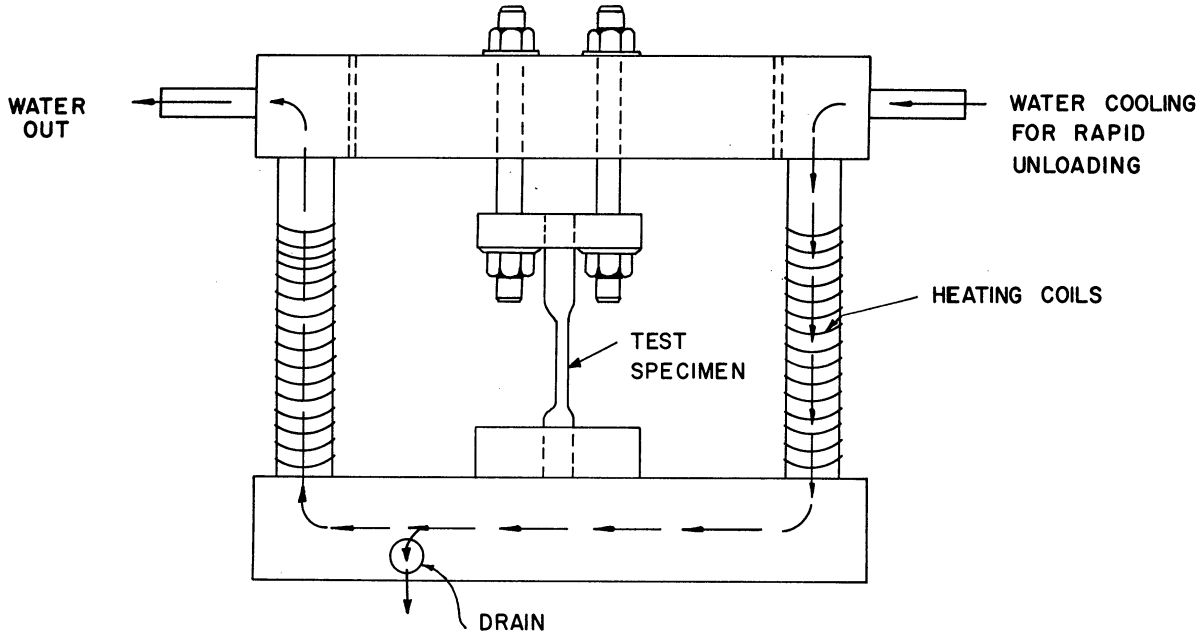

Figure 2.4. Thermally Operated Loading Machine

C. Acoustic Testing

1. Loading Machine

Some preliminary experiments were conducted using a thermally operated loading machine (Figure 2.4). This machine was made up of two parallel beams supported by two columns which were welded to them. The specimen was threaded into one of the beams and bolted to the other. As the columns were heated by the use of electric coils these columns expanded and loaded the specimen in tension. The unloading was accomplished by allowing the loading machine to cool in air or by passing water through the columns. This particular machine had the following disadvantages: (a) In order to be effective the coupling between the specimen and the machine had to be very rigid. Hence the acoustic transmission loss between the specimen and the machine was low, and ambient noises were easily transmitted to the transducer. (b) Electrical as well as mechanical noises produced during the heating process were at times large enough to be picked up by the sensitive acoustic pickup. (c) The time required to load a specimen to the desired level was approximately 15-20 minutes and the time required to unload a specimen (silently with ambient cooling) was about 40-60 minutes. Cooling by means of water was more rapid but gave rise to excessive noise. (d) The strain rate was not linear but exponential. (e) The maximum strain that this machine could produce in a specimen was too low. If a specimen were to undergo a permanent deformation of .022 inches the load would drop by more than 95%.

In order to avoid all these drawbacks another loading device called the acoustic test machine was designed. This machine and its various parts are shown in Figure 2.5. Figure 2.5(a) shows a schematic view of the machine. Figure 2.5(b) shows only its front end where the specimen is situated. When the reservoir (l) is lowered using the drive unit (e) the water flows from the support tank (m) to the reservoir. The ballast tank (h) (which is buoyant at zero load) gradually exerts its weight on the lever (b) which in turn applies the load to the specimen (s) in the grips (n) through the hanger (q). The load rate could be easily governed by the use of valve (k) and was kept constant at about 350 lb/min. A plastic deformation of about .022 inches at the specimen changed the load by less than 5%. Thus this system was considered to be very "soft". The power requirement was only 1/60 h.p. The specimen was isolated[2, 3, 6, 9, 10, 14] first of all by putting the acoustic test machine in a soundproof room having noise reduction capability given by Table 2.2.

Table 2.2

NOISE REDUCTION CAPABILITY OF SOUNDPROOF ROOM

Octave bands cps	Noise reduction in db
37.5 - 75	22
75 - 150	28
150 - 300	36
300 - 600	46
600 - 1200	53
1200 - 2400	58
2400 - 4800	61
4800 - 9600	63

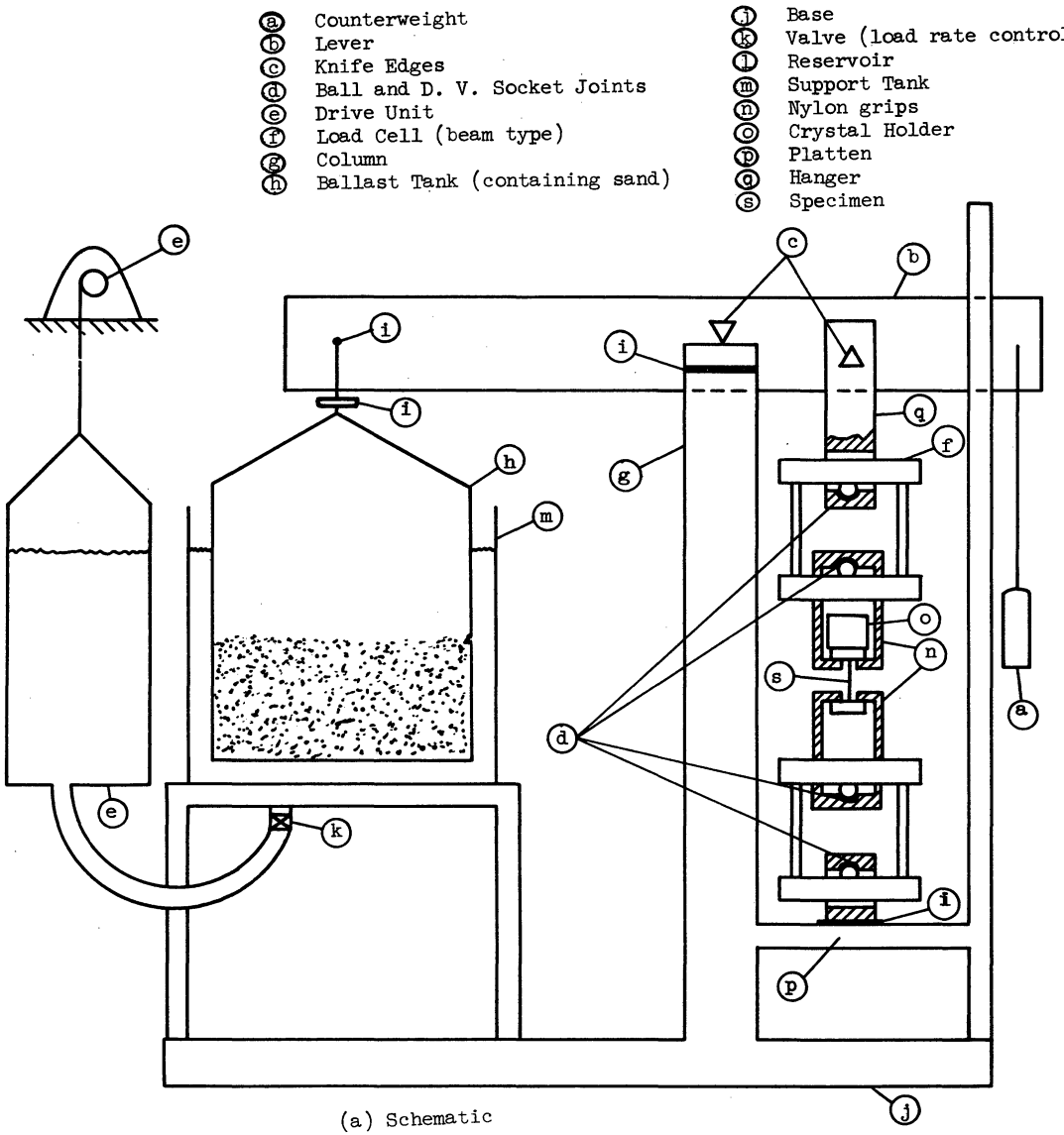

(a) Schematic

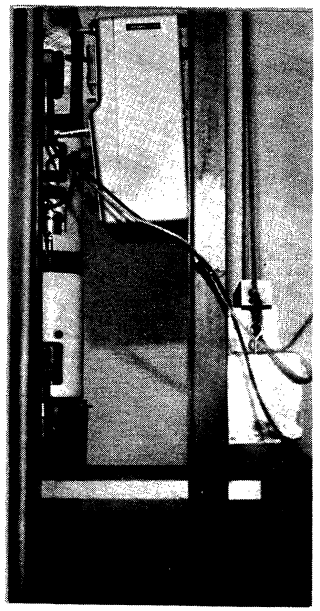

(b) Photograph of the Front End

Figure 2.5. Acoustic Test Machine

Next the acoustic test machine was placed on a rubber floor mat and sound isolation was provided at the places marked (i) in Figure 2.5(a). Finally the specimen was placed in nylon grips. Prior tests conducted by Schofield revealed that nylon has good damping qualities as compared to metals like steel or aluminum.

The load cell in the acoustic test machine was calibrated by the use of the load cell on the fatigue machine. A certificate of calibration of the load cell on the fatigue machine was supplied by the manufacturer. This cell was used as a standard throughout the experiments.

The problem of eccentricity was solved by using four ball and socket joints which were co-axial with the axis of the specimen. These sockets were made of DU material which is a porous bronze impregnated with teflon and lead (coefficient of friction = 0.05). When the stainless steel balls rub on the DU material they do not exhibit a stickslip friction phenomenon. The final check on eccentricity was made by loading a dummy specimen with highly sensitive solid state strain gages on it. This method revealed that the bending stress on the specimen did not exceed 4.0% of the total uniaxial tensile stress.

2. Electronic Equipment:*

The three quantities that were measured and recorded during an acoustic test were:

---

* See Figure 2.6 and Figure 2.7 also see appendix for detailed specifications of various equipment.

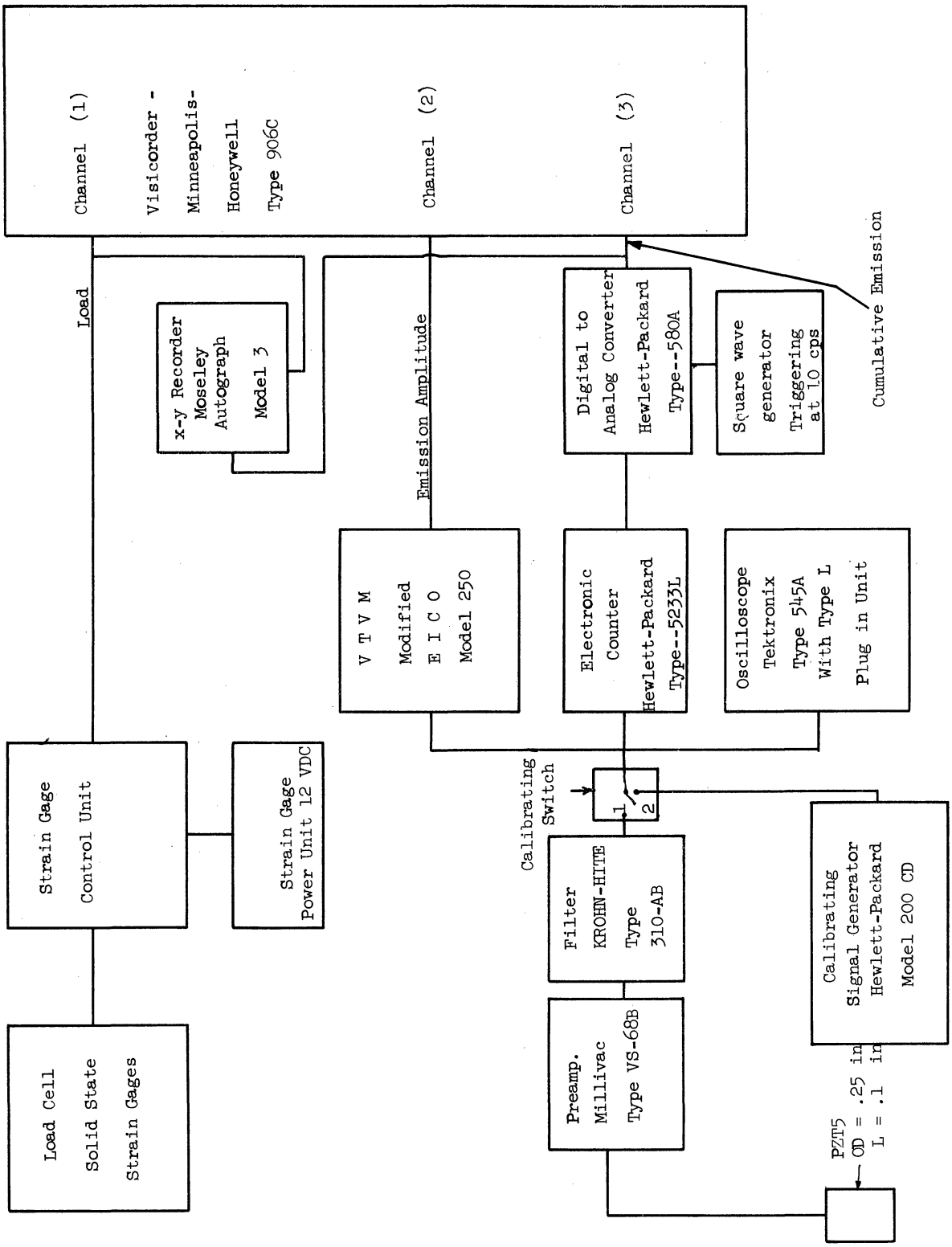

Figure 2.6. Electronic Equipment - Schematic

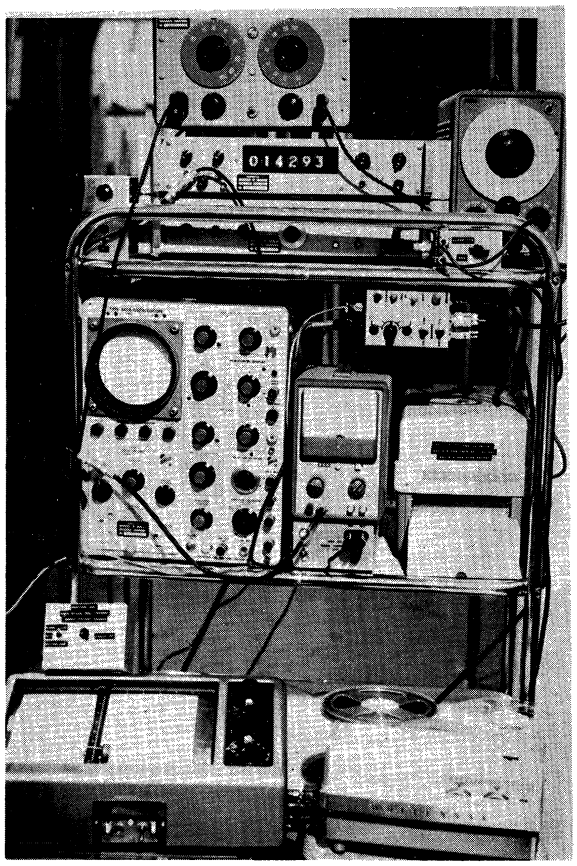

Figure 2.7. Electronic Equipment - Photograph

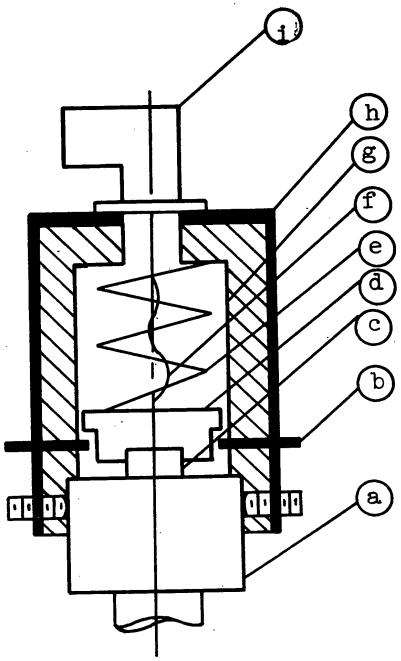

a Specimen
b Shorting Screw
c Crystal
d Backing plate
e Spring
f Positive Lead
g Nylon Holder
h Copper Shielding
i B. N. C. Connector

(a) Crystal holder and Specimen Sectional View

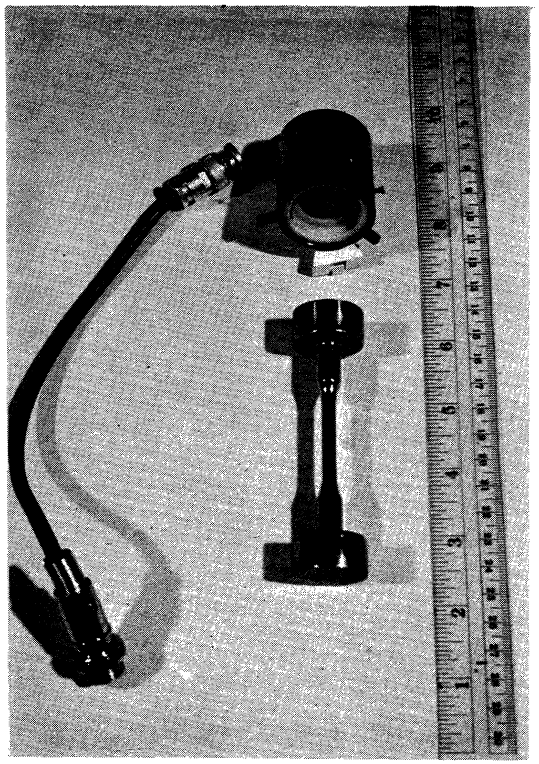

(b) Crystal holder disassembled from Specimen

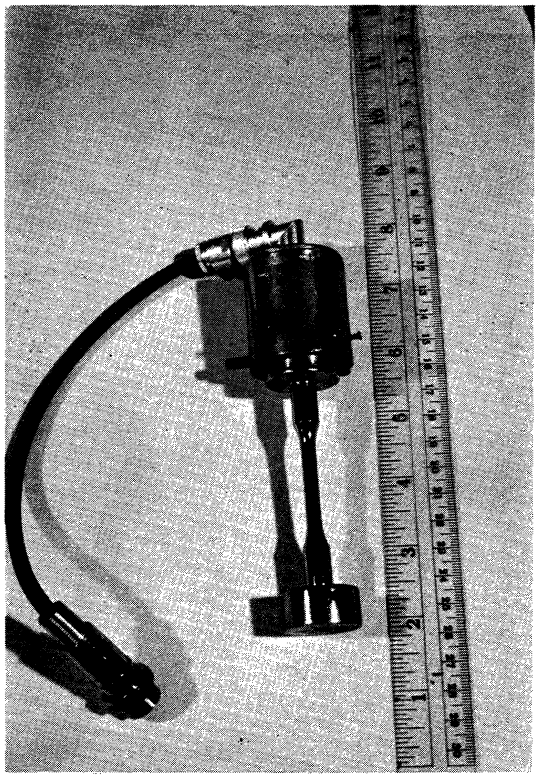

(c) Crystal holder assembled on top of Specimen

Figure 2.8. Crystal Holder and Specimen

a. Load on channel (1) of the Visicorder oscillograph

b. Emission amplitude on channel (2) of the Visicorder oscillograph

c. Cumulative emission on channel (3) of the Visicorder oscillograph.

The load was measured using a beam type load cell having solid state strain gages which were temperature compensated. The output of the load cell was displayed on channel (1) of the Visicorder, and the overall drift at the output during a load-unload sequence was less than 1%.

The acoustic pulses were picked up by the help of a lead zirconate titanate piezoelectric crystal (PZT-5) of 0.25 in. diameter and 0.1 in. thickness. The crystal was mounted on a copper disc inside a holder which was made of nylon and shielded electrically by copper. Figure 2.8(a) gives a sectional view of the crystal holder attached to a specimen. Figure 2.8 (b) and Figure 2.8 (c) are photographs of the same.

The other side of the crystal holder was kept in constant electrical and acoustic contact with the specimen (s) by the help of spring (e), Figure 2.8. The crystal was connected to a preamplifier by means of a very short cable to avoid electronic noise pickup. The specimen was grounded to the copper shield (of the crystal holder) which in turn was grounded through the cable, thereby avoiding ground loops.

The preamplifier was a "hushed" transistor amplifier (Millivac) and was chosen because it was capable of having a wide band and a low noise level. The output of the preamplifier was connected through a

filter to three separate devices in parallel; an EICO Vacuum tube volt meter (V.T.V.M.), a Tektronix oscilloscope and a Honeywell Visicorder. The V.T.V.M. was modified so that its output could be displayed on the Visicorder in order to obtain a permanent record. The oscilloscope display was used so pictures of waveforms could be taken. The electronic counter had a binary coded decimal output which was connected to a digital-to-analog converter. The output of the converter was triggered externally at 10 cps by a square wave generator and the analog pulse, corresponding to the total number of pulses counted (cumulative emission), was recorded on channel (3) of the Visicorder. At the beginning of each run the load cell was balanced and its gain was checked using a calibrating resistor. Hence the cell's output on the Visicorder was always 500 lb/in. of deflection. The "hushed" transistor amplifier was always set to accept a band width of 2.0 - 180,000 cps at a gain of 70 db. The Krohn-Hite band pass filter was used to attenuate all frequencies below 300 cps. All electronic equipment except the preamplifier was left outside the soundproof room as shown in Figure 2.7. In this manner the overall noise level was maintained below 4 microvolts R.M.S. as referred to the input of the preamplifier. The acoustic detection system was calibrated by transfering the calibration switch (Figure 2.6) to position (2) and applying a known 1 kc/sec. signal (.055 volts R.M.S.) from the calibrating signal generator. This voltage was checked by using the V.T.V.M. and then the trigger level on the counter was set so that all the signals above .055 volts R.M.S. were counted. In

this manner the sensitivity was kept constant throughout the whole series of tests and the calculated values of the sensitivities referred to the input of the preamplifier were as follows:

Minimum voltage at preamplifier input that could trigger the counter = 24.8 microvolts peak to peak

Minimum pressure at the crystal that could trigger the counter = .394 Newtons/sq meter

Minimum intensity of sound at the crystal that could trigger the counter = 3.88×10^{-13} watts/sq cm.

D. Mechanical Testing

Three types of mechanical tests were performed for the purpose of this investigation. These were tensile (static) tests, fatigue tests, and microstrain tests. Because of the limitations of each testing facility, these tests had to be conducted on three different machines using three different types of specimens. The details of each type of test are given in the following paragraphs.

1. Tensile Tests

The tensile tests were conducted on a 60,000 lb Baldwin Southwark testing machine using a standard (A.S.T.M. Designation E 8-61t) round test specimen of .505 in. diameter and 2 in. gage length. For low strain rates stress-strain curves were obtained using a stress-strain plotter supplied with the machine. For higher strain rates the stress-strain curves were plotted manually. The strain rate was held within .05 to .002 per min. These specimens were stressed to fracture in monotonic tension.

2. Fatigue Tests

These tests were conducted on a 20,000 lb Research Incorporated Materials Testing System Model 900.29 shown in Figure 2.9(a). The specimens (Figure 2.2) that had undergone acoustic as well as surface observations were fatigued using this machine. The grips of this machine were made of steel and are shown in Figure 2.9(b). They are similar to those used in the acoustic test machine (Figure 2.5(a)). The alignment is obtained by the use of four coaxial ball and socket joints, Figure 2.9(b). These balls were made of stainless steel and the sockets were made from porous bronze impregnated with lead and teflon (DU material). The total bending stress on a specimen (measured using a dummy specimen with solid state strain gages) was found to be less than 5.58% of the total axial stress. Figure 2.9(c) gives a closer view of the ball and socket joints. This fatigue machine is an electronically controlled hydraulic system operating on a closed loop principle (Figure 2.10). Hence it is capable of delivering a wide range of inputs to the specimen. The input during all the tests was such that the stress ratio

$$A = \frac{\text{Stress Amplitude}}{\text{Mean Stress}} = \frac{S_a}{S_m} = 1$$ as indicated in Figure 2.11.

During the tests the load waveform used was sinusoidal and the load cell output was monitored on an oscilloscope. The cyclic frequency of this machine was held constant at 30 C.P.S. during the testing period.

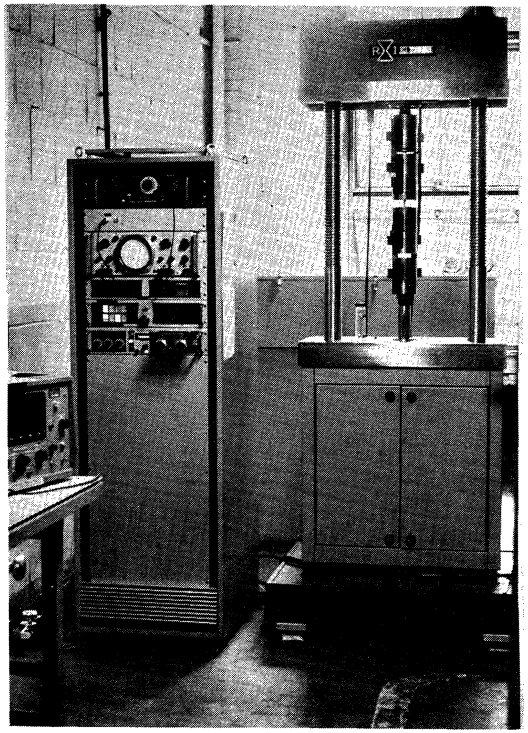

(a) Research Incorporated Materials Testing System

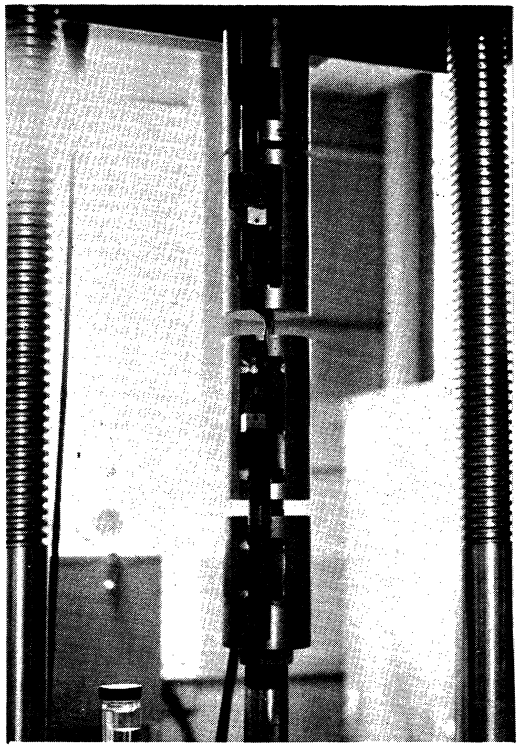

(b) Grips for Research Incorporated Machine

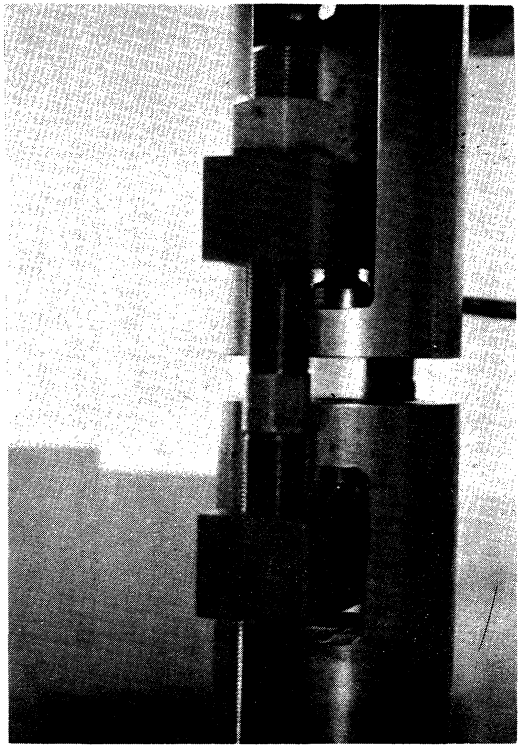

(c) The Ball and Socket Joints in the Grips

Figure 2.9. Research Incorporated Materials Testing System Model 900.29 Used for Fatigue Testing

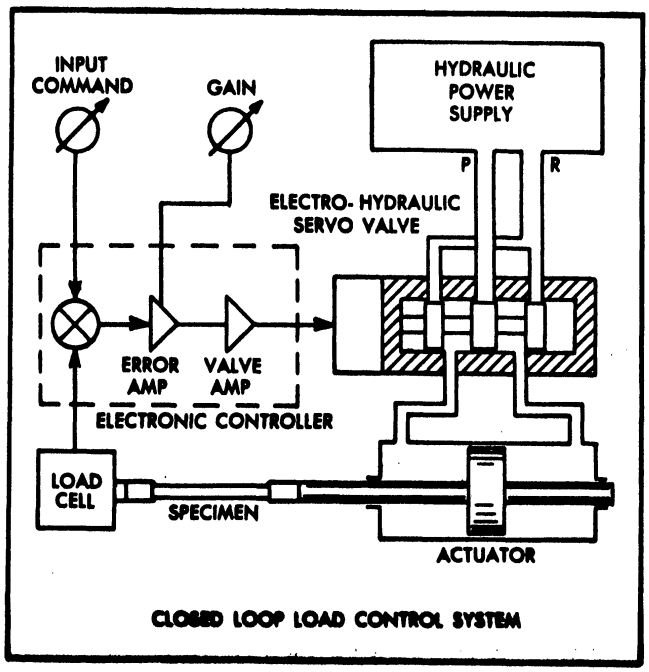

Figure 2.10. Schematic of the Closed Loop Control System of the Fatigue Machine

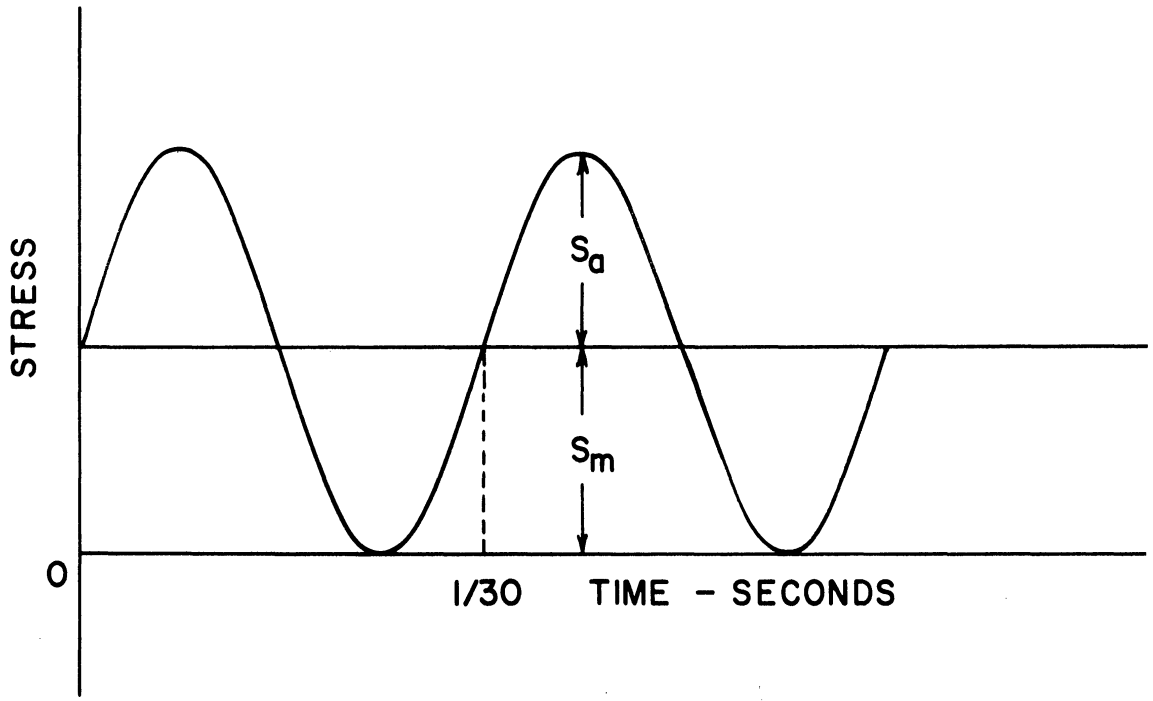

Figure 2.11. Stress Pattern Used in Fatigue

3. Microstrain Tests

The microstrain tests were carried out on an Instron Tension-Compression Machine. This machine was a constant strain rate machine and had two types of readouts. The first readout was an x-y plot of microstrain (abscissa) versus load (ordinate). The microstrain pickup was of the capacitive type and had a sensitivity of 1.865×10^{-6} inches per 1/20 in. on a Mosely x-y recorder. This readout was used to measure the amount of plastic deformation at the end of each cycle of load. The second readout was a plot of load versus time. Whenever the observed strain was beyond the range of the microstrain readout the strains were calculated from the chart of the second readout.

The strain rate was held constant at .05 per min during the microstrain tests. The specimen shape and size are given by Figure 2.12.

E. Surface Observations

Surface observations were made by the use of a Unitron light microscope using reflected light. Photographs were taken using a Honeywell Pentax camera with Panatomic X fine grain film. The magnifications used ranged from 75X to 1500X (oil immersion). Owing to the curvature of the specimen shank (0.2 inches diameter), the depth of field was not sufficient to obtain the necessary details for this particular study; hence this technique was used only to make gross surface observations.

In order to overcome the deficiency of the light microscope the surface of the specimen was replicated and the replicas were examined under an electron microscope (J.E.M. 6-A). Both single and

double stage replication techniques were tried and it was found that the double stage technique was in no way superior to the single stage one. Hence single stage replicas, made out of collodion and shadowed with platinum and palladium at an angle of about 30 degrees, were used extensively.

A micro etchant was used only on those specimens that had survived 10^7 cycles of load. This etchant was Fry's reagent whose composition is 5gm Cu Cl_2, 40ml conc. HCl, 30ml H_2O, 25ml C_2H_5OH. Only half of each specimen was etched in this reagent for 10 seconds. The other half was left unetched for comparison.

Both halves of the specimens were then subjected to surface observations. The results are discussed in the next section.

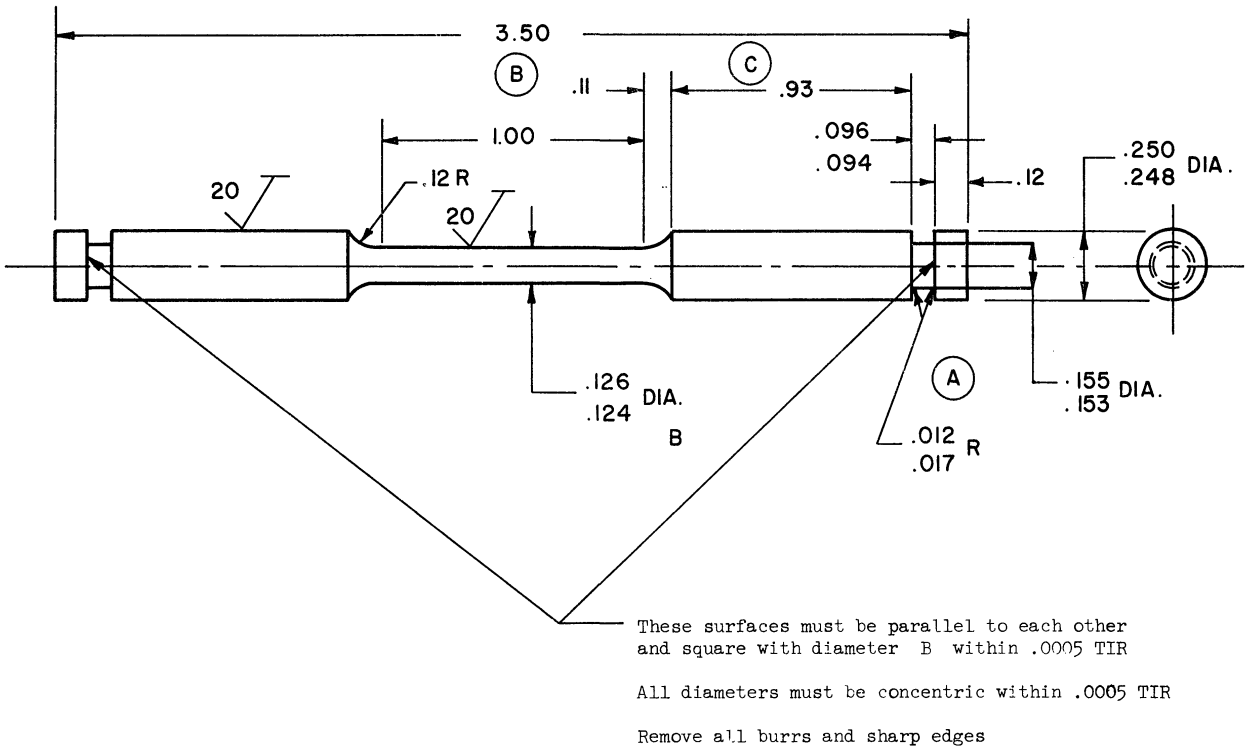

Figure 2.12. Microstrain Specimen

III. RESULTS

A. Acoustic Emission

1. Load-Unload Characteristics of a Virgin Specimen

For the purpose of this study the term "virgin specimen" will apply to a specimen in its as-received, machined, and electro-polished condition, prior to the application of any tensile stress.

There is a great deal of information available regarding the fatigue limits of the materials chosen for this investigation. From this information the maximum ($S_{e_{max}}$) and minimum ($S_{e_{min}}$) values of the scatter bands on the fatigue limit of each of the materials was determined (see Figure 3.1). In case of each material two stress levels, S_1 and S_2, were chosen, one above and the other below the scatter band of the fatigue limit data. In order to prevent this scatter from creating an ambiquity in the results, one of the specimens of each type of material was fatigued at the stress level S_2 below the $S_{e_{min}}$ and the other specimen was assigned to be fatigued at a level S_1 above the $S_{e_{max}}$. During the acoustic tests both of these specimens were stressed only to S_1.

Table 3.1 shows the values of S_1 and S_2 together with the mechanical properties for each steel used.

The characteristics of the acoustic emission obtained during the loading of a hot rolled material were significantly different from that of the cold rolled material. Figure 3.2(a) shows a typical Visicorder chart obtained during the acoustic test of a hot rolled 1020

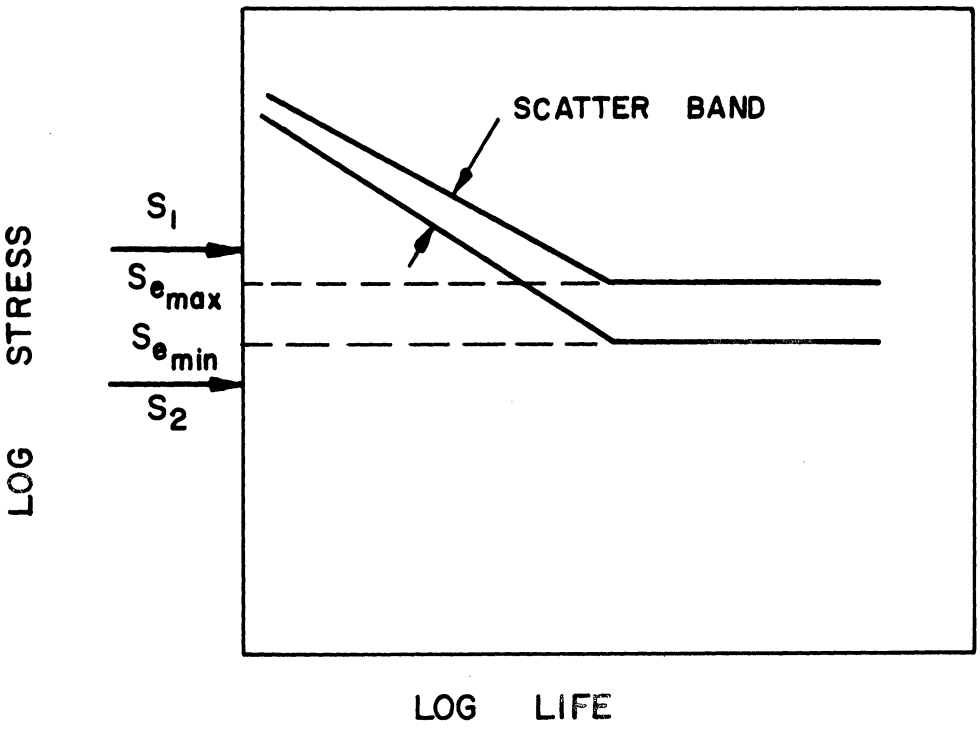

Figure 3.1. Selection of Fatigue Stress Levels

Table 3.1

MECHANICAL PROPERTIES OF THE MATERIALS USED FOR THIS INVESTIGATION

Material (Steel)	Brinell Hardness Number	Rockwell Hardness	S_u, ksi	upper yield point in ksi			Yield Strength - Sy(0.2% offset) ksi	S_1 ksi	Se_{max} ksi	Se_{min} ksi	S_2 ksi	S* ksi - Two specimens
				0.505 in Dia. - BLH Testing Machine Specimen	0.2 in. Dia. - Acoustic Test Machine Two Specimens	0.125 in. Dia. - Instron Tensile Testing Specimen Machine						
1018 Cold Rolled	168	85_{R_B}	83.5				71.5	71.0	67.0	43.4	39.4	62.0 62.0
1020 Hot Rolled	114	$65R_B$	58.5	32.0	29.8 29.2	37.8		40.9	36.9	32.4	28.4	39.5 39.5
1042 Cold Rolled	244	$22R_C$	112.0				91.2	68.2	64.2	38.8	34.8	48.0 63.0
1045 Hot Rolled	179	$87R_B$	88.5	52.5	48.0 48.4	62.5		50.4	46.4	43.0	39.0	46.0 47.0

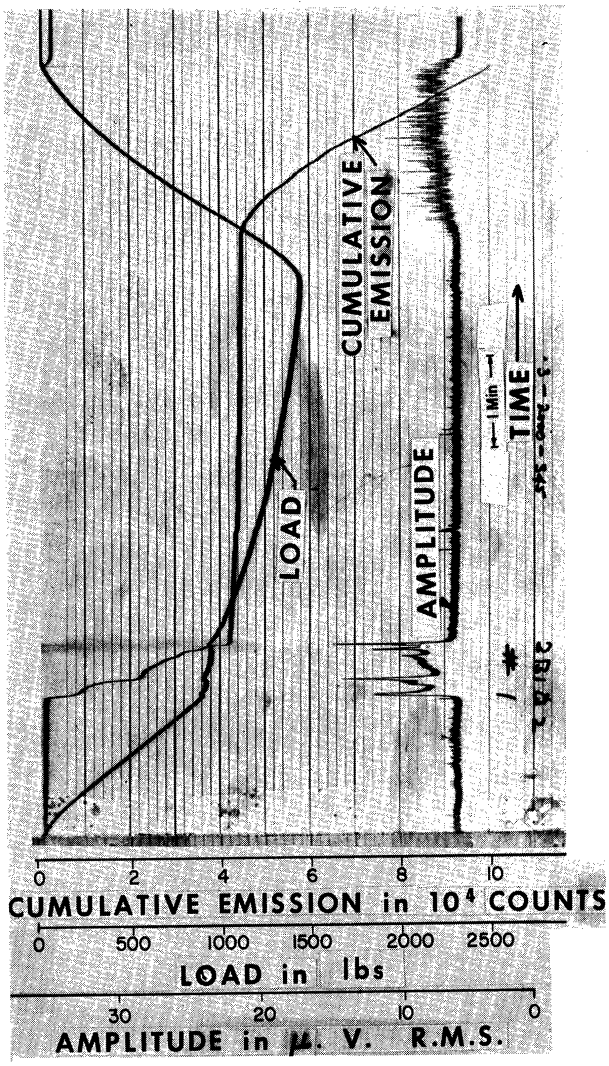

(a) Visicorder Output

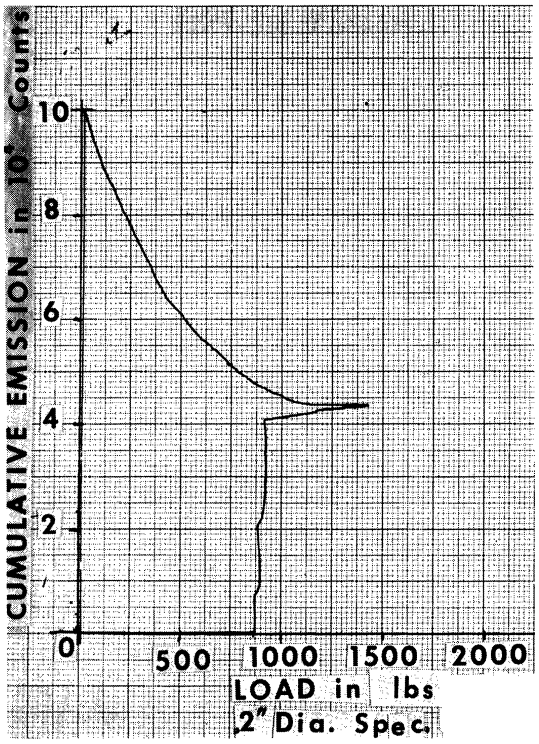

(b) x-y Recorder Output

Figure 3.2. Typical Test Results from an Acoustic Test on 1020 Hot Rolled Steel Virgin Specimen. (Data Recorder Simultaneously on Visicorder and x-y Recorder.)

steel (note that time increases upwards and amplitude to the left). The emission is quite low until the upper yield stress is reached. At that point there is a sudden increase in emission until the lower yield stress is reached. This emission beyond the upper yield is designated in the discussion that follows as high frequency emission and it tapers off gradually as soon as the load begins to increase once again. Figure 3.3 shows plots of the cumulative emission versus the load for each of the hot rolled steel specimens tested. It should be mentioned that even though the general trend in the emission behavior during the loading of hot rolled steel virgin specimens is the same, no two specimens (cut from adjacent pieces of a single bar) were exactly alike in their acoustic behavior.

When the stress on these specimens was released it was observed that the unloading operation also produced acoustic emission in each case as shown in Figure 3.3.

The general acoustic behavior can be summed up by the use of Figure 3.4 which shows schematic diagrams of cumulative emission from steel specimens while they were loaded to a predetermined stress S_{max} and then unloaded. Curve oabcd represents the behavior of a virgin hot rolled steel specimen during its first load-unload cycle. From o to a the specimen is relatively silent. At the point a just prior to the upper yield point the specimen starts to emit copiously and between points a and b the high frequency emission is observed. From b to c the emission drops off once again as strain

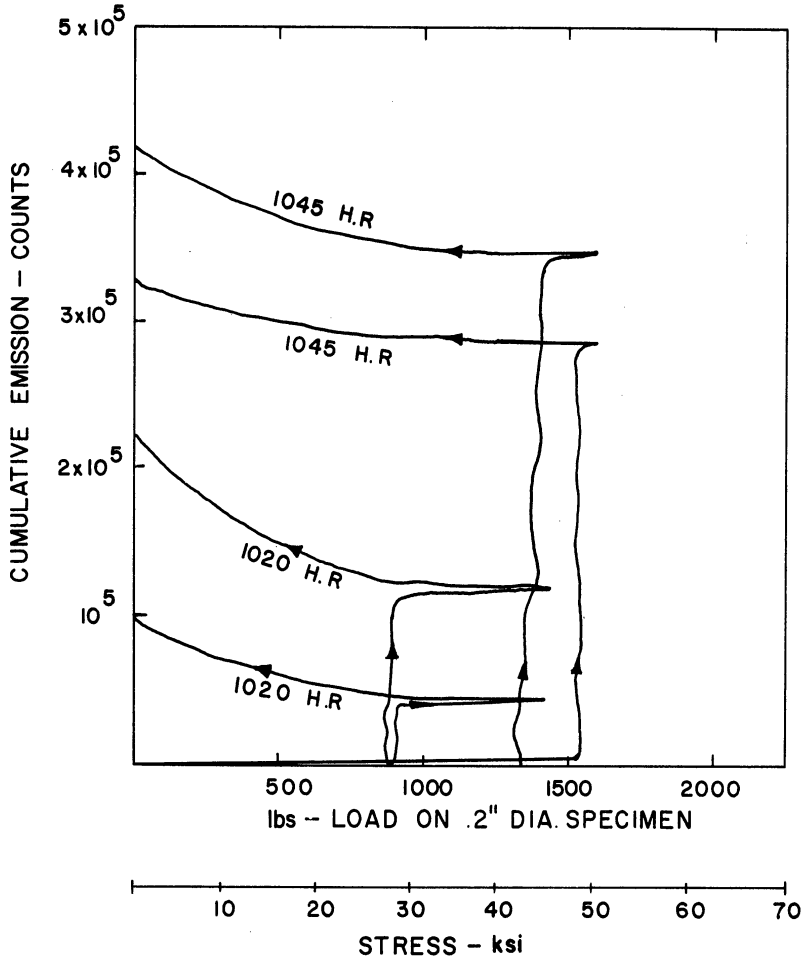

Figure 3.3. Emission Behavior of Virgin Hot Rolled Steels (x-y Recorder Output)

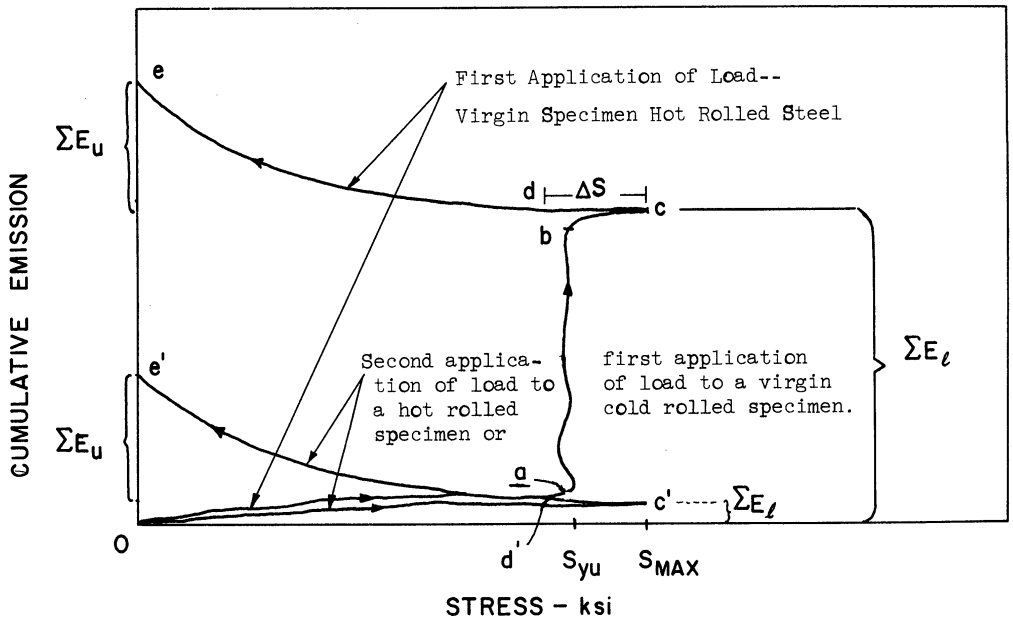

Figure 3.4. Schematic Diagram of Cumulative Emission Versus Stress when the Specimen is Loaded to a Predetermined Stress S_{max} and then Unloaded

hardening begins to occur. At the point c the direction of loading is reversed. On the unload part of the cycle there is first a region cd where no significant emission takes place. After point d the emission gradually begins to reappear. The emission continues from d to e and it keeps increasing in its rate until point e is reached.

The nomenclature that will be used in describing the results is clarified by Figure 3.4. The cumulative emission from o to c will be called the total emission on load and will be denoted by ΣE_ℓ. The total number of acoustic pulses counted by the electronic counter between c and e will be called the total emission on unload and will be denoted by ΣE_u. The maximum stress reached during a load-unload cycle will be denoted by S_{max}. The difference in stress between points c and d will be called the stress delay and will be denoted by ΔS.

Figure 3.2(a) shows a typical Visicorder output for a test run on a virgin 1020 hot rolled steel specimen with its x-y recorder counter part in Figure 3.2(b). It will be noted that the amplitude of the emitted pulses and the cumulative emission are not related during the load or the unload part of the curves. The emission on unloading is predominantly of the burst type. The emission during the loading is also of the burst type except for the region between points a and b where high frequency emission is present.

When a virgin cold rolled steel specimen is stressed its behavior is quite similar to that of the hot rolled specimen except for the fact that the high frequency region ab (Figure 3.4) is completely missing in the case of a cold rolled specimen. Figure 3.4 illustrates schematically this marked difference in behavior. The obvious consequence of this difference in behavior is that ΣE_ℓ for a cold rolled steel specimen is remarkably lower than ΣE_ℓ for a hot rolled specimen. The general trend of the emission on unloading for a cold rolled steel specimen is very similar to that of the hot rolled steel specimen. Figure 3.5 shows the emission behavior of the cold rolled steel specimens used during these tests.

2. Changes in the Emission Behavior that Result From Repeated Loading.

When a hot rolled specimen prestressed above the S_{y_u} is reloaded to the same value of S_{max} the emission pattern changes from o a b c d e to o c' d' e (Figure 3.4). In other words the high frequency emission between points a and b is absent. The unload emission is still present and c' e' resembles c e . The hot rolled virgin specimen stressed such that $S_{max} > S_{y_u}$, on reload behaved in a very similar way to a virgin cold rolled specimen if the previous value of S_{max} was not exceeded on reload. The cold rolled specimens did not show any marked changes in behavior when they were reloaded.

Each specimen was next reloaded for the third, fourth, fifth, etc., times. Each time the S_{max} attained was lower than that attained previously. Figure 3.6(a) shows the results obtained on a 1020 hot

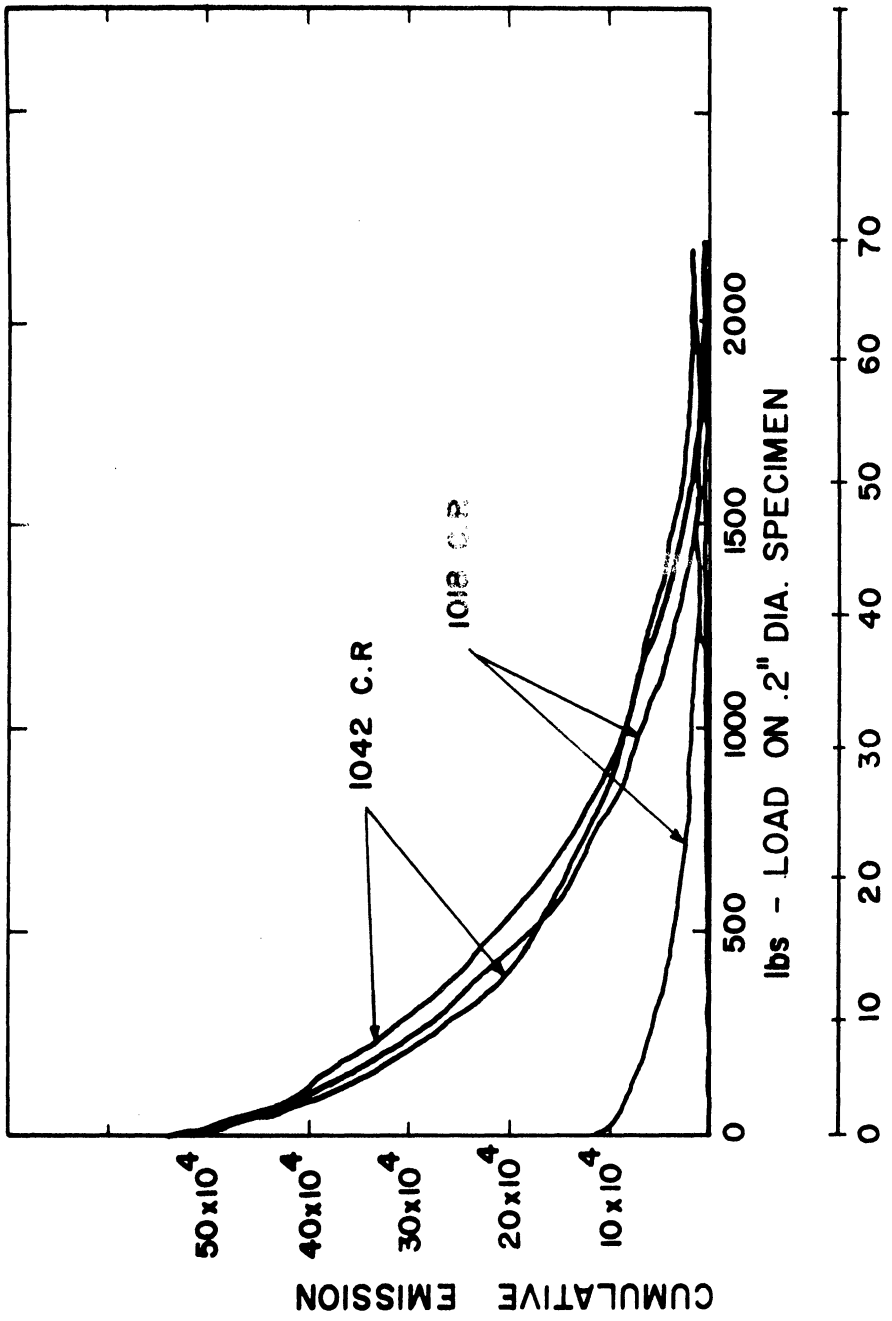

Figure 3.5. Emission Behavior of Virgin Cold Rolled Steels (x-y Recorder Output)

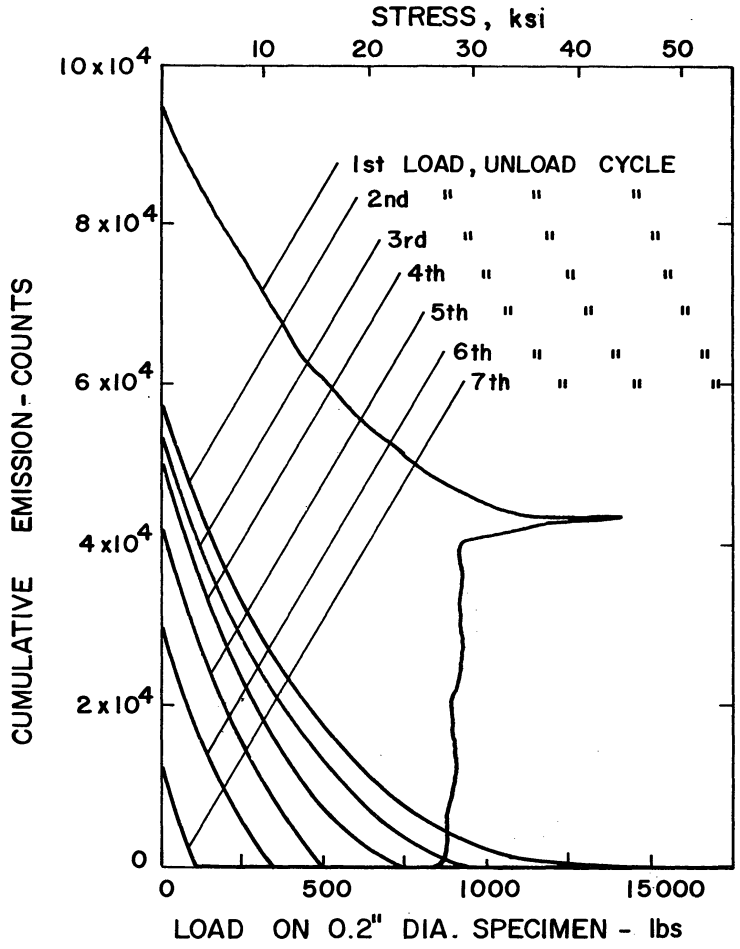

(a) x-y Recorder Output

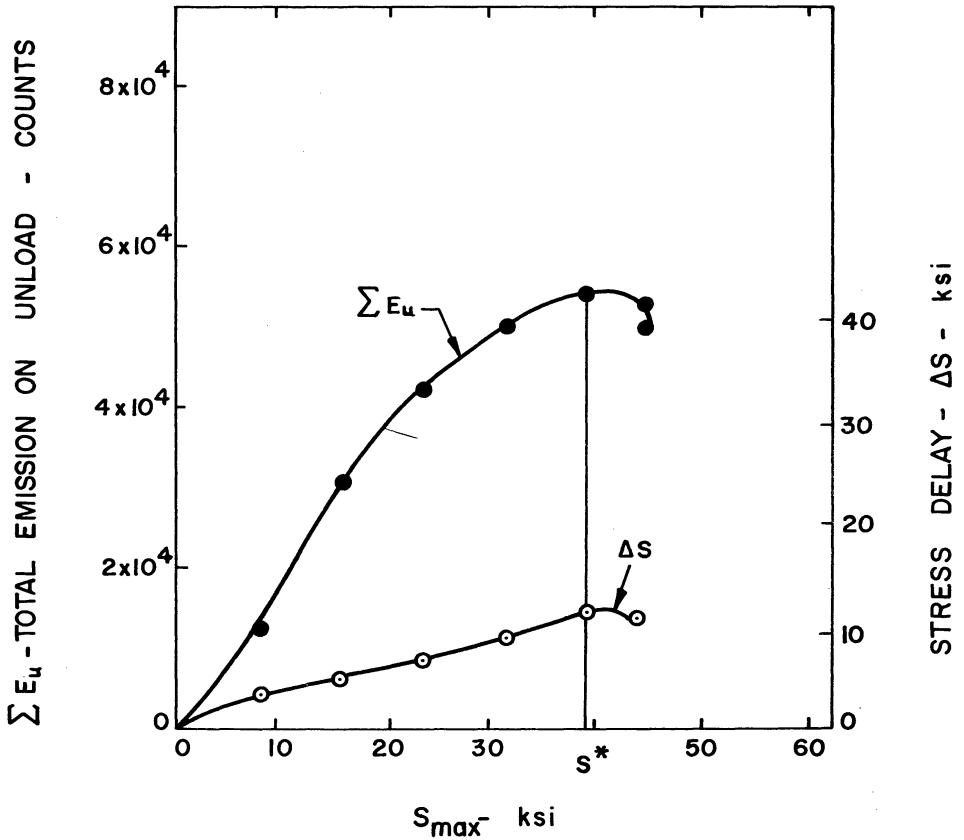

(b) Dependence of ΔS and ΣE_u on S_{max}

Figure 3.6. Acoustic Emission Behavior Shown by 1020 Hot Rolled Steel When Subjected to Repeated Loading

rolled steel specimen that was loaded consecutively to maximum stresses of 46.2, 46.2, 39.8, 31.8, 23.8, 17.5, and 8.7 ksi. Such a load pattern will be called a decreasing load pattern. The first observation that can be made from the set of curves in Figure 3.6(a) is that all the load-unload curves follow the same general trend. The second observation is that the stress delay ΔS and the total emission on unload ΣE_u, depend on the value of S_{max}. Figure 3.6(b) shows a plot of S_{max} versus ΣE_u and ΔS and a definite relationship is observed between these three variables. When the logarithm of S_{max} was plotted against ΣE_u the relation shown in Figure 3.7(a) was obtained. This relation will be called the unload emission characteristic. This relationship was found to be typical of all materials tested and the unload emission characteristics for all the virgin specimens are shown in Figure 3.7(b). Each curve always reached a single maximum at a stress value denoted by S^*. The part of the curve below S^* was very nearly a straight line while at $S_{max} > S^*$, ΣE_u dropped quite rapidly. It was also noted that below S^* the unload emission pattern did not change with the repetition of loading. In fact for each $S_{max} < S^*$ the value of ΣE_u obtained did not fluctuate more than 5% from one loading cycle to another. On the other hand for $S_{max} > S^*$ the value of ΣE_u obtained had a tendency to increase slightly with each successive load cycle until a saturation value was reached. This is shown in Figure 3.8 by plotting the values of ΣE_u obtained from a 1045 hot rolled steel specimen,

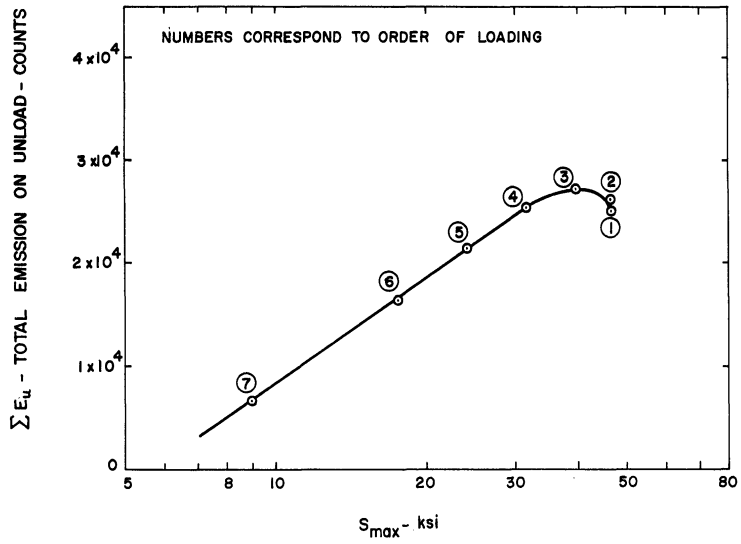

(a) 1020 Hot Rolled Virgin Specimen When Subjected to Repeated Loading

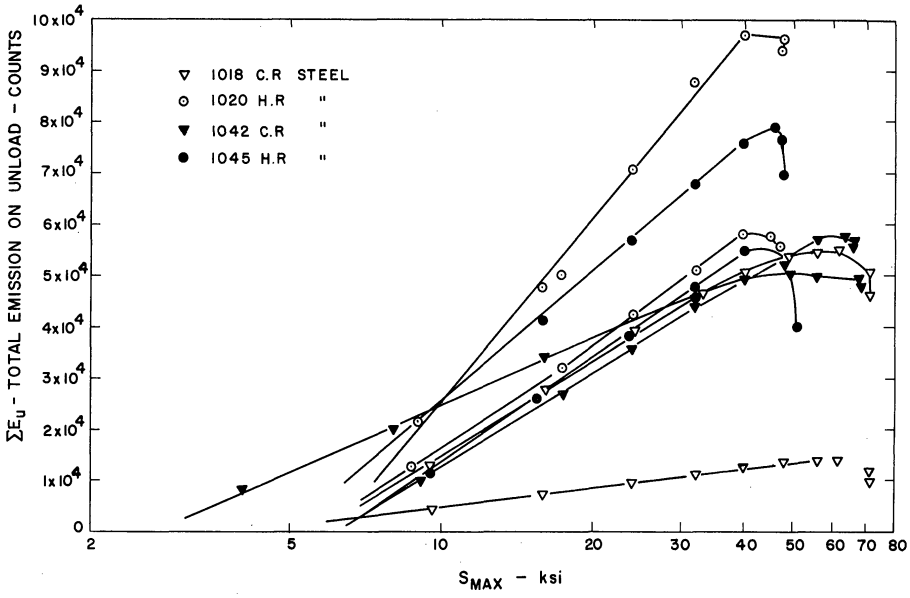

(b) All the Virgin Specimens Tested Under Repeated Loading

Figure 3.7. Unload Emission Characteristics with Decreasing Load Pattern

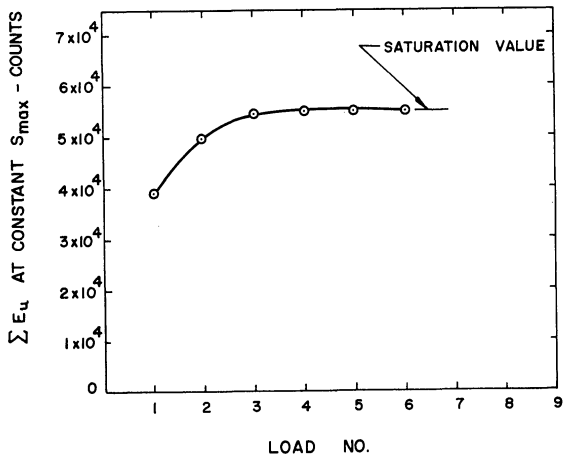

Figure 3.8. Effect of Repeated Loading Above S* on ΣE_u for a 1045 Hot Rolled Steel Specimen

which was loaded to $S_{max} > S^*$. It should be borne in mind that all the observations discussed in this part hold only for unload emission characteristics obtained with a decreasing load pattern. The emission behavior during the loading part of each cycle did not show a consistent pattern on repeated loading.

3. Effect of Strain Rate on Load and Unload Emission

In order to find the effect of strain rate on the acoustic emission, a steel specimen (1045 hot rolled) was subjected to an uninterrupted load and unload cycle while making sure that $S_{max} < S^*$. The stress versus cumulative emission curve from this test is shown in Figure 3.9(b). Next the specimen was reloaded to the same value of S_{max} and then unloaded. But this time the unload was interrupted at points a, b, and c as shown on the Visicorder record in Figure 3.9(a). The x-y plot of this interrupted unload behavior is shown in Figure 3.9(b) and the outcome apparently does not deviate much from the previous one obtained from uninterrupted unloading. The only deviation occurred near b and c where the strain rate was too low. The interruption at a had no apparent effect on the stress delay ΔS . This experiment clearly demonstrated that the unload emission behavior is strain rate dependent. Figure 3.9(a) also demonstrates that the unload emission is not only a function of the load but it also increases with the strain rate. Experiments in which the loading was interrupted were also conducted and it was found that even the emission behavior on loading was strain rate dependent- an observation

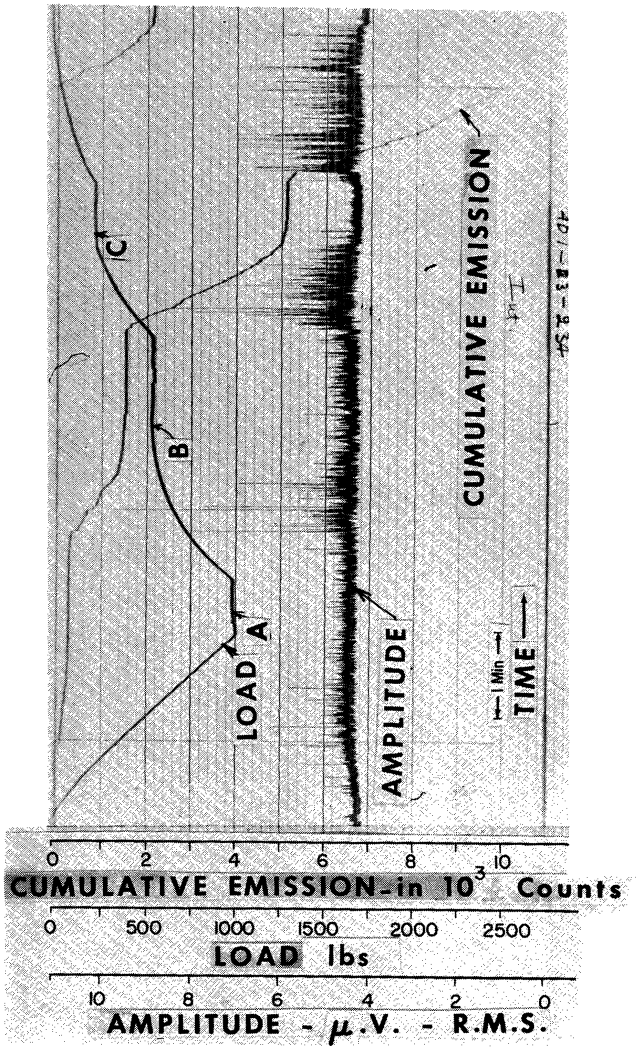

(a) Visicorder Output

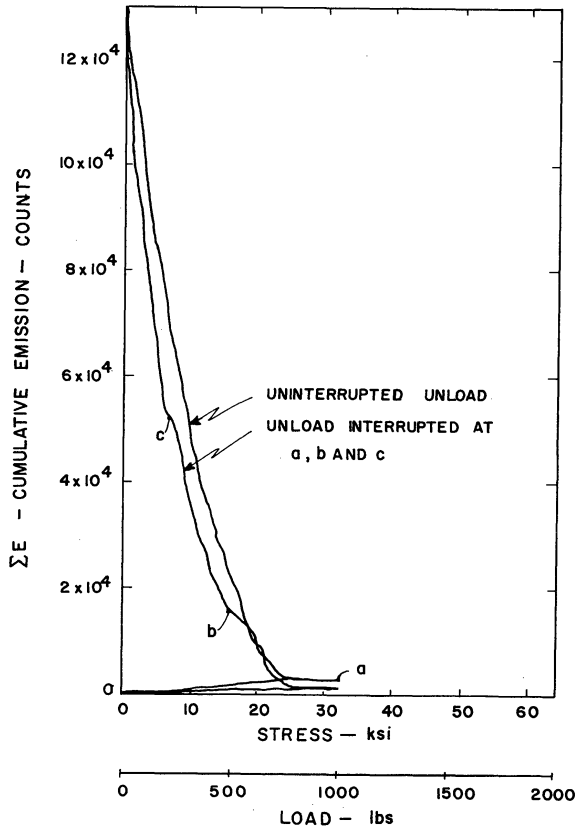

(b) x-y Recorder Output

Figure 3.9. Effect of Interruption on Unload Emission Behavior of 1045 Hot Rolled Steel.

verified by Schofield in the case of single crystals of aluminum[110].

4. Effect of the Load Pattern on the Unload Emission Characteristic

The curve obtained in Figure 3.7 is called the unload emission characteristic. This curve was obtained by loading the specimen to a value of $S_{max} = S_1$ (Figure 3.1) and then consecutively lowering the S_{max} for each following cycle as explained in Figure 3.7(a). This type of load pattern, which is called a decreasing load pattern, gives rise to the question, "What effect does the load pattern have on the unload emission characteristic?" In order to answer this question a virgin 1045 hot rolled steel specimen was loaded repeatedly eight times (1 through 8) in such a manner that the S_{max} was increasing from one cycle to the next. The same specimen was then loaded for seven more times but this time the S_{max} was decreased from one cycle to the next (Figure 3.10). The S_{max} was plotted versus $\sum E_u$ and the results are shown in Figure 3.10. Figure 3.10 indicates that the unload emission characteristic of a virgin hot rolled steel specimen changed by less than 20% when two different loading patterns were followed on the same specimen in this sequence. During this series of loads and unloads this specimen had undergone a permanent elongation of 0.8%. This specimen was allowed to age for 326 hours at room temperature and a series of loads and unloads was performed on it using the same two load patterns as before. Figure 3.11 shows the results in the same way as in Figure 3.10; the numbers on each point indicate the order of loading. From load cycles

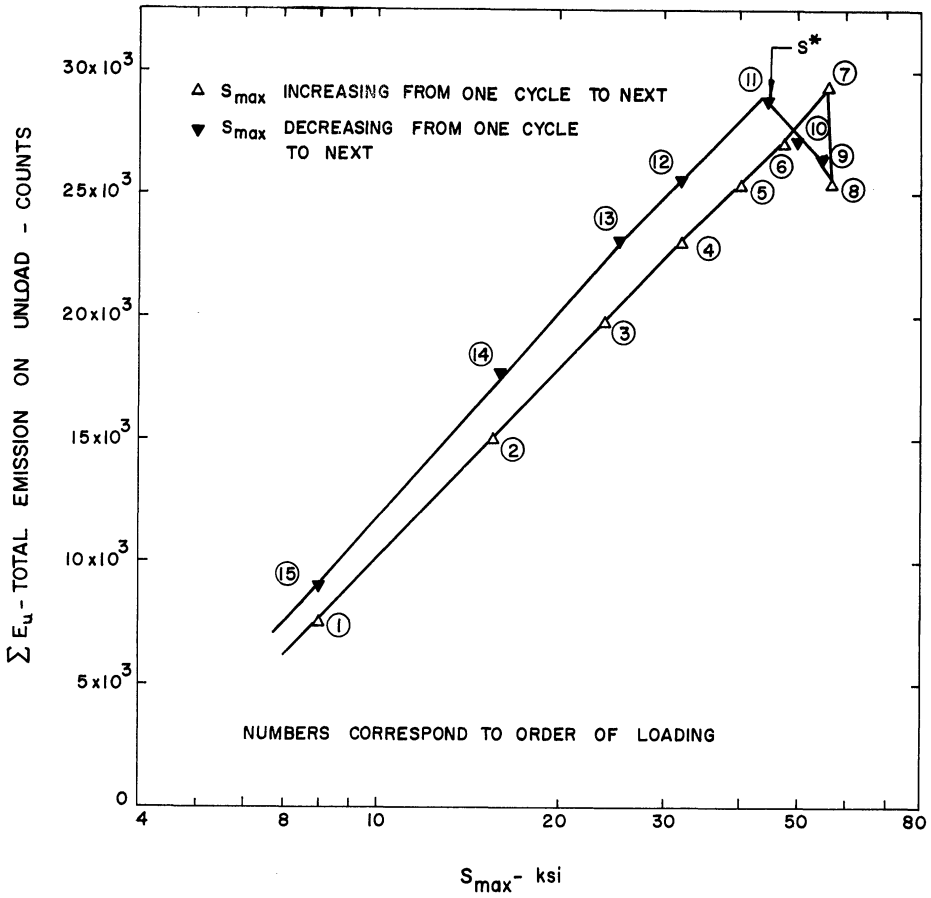

Figure 3.10. Unload Emission Characteristics Obtained Using Two Patterns of Loading on a Virgin 1045 Hot Rolled Steel Specimen

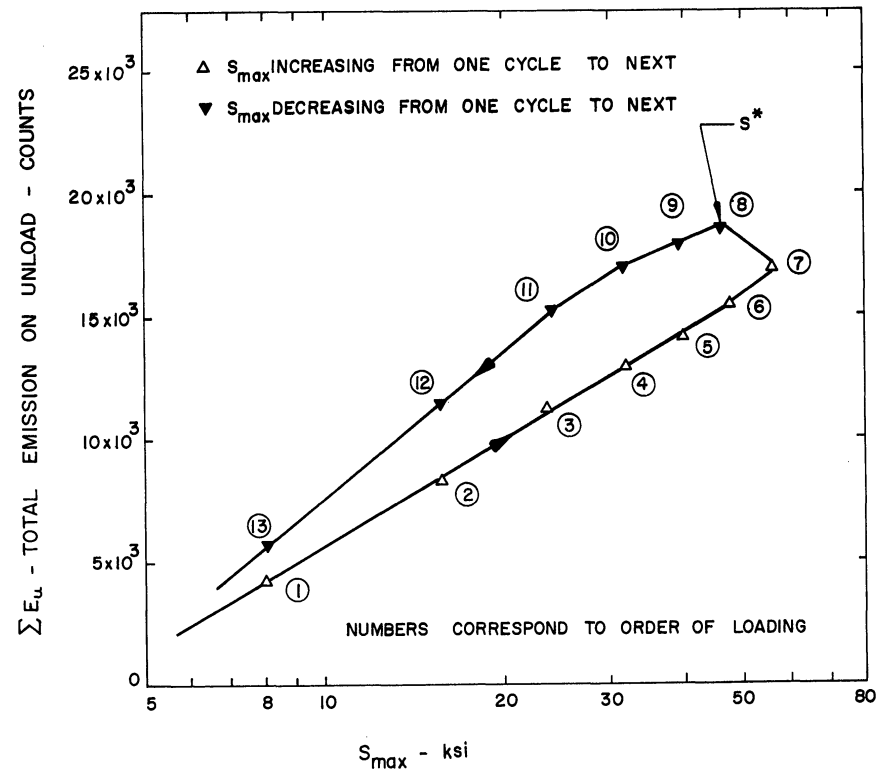

Figure 3.11. Unload Emission Characteristics Obtained Using Two Patterns of Loading. 1045 Hot Rolled Steel after 0.8% Elongation and 326 Hours of Aging at Room Temperature

(1) through (7) the S_{max} was increased on each consecutive cycle. From cycles (8) through (13) S_{max} was decreasing. The total emission on unloading was higher when the S_{max} was decreasing from one cycle to the next. The interesting feature to note here is that in Figures 3.10 and 3.11 there is a stress S* at which emission was highest (using a decreasing load pattern) and this stress is very nearly the same in both cases for a decreasing load pattern.

The material (1045 hot rolled steel) undergoes substantial plastic deformation during the eighth reload (Figure 3.10). It will be observed that a corresponding departure from a straightline relationship between ΣE_u and S_{max} takes place at that point.

5. The Kaiser effect

After conducting his series of tests Kaiser concluded that when a specimen previously stressed to a certain prestress is restressed the emission does not reappear until that prestress is exceeded. This effect has been called the "Kaiser Effect." Kaiser indicated that this effect could be used to detect the amount of prestress in a part. In order to check the validity of this effect a 1045 H.R. steel specimen was consecutively stressed to seven increasingly higher levels of stress and the cumulative emission was recorded during the reapplication of the stress.

The results of these tests are shown in Figure 3.12. It can be readily seen that the Kaiser effect does not occur from loads nos. (1) through (6). At load (7) the specimen went through the upper

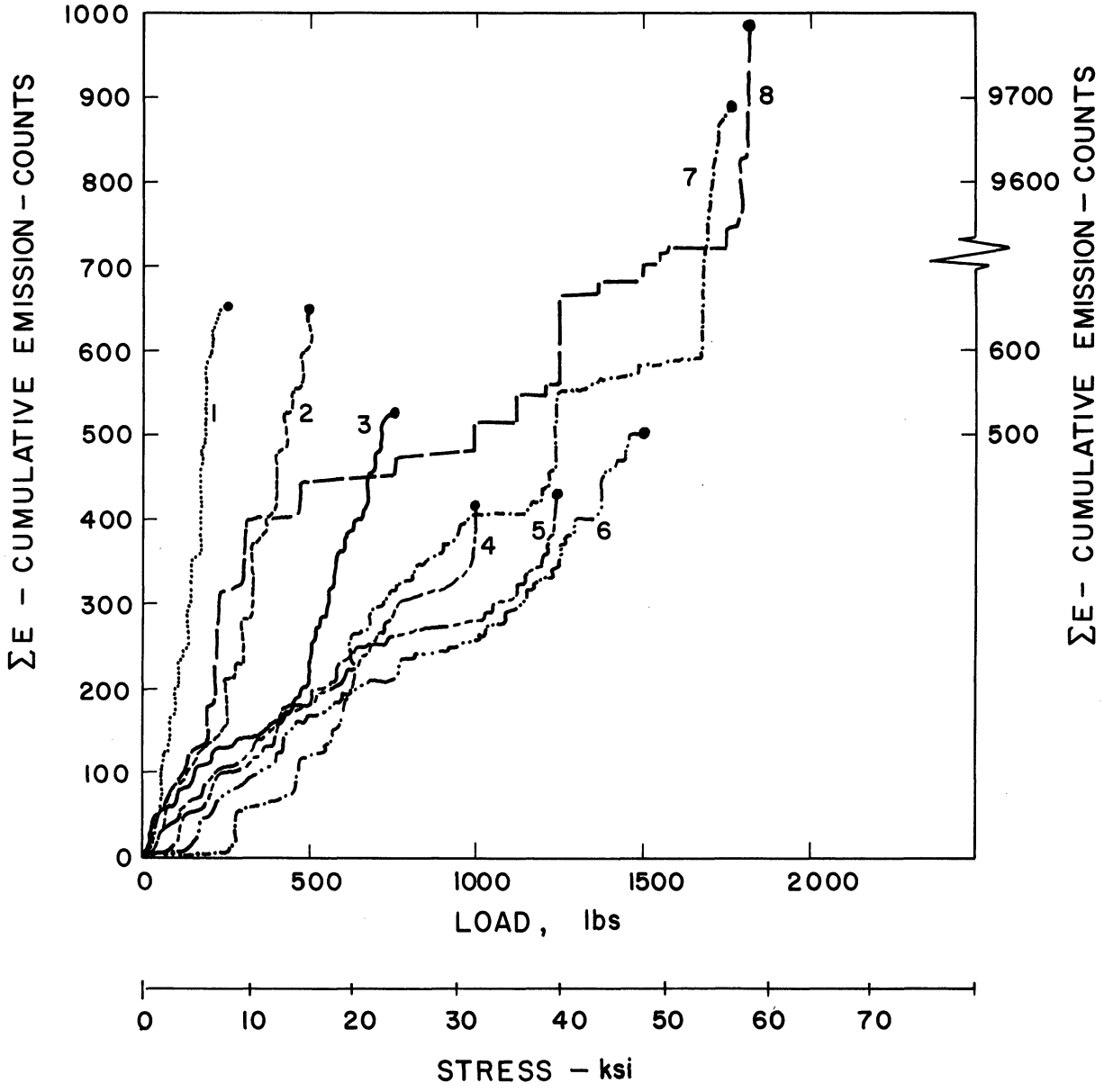

Figure 3.12. Absence of Kaiser Effect in 10[1]5 Hot Rolled Steel Virgin Specimen

yield point (at 1675 lb) giving rise to an increased rate of emission. This emission began to diminish after the load reached 1725 lb. At 1775 lb the load was released and the specimen was reloaded for the eighth time (load No. 8). During the eighth load the emission followed a generally increasing path until a load of 1775 lb was reached. Beyond this load a very abrupt increase in emission was observed and the oscilloscope revealed that the high frequency emission which had stopped during the previous loading had started once again. An explanation of this will be given in Section IV. At present it can be said that the Kaiser effect is not a universal effect occurring at all stress levels.

6. Effect of Strain Aging at Room Temperature on the Acoustic Emission

In Section III A. 2. it was observed that whenever an unload emission characteristic was obtained using a decreasing load pattern the ΣE_u was constant for a given $S_{max} < S^*$. It was also noted for a given material at a given time that two unload emission characteristics obtained using a decreasing load pattern were identical for $S_{max} < S^*$. Yet it was found that for the same material the ΣE_u for a given $S_{max} < S^*$ was not a constant over a long and extended period of time. A 1045 hot rolled specimen was subjected to a series of loads and unloads and an unload emission characteristic using a decreasing load pattern was obtained. This characteristic showed that at an S_{max} of 31.8 ksi the ΣE_u appeared to be quite stable when the specimen was reloaded instantly to the S_{max} of 31.8 ksi.

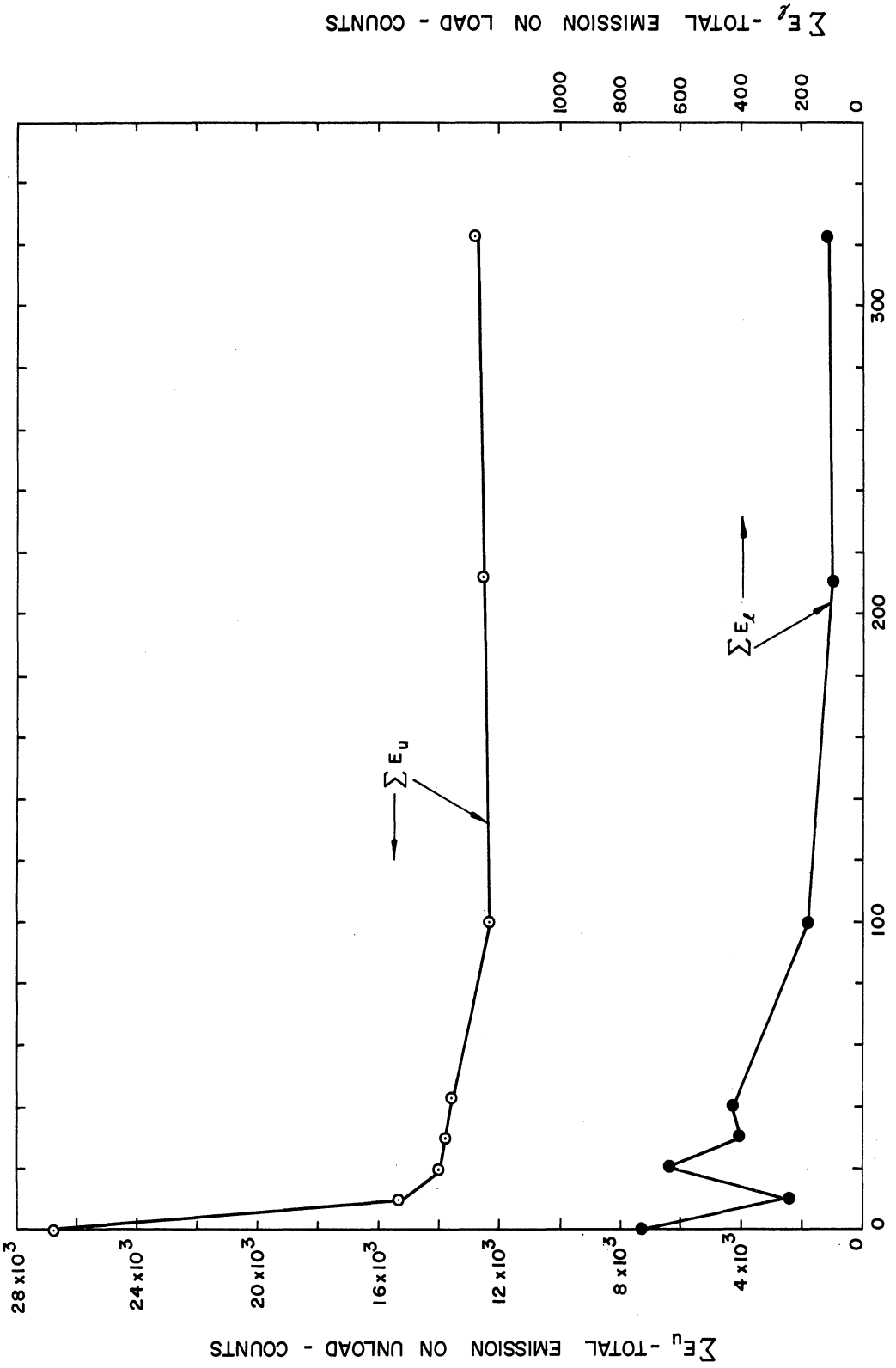

Figure 3.13. Effect of Strain Aging at Room Temperature on ΣE_u and ΣE_ℓ in 1045 Hot Rolled Steel.

This specimen was left undisturbed in the grips and reloaded to S_{max} of 31.8 ksi after periods of rest.

Figure 3.13 shows the values ΣE_u and ΣE_ℓ obtained when the specimen was reloaded to the S_{max} of 31.8 ksi after varying lengths of time. It was observed that ΣE_u dropped to about 50% of the value obtained for a virgin specimen within the first 30 hours. After 100 hours there was no further significant change in the value of ΣE_u .

7. Effect of Fatigue on Emission

Each of the specimens being investigated in the program was subjected to extensive acoustic tests in its virgin state and after every 10^3, 10^4, 10^5, and 10^6 cycles of fatigue loading. The results are as follows.

(a) Emission During Loading

The following three observations of the emission behavior on loading were made as the specimens were progressively fatigued:

(i) The high frequency emission phenomenon observed in the hot rolled virgin specimens did not appear in the specimens that had been fatigued.

(ii) The total emission on load (ΣE_ℓ) decreased at first during fatigue and then increased again after reaching a minimum value in the region of 10^4 or 10^5 cycles. After 10^6 cycles of stress

ΣE_ℓ reached a maximum in case of those specimens which were fatigued above the S_e . There was also an increase in ΣE_ℓ in the case of those specimens which were stressed below S_e for 10^6 cycles, but this increase was not as pronounced as in the previous case. This is shown in Figure 3.14(a).

(iii) The amplitude of the emitted bursts also seemed to follow a pattern similar to that of the ΣE_ℓ. Figure 3.14(b) shows Visicorder chart recordings of the amplitude of emission obtained for two 1020 cold rolled steel specimens stressed in their virgin state and after 10^4 and 10^6 cycles of fatigue. It can be seen that the emission amplitude observed after 10^6 cycles of stress was much higher than that observed after 10^4 cycles of stress. The amplitude of emission from the specimen fatigued for 10^6 cycles above $S_{e_{max}}$ was much higher than that of the specimen fatigued below $S_{e_{min}}$.

(b) Emission during unloading.

Figure 3.15 shows the unload emission characteristics observed using a decreasing load pattern at five different stages in the fatigue life of a 1042 cold rolled steel specimen. From this figure the following observations can be made:

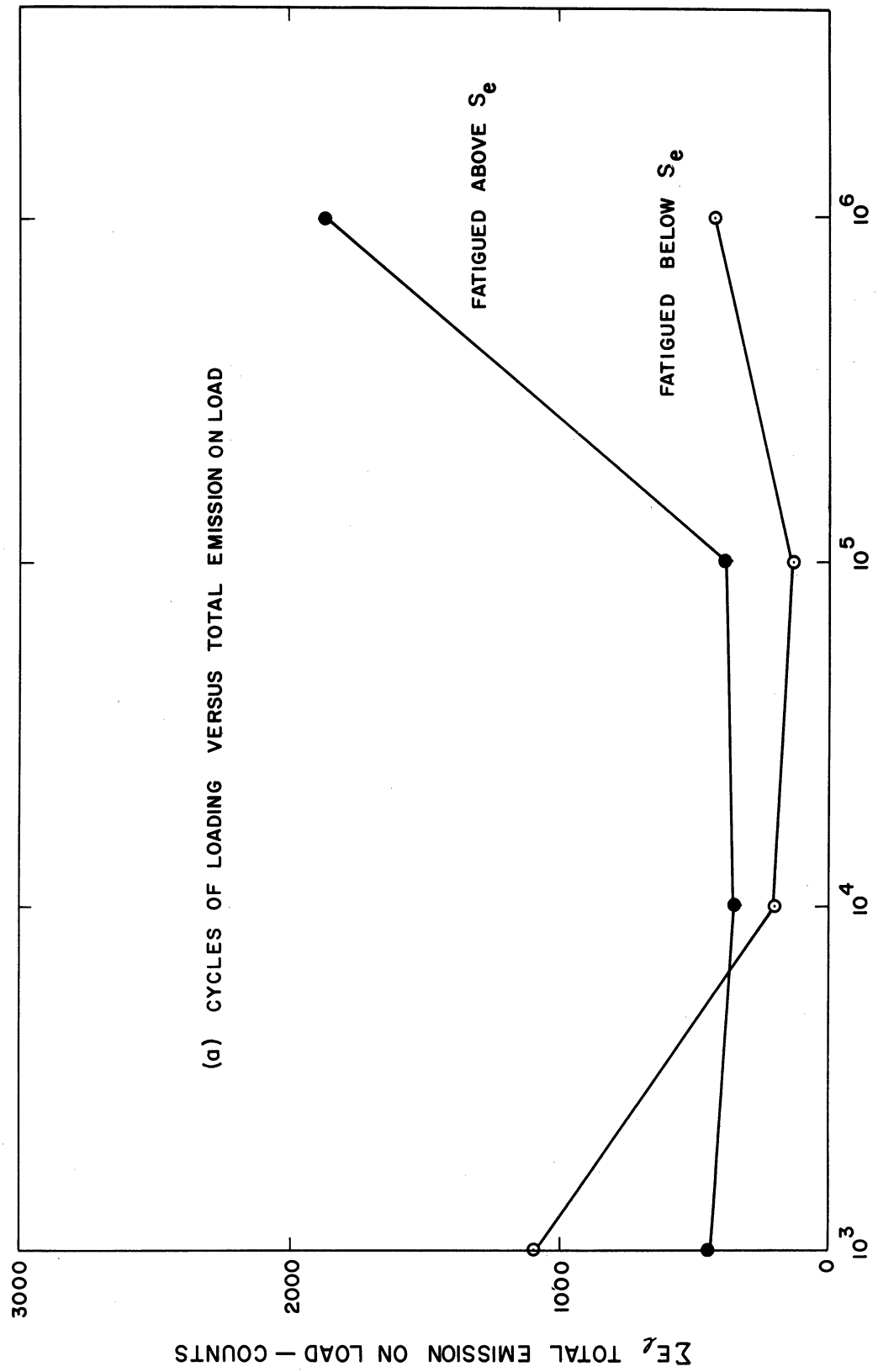

(a) Cycles of Loading Versus Total Emission on Load

Figure 3.14. Effect of Fatigue on the Acoustic Emission Obtained on Loading a 1018 Cold Rolled Steel

1018 C.R. Specimen Fatigued Above $S_{e_{max}}$

After 1st Cycle of Loading

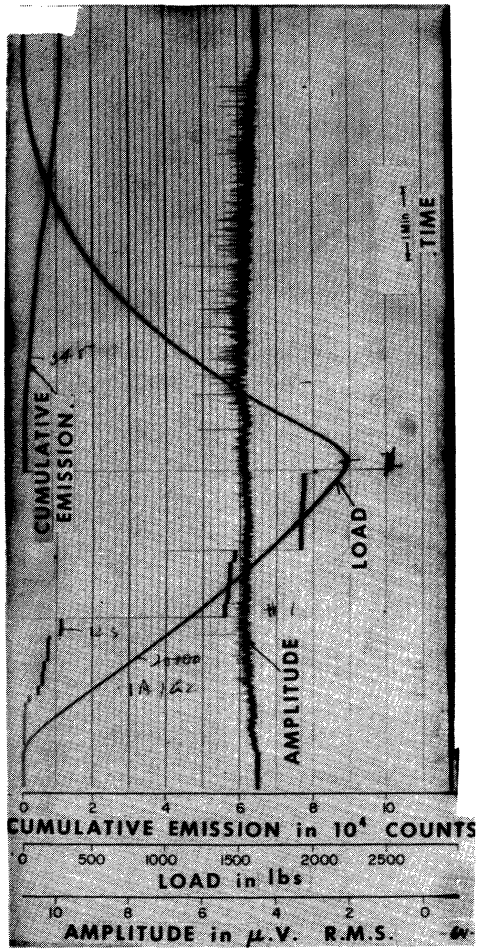

After 10^4 Cycle of Loading

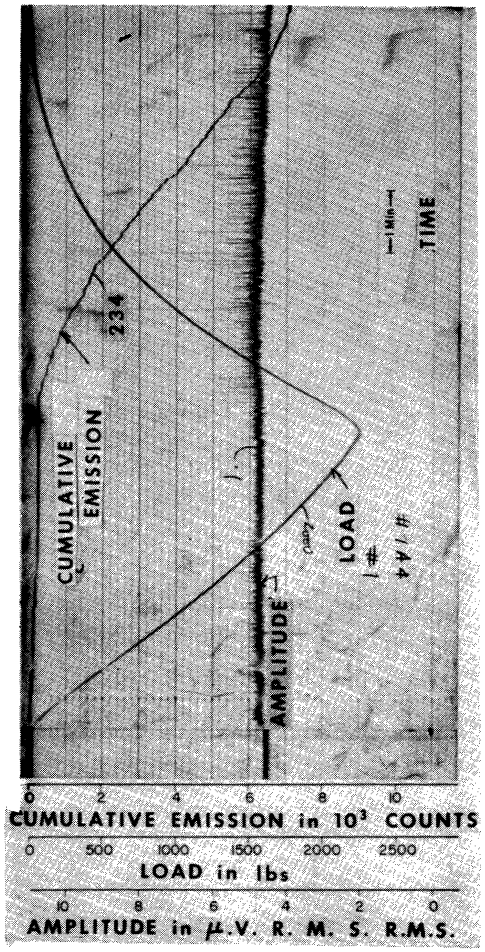

After 10^6 Cycles of Loading

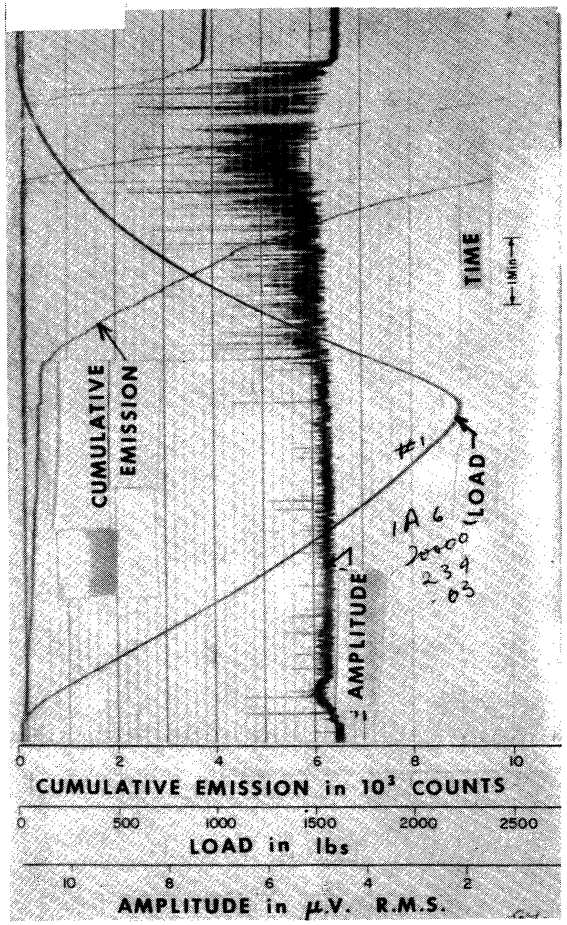

Figure 3.14 (Continued). (b) Visicorder Charts Showing Emission Amplitudes after 1, 10^4, and 10^6

1018 C.R. Specimen Fatigued Below $S_{e_{min}}$

After 1st Cycle of Loading

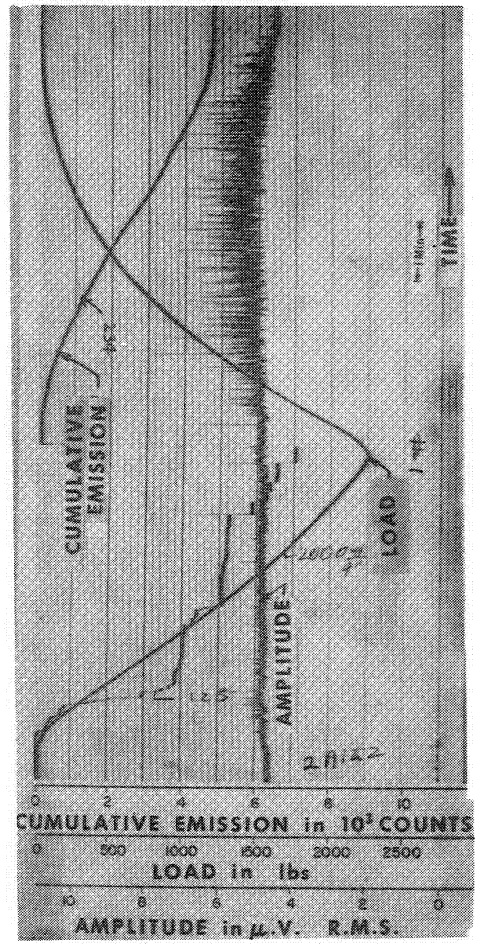

After 10^4 Cycles of Loading

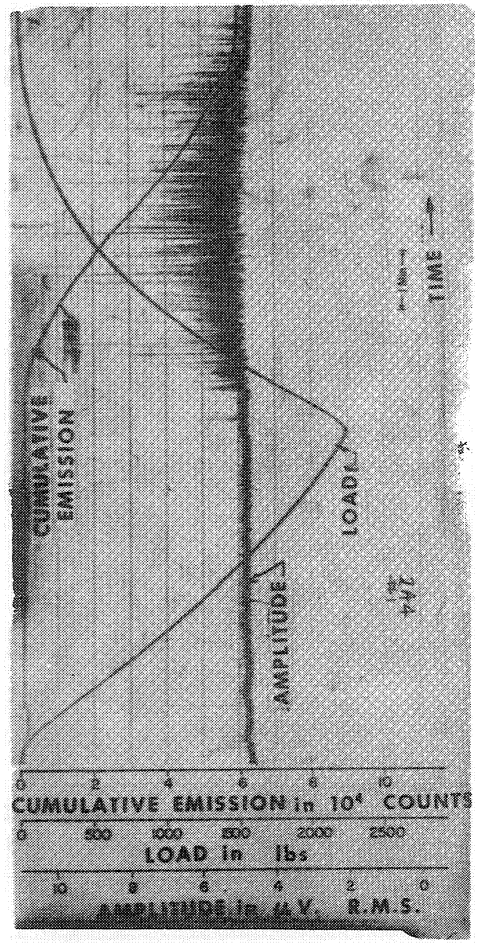

After 10^6 Cycles of Loading

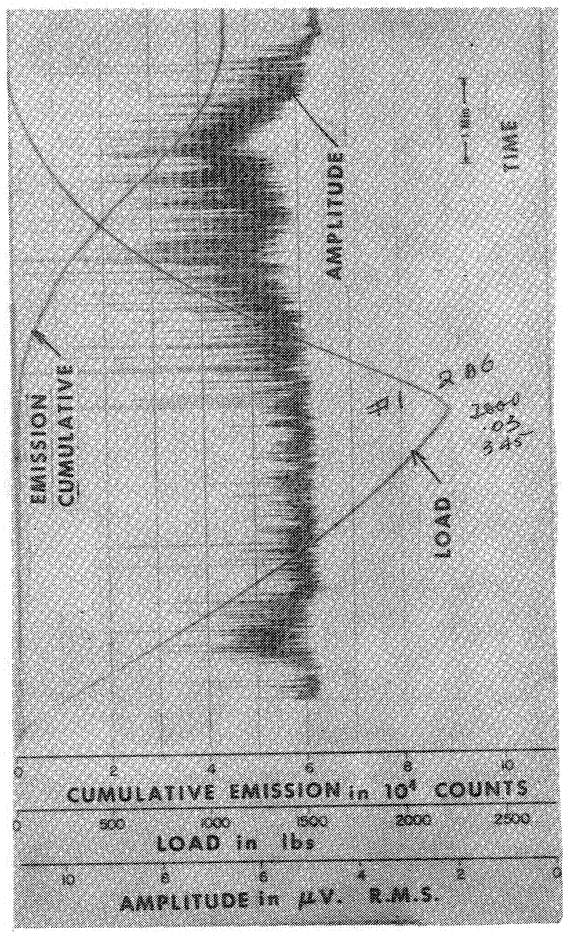

Figure 3.14 (Continued). (b)(Continued)

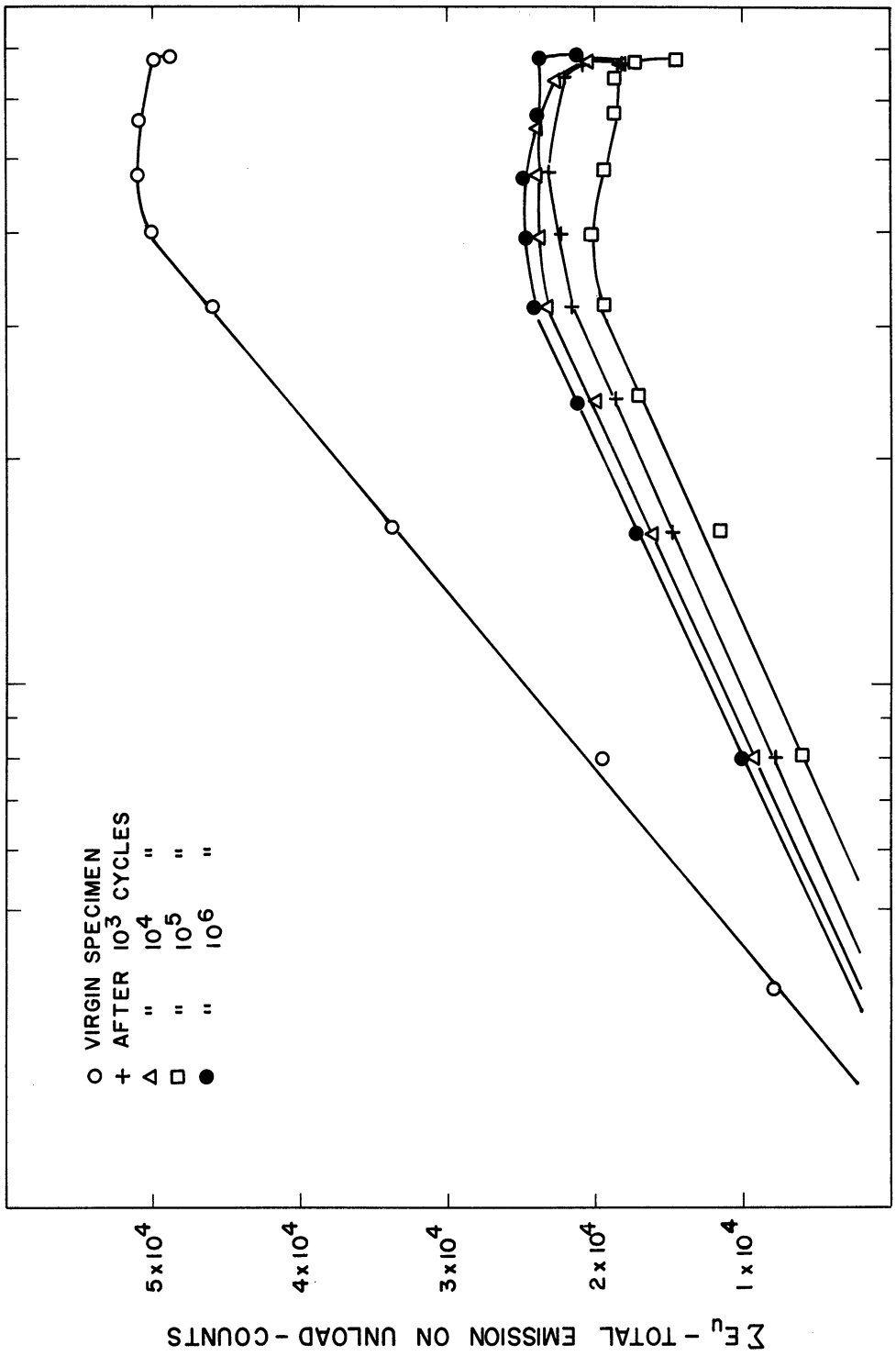

Figure 3.15. Effect of Fatigue on Unload Emission in 10 2 Cold Rolled Steel (Decreasing Load Pattern)

(i) The unload emission ΣE_u for a virgin specimen is about twice as high as the emission obtained after it has been fatigued.

(ii) The maximum required stress for peak emission on unload S^*, does not change appreciably as the specimen is fatigued.

(iii) The general pattern of the unload emission characteristic is unchanged even after 10^6 cycles of fatigue.

B. Surface Observations

1. Virgin Specimens

At the outset it was decided to observe progressively the behavior of the surface of all the specimens as they were undergoing fatigue. In order to make any meaningful observations it was further decided to electropolish the surface using the technique discussed in Section II A. 2. The electrolyte used was a mixture of chromium trioxide, water, and acetic acid. After trying various other electrolytes such as a mixture of sulphuric acid and orthophosphoric acid, or a mixture of nitric acid and acetic anhydride at different current densities, it was found that the chromic-acetic acid electrolyte used gave the best polish on the surface of the specimens.

The steels used were of the commercial quality and contained inclusions in the form of elongated stringers of non-ferrous material. These inclusions were removed preferentially during the electropolishing process and hence shallow and polished elongated craters were left

behind. These craters were always oriented parallel to the axis of the specimen. Their widths varied between 0.001 and 0.003 inches, and their lengths varied from 0.003 to 0.1 inches. Figure 3.16 shows the elongated craters on the surface of a virgin specimen of 1018 cold rolled steel at a magnification of 330x

2. After the First Load Cycle

All the specimens were first loaded in the acoustic test machine (Figure 2.5) to a stress S_1 as described in Section III A. 1. During this loading all the 1020 hot rolled steel specimens exhibited the formation of primary slip lines on the shank part of the specimen. This change manifested itself between the upper and lower yield points. The electron micrographs in Figure 3.1 7(a) through 3.17(e) show the various aspects of these primary slip lines. The spacing of these slip lines was about 0.5×10^{-3} to 1.2×10^{-3} inches yet they were quite wavy in their appearance. When these lines were observed at higher magnification they were not precisely step-like in nature but were more like ripples on the surface (Figure 3.17 (a)). The slip lines in one grain were not parallel to those in other grains. Even in a single grain these slip lines were never exactly colinear or parallel. On the contrary they followed no general contour. Their spacings generally grew more dense near the grain boundaries (Figure 3.17(b)). These 1020 hot rolled steel specimens were stressed beyond the upper and lower yield points and the loading was continued well into the strain hardening region as observed from the load versus time curve,

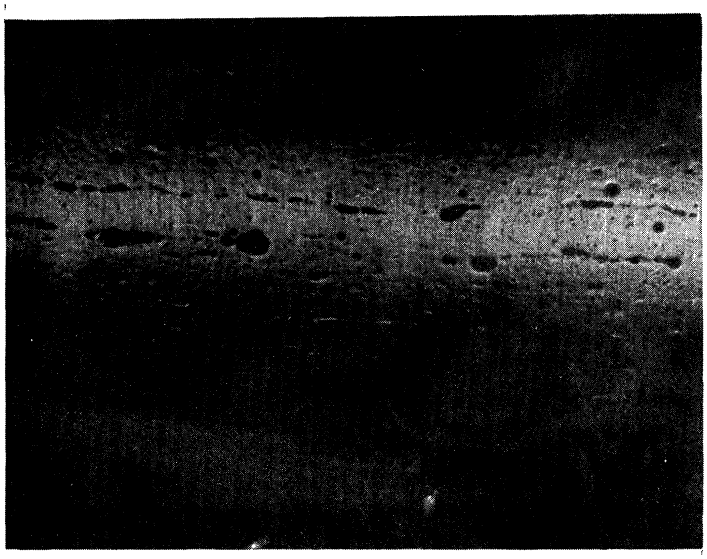

Figure 3.16. Typical Craters Left by Inclusions. Light Micrographs at 330x. Virgin 1020 Cold Rolled Steel.

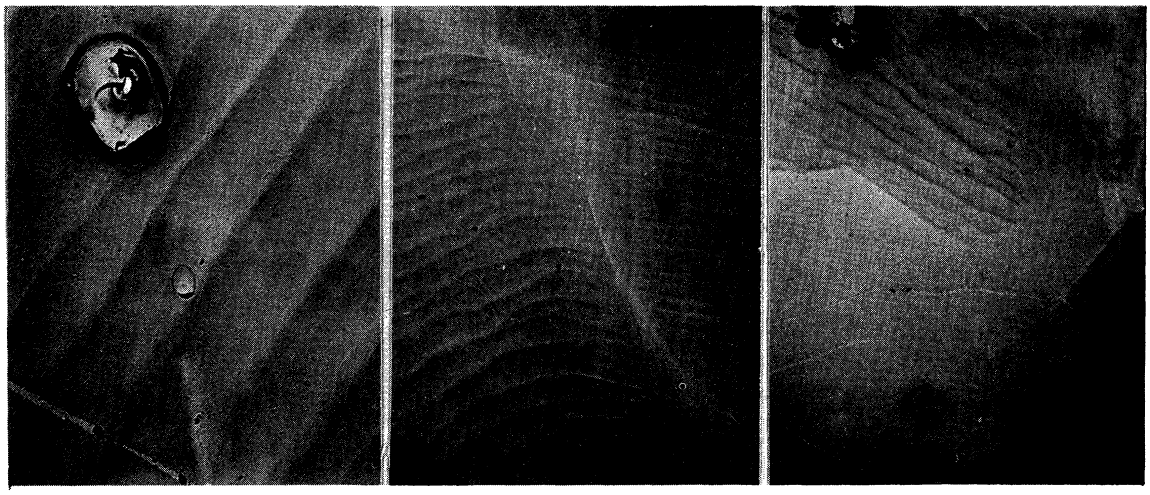

(a) Primary Slip in the Center of the grain 5000X

(b) Primary Slip Near Grain Boundary 1400X

(c) Grains With and Without Primary Slip 1400X

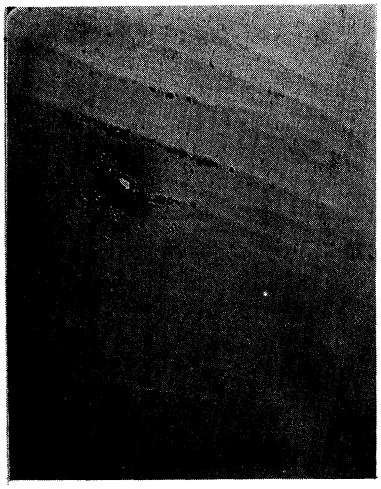

(d) Duplex Slip 2100X

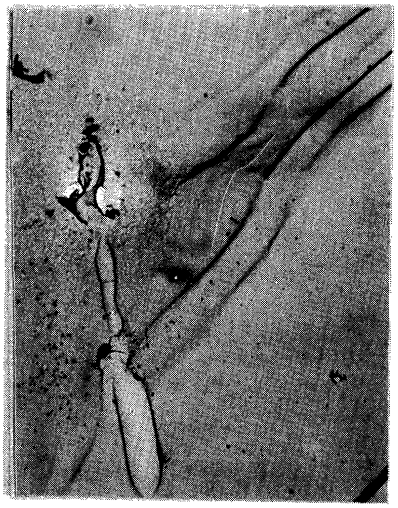

(e) Primary Slip lines in the Vicinity of an Inclusion Crater 2900X

Figure 3.17. Primary Slip Lines in 1020 Hot Rolled Steel Virgin Specimen Electron Micrographs of Replicas.

Figure 3.18. Yet it was observed that all of the pearlite grains and some of the ferrite grains did not show any semblance of primary slip even when their neighbors did (Figure 3.17(c)). Figure 3.17(d) shows the existence of duplex slip which occurred during this upper and lower yield point region. Duplex slip[121] was not as predominant as the single slip mentioned above.

The inclusion craters had a marked effect on primary slip lines and they seemed to be able to disrupt the smooth contour of these lines to a great extent (Figure 3.17(e)).

The 1045 hot rolled steel specimens did not exhibit any detectable surface change (in the form of primary slip lines) at all during the first load cycle, even when undergoing the upper and lower yield point phenomenon.

The cold rolled 1018 and 1042 steel specimens exhibited no change in their surface when they were loaded up to a stress S_1 given in Table 3.1.

None of the specimens showed any sign of necking when subjected to loads up to S_1. In order to determine the acoustic and surface behavior during the necking period, a cold rolled 1042 steel specimen was subjected to loading beyond S_1 until very substantial necking took place (this specimen was prepared and used exclusively for this test only). It was noted that in the necked region slip lines were formed. These slip lines occurred in ferrite as well as in pearlite grains and were very step-like and abrupt in appearance as can be seen in Figure 3.19 which shows electron micrographs of a replica made of the surface in the center of the necked region.

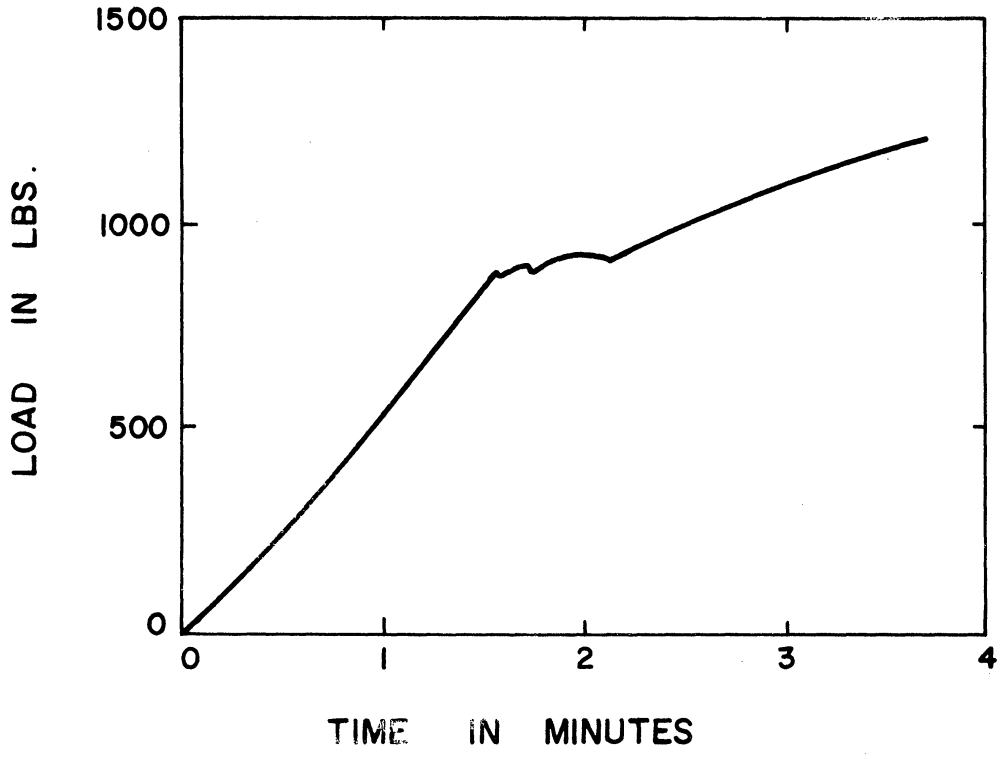

Figure 3.18. Curve Showing the Upper and Lower Yield Points Obtained on the Acoustic Test Machine

(a) Slip lines in neighboring Ferrite and Pearlite grains 4400X

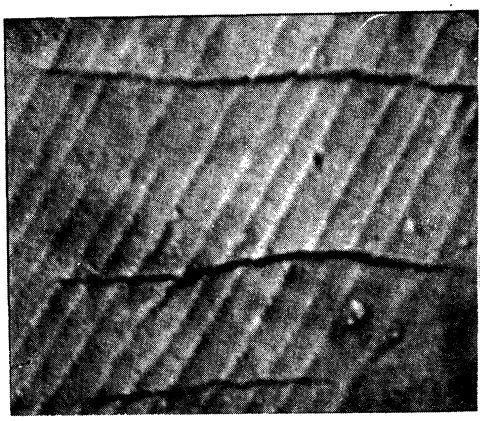

(b) Slip lines in Pearlite - 16000X

Figure 3.19. Slip Lines Appearing on the Surface in the Necked Region of a 1042 Cold Rolled Steel Electron Micrographs of replicas

3. After Cyclic Loading Below the Fatigue Limit

The surfaces of the four specimens 1018 cold rolled, 1020 hot rolled, 1042 cold rolled, and 1045 hot rolled which were subjected to cyclic loading at a stress S_2 below $S_{e_{min}}$ (Figure 3.1) were examined after every 10^3, 10^4, 10^5, 10^6, and 10^7 cycles of load. It was found that no slip lines or surface changes could be observed on any of them even after using electron micrography on collodion replicas shaded at various angles (20 to 50 degrees). Even the 1020 hot rolled steel specimen that showed primary slip after the first application of a load showed no further change (Figure 3.20(d)).

Etching of the surface did reveal some structure, however. After 10^7 cycles of load, half of the shank portion of each of these specimens was etched for 10 seconds using Fry's reagent. Then both the etched and unetched portions were replicated and examined under the electron microscope.

The results showed that there were some very fine and diffuse slip lines which were revealed by the etchant in all these specimens. These slip lines were not present in all areas as can be seen in Figure 3.20(a)). The fine structure of slip lines revealed by etching is shown at two different magnifications in Figures 3.20(b) and 3.20(c). The difference between the unetched and etched parts of a 1020 hot rolled specimen is revealed in Figures 3.20(d) and 3.20(e). It can be seen that the fine slip observed after fatigue appears to have a direction which is not the same as that of the coarse primary slip.

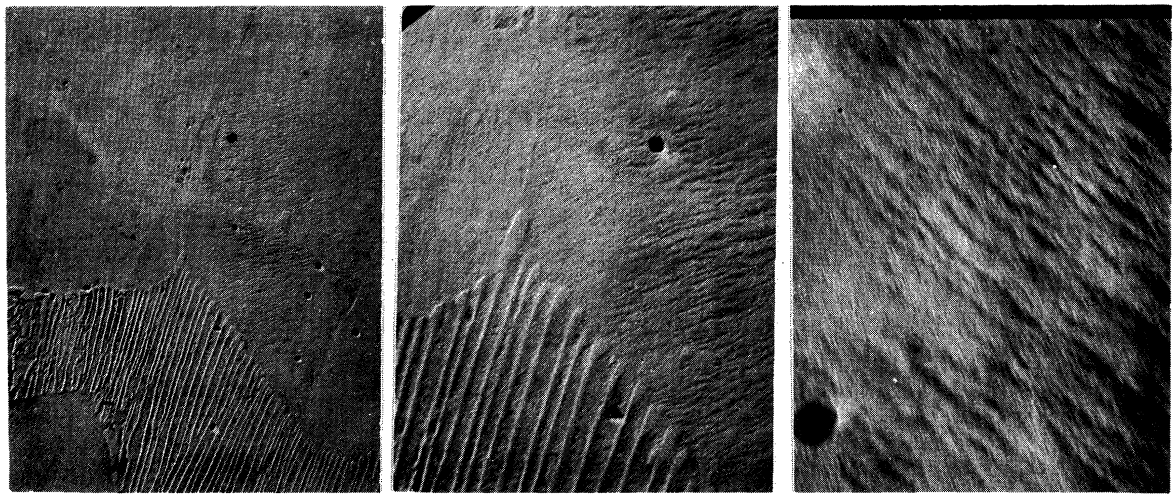

(a) 1018 Cold Rolled Steel Etched 2200X

(b) 1018 Cold Rolled Steel Etched 3600X

(c) 1018 Cold Rolled Steel Etched 18000X

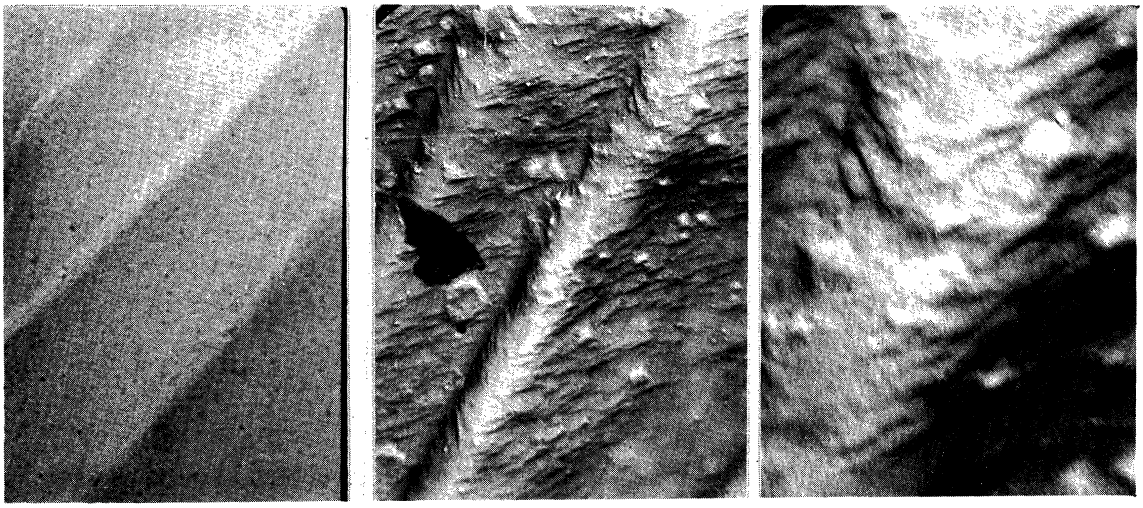

(d) 1020 Hot Rolled Steel Unetched 10000X

(e) 1020 Hot Rolled Steel Etched 10000X

(f) 1020 Hot Rolled Steel Etched 28000X

Figure 3.20. Surface Observations on Steel Specimens Fatigued Below the Fatigue Limit for 10^7 Cycles - Election Micrographs of Replicas

4. After Cyclic Loading Above the Fatigue Limit

Examination of the surface of the specimens stressed cyclically for 10^3 and 10^4 cycles showed no discernable changes in the surface. After 10^5 cycles, however, the specimens began to show slip lines localized in sharp bands in the middle of some of the grains (about one grain in fifty). These bands will be referred to as slip bands in the following discussion even though there are only very few of them. After 10^6 cycles of loading these markings increased in size, number, and intensity. There were usually two to six slip bands per grain and about one grain in every five possessed these slip bands (Figure 3.21(a)). These bands generally started at the center of a grain and progressed towards the grain boundaries. There the bands would connect with the slip bands in the neighboring grains and thus give rise to a crack as shown in Figure 3.21(b) and at a larger magnification in 3.21(c).

The fine structure of these bands was observed using high magnification light microscopy and replica techniques with electron microscopy. The results showed a region of very severe slip which also seemed to show profuse cross slip (Figures 3.22(a), 3.22(b), 3.22(c)). These bands progressed in a direction parallel to the band until they reached a grain boundary (Figure 3.22(c)) or an inclusion crater (Figure 3.22(d)). None of the slip bands observed on the surface began to appear at the grain boundaries or inclusion craters. On the contrary they first appeared in the middle of a grain and progressed towards an inclusion crater or a grain boundary. After being stopped

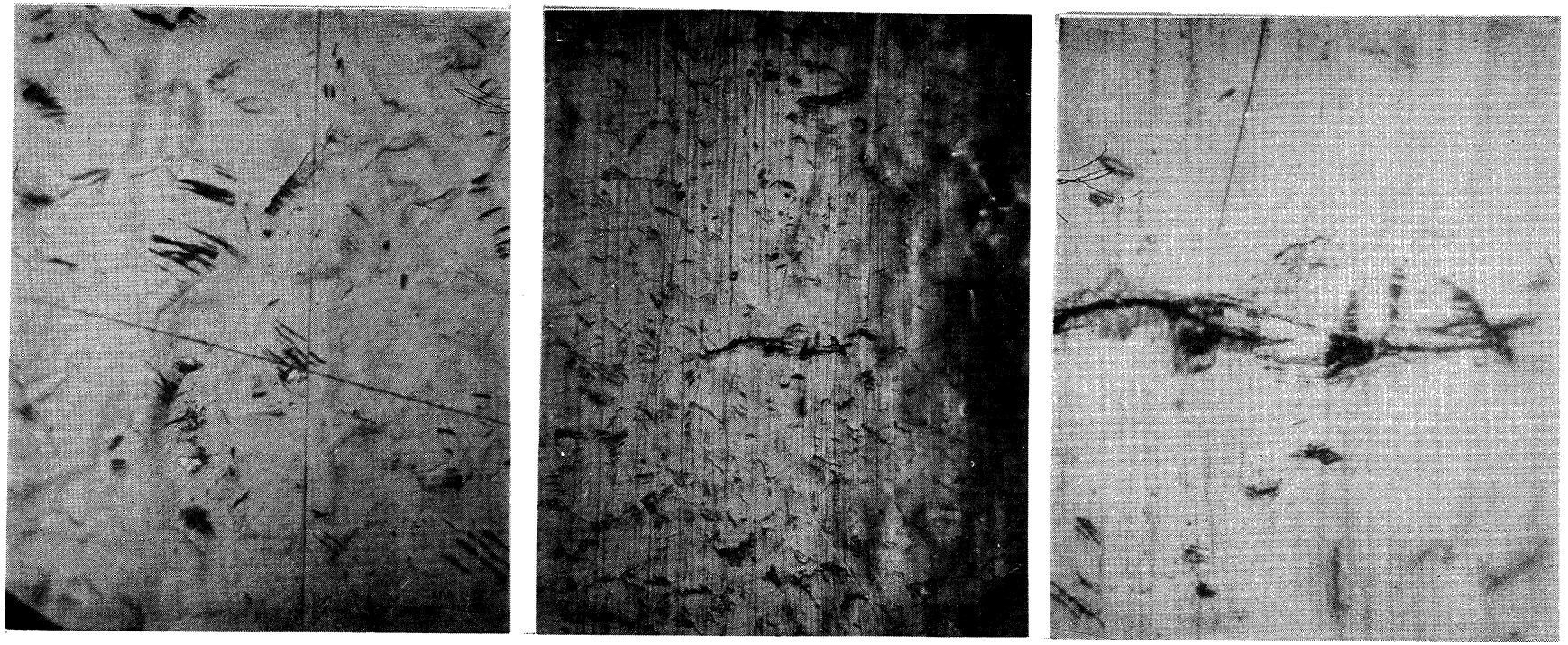

(a) Slip Bands after 10^6 Cycles.
1045 Hot Rolled Steel
Light Micrograph - 1320X.

(b) Slip Bands Forming a Crack
after 10^6 Cycles
Light Micrograph - 330X
1042 C. R. Steel.

(c) Same as (b) Butat 1320X
to Show the Details of
the Crack.

Figure 3.21. Slip Bands and Fatigue Cracks at Low Magnification.

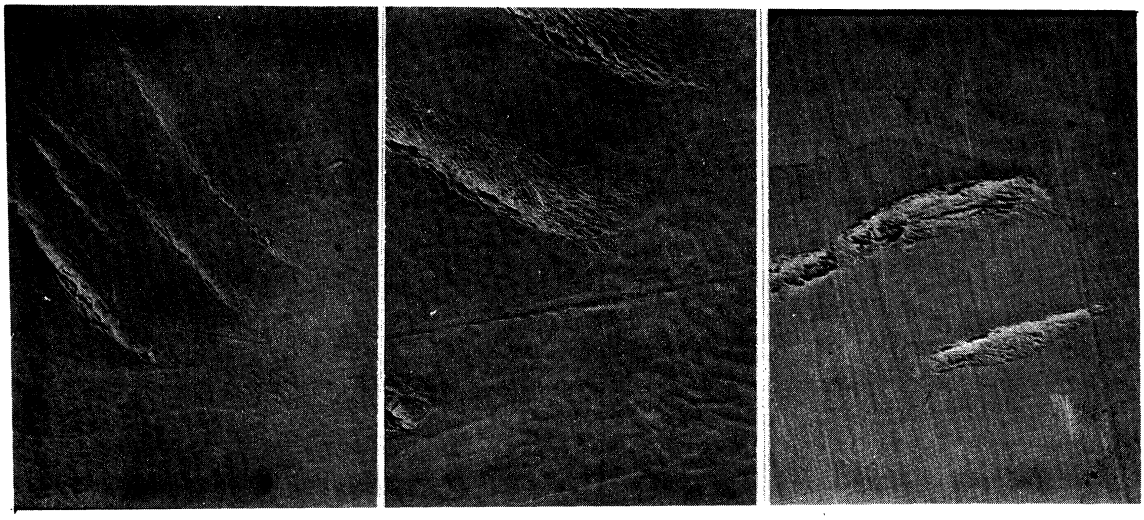

(a) Slip Bands 1045 Hot Rolled Steel after 10^6 Cycles 1800X Electron Micrograph

(b) Slip Bands 1045 Hot Rolled Steel after 10^6 Cycles 2500X Electron Micrograph

(c) Slip Bands 1042 Cold Rolled Steel after 10^6 Cycles 6500X Electron Micrograph

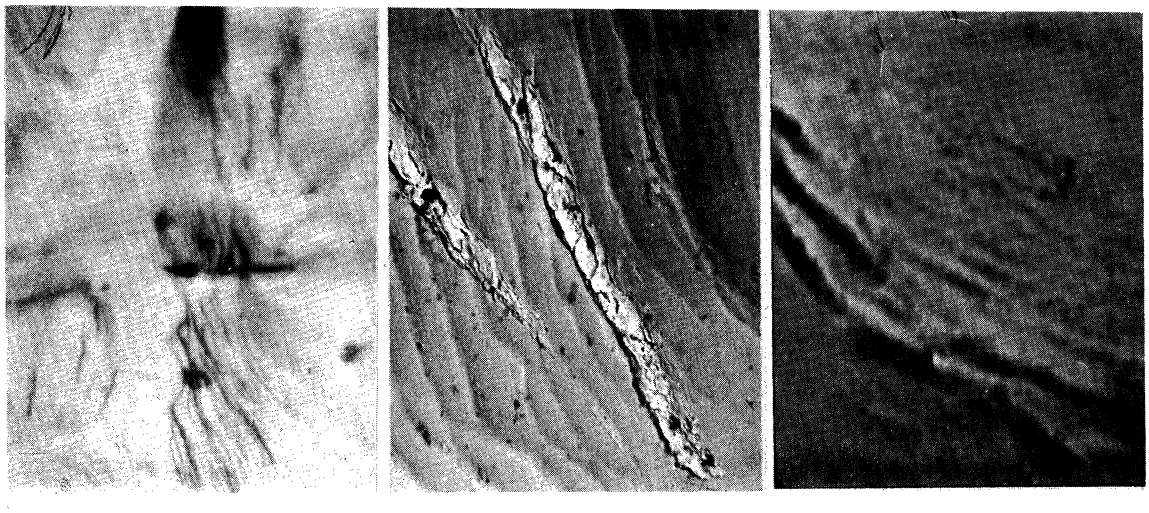

(d) Slip Bands and Primary Slip at an Inclusion Crater in 1020 Hot Rolled Steel after 10^6 Cycles 1800X Light Micrograph

(e) Slip Bands and Primary Slip 1020 Hot Rolled Steel after 10^6 Cycles 1400X Electron Micrograph

(f) Fine Stucture of the End of a Slip Band 1020 Hot Rolled Steel after 10^6 Cycles 10000X Electron Micrograph

Figure 3.22. Surface Observations on Steels Fatigued above the Fatigue Limit.

by the grain boundary they began to spread in a direction normal to the band and finally completely extended along one side of a grain boundary or an inclusion crater. The primary slip lines appeared to play no role in the generation or propagation of slip bands. The direction of these bands was not the same as the direction of the primary slip lines (Figure 3.22(e)) and the orientation of these slip bands was never parallel to the tensile axis but always inclined to it (Figures 3.21(a) through 3.21(c)). The appearance and fine structure of these bands was the same for hot rolled and cold drawn specimens and as such these bands were typical of all the specimens that failed between 10^6 and 10^7 cycles.

C. Results of the Microstrain Tests

One microstrain specimen of the type shown in Figure 2.12 was prepared from each of the four materials used. These specimens were later tested using an Instron tensile testing machine equipped with a constant strain rate loading system. The purpose of this microstrain study was twofold. First of all the specimens were observed to emit acoustic energy during both the loading and the unloading parts of a tensile test. Kaiser had concluded that the stress-strain curve is a many leveled curve instead of being smooth and continuous. Since the capacitive pickup used to measure microstrain at the Ford Scientivic Laboratory was capable of measuring one microinch it was decided to use it to detect any steps in the stress strain curve. The observations showed that even with such a sensitive pickup the steps in the stress-strain curve were hard to discern. The second reason for

using the microstrain tests was to determine the amount of plastic strain in each of the materials at various stress levels.

In order to be able to correlate the findings of the microstrain tests with the acoustic observations made in the acoustic test machine, it was decided to stress the microstrain specimens in a manner similar to that used in obtaining the unload emission characteristics. Thus each microstrain specimen was stressed to the same values of S_{max} as its counterpart used in the acoustic tests. Each specimen was first stressed using an increasing load pattern, that is, the S_{max} (the maximum stress reached during each cycle) was increased from one cycle to the next until S_{max} reached a value close to S_1. Then the specimen was subjected to a decreasing load pattern, that is the S_{max} was decreased from one cycle to the next. The values of S_{max} reached at each loading of a microstrain specimen were kept identical to those reached by their counterparts during the tests on the acoustic test machine. Figure 3.23 shows a typical plot of load versus time displayed by the recorder on the Instron Machine.

There was also an x-y recorder which plotted the applied load versus the extension of the specimen. Figure 3.24 is a schematic representation of a typical hysteresis loop that was obtained. It can be observed that as a specimen is cycled from zero to S_{max} and back to zero stress, it will undergo a certain amount of plastic deformation. This plastic deformation is represented by ϵ_p. The plastic strain is then plotted against S_{max} for each cycle and curves shown in Figures

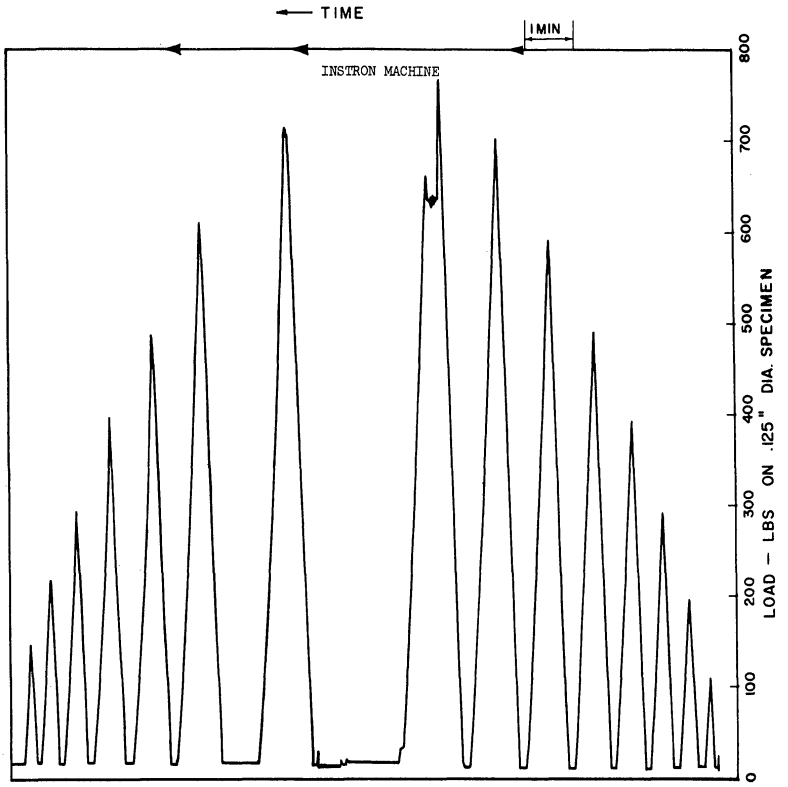

Figure 3.23. Load-Time Chart Output from the Instron Machine for 1045 Hot Rolled Steel Microstrain Specimen.

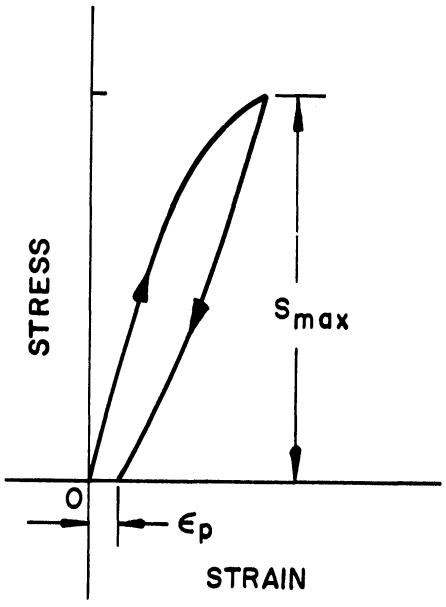

S_m = Maximum Stress Reached During the Load Cycle

ϵ_p = Plastic Strain at the End of this Load Cycle

Figure 3.24. Schematic Representation of a Hysteresis Plot During a Stress Versus Microstrain Test.

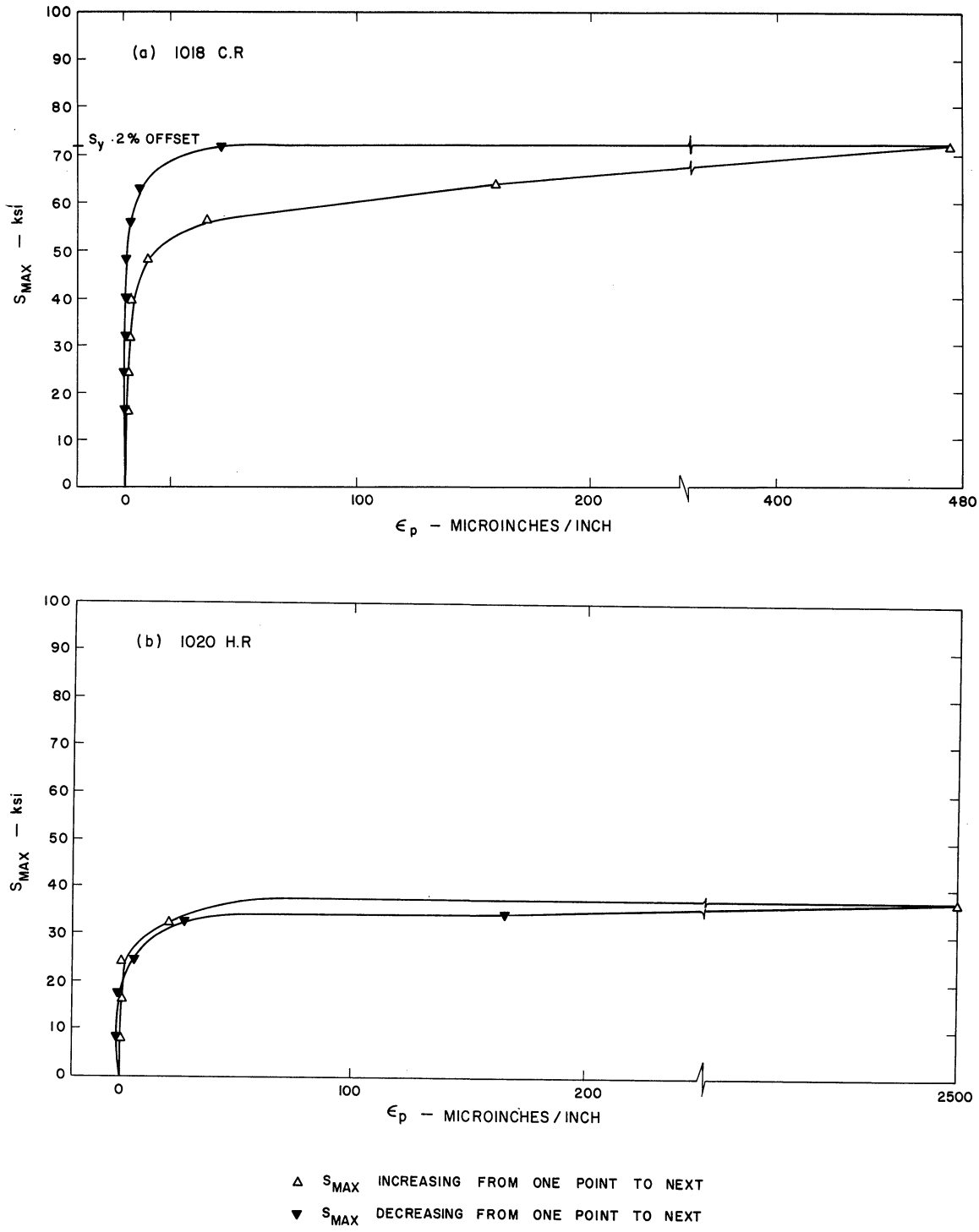

Figure 3.25. Relationship Between the Maximum Stress Attained During a Cycle (S max) and the Plastic Strain at the End of that Cycle (ϵp) .

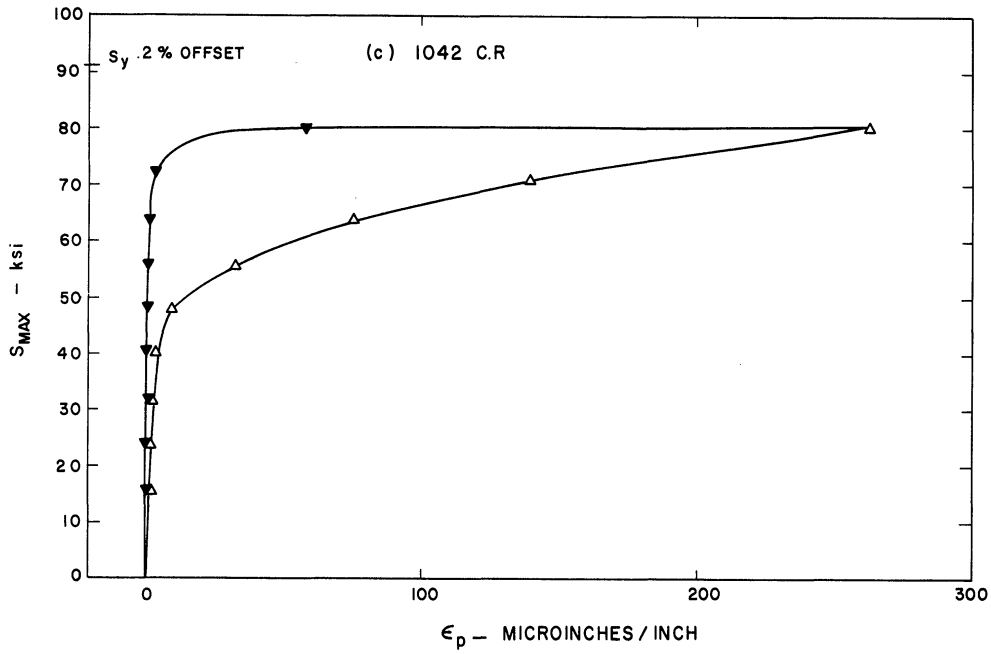

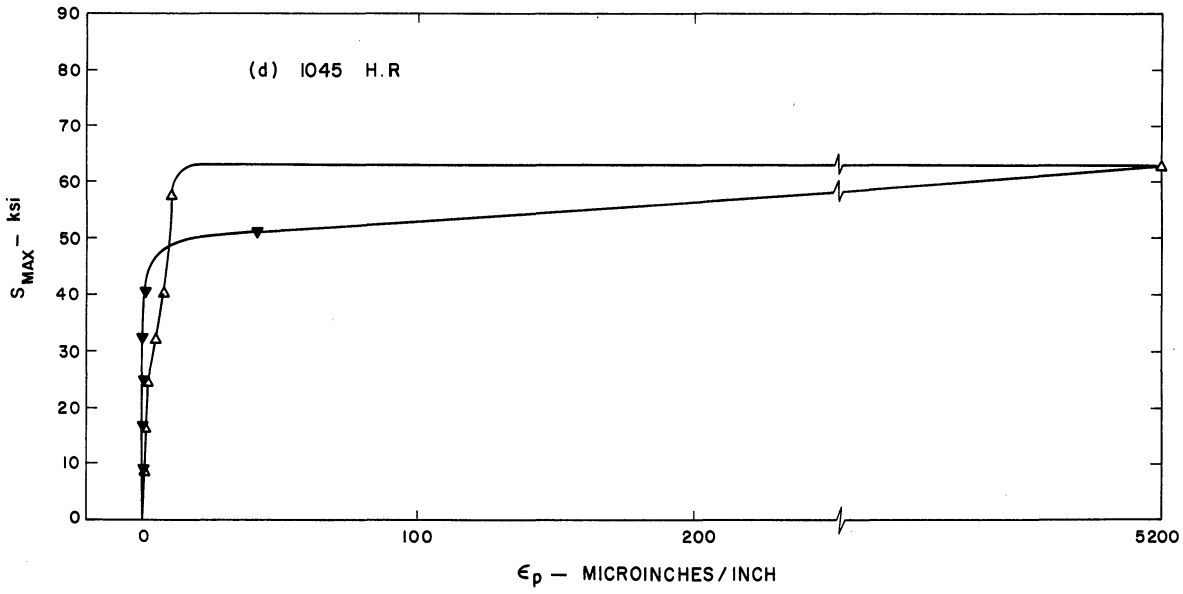

Figure 3.25. (Continued)

3.25(a) through 3.25(d) are obtained. In these figures it should be born in mind that the points labelled by erect triangles (△) were obtained by using an increasing loading pattern while points labelled by inverted triangles (▽) were obtained by using a decreasing loading pattern. The data obtained during the microstrain work are also included in the Table 3.1.

Examination of the data has revealed significant facts. First of all the values of upper yield point are markedly different for each of the three loading machines used in the whole program. The lowest value of the upper yield point that was observed was the one which was measured on the acoustic test machine. This is not believed to be due to an error in the calibration of the load cell in the acoustic test machine because this calibration was checked constantly by using the technique mentioned in Section III. There were other factors which could have caused this difference. These factors are tabulated in Table 3. It is possible that any of the factors mentioned in Table 3.2 could affect the value of the upper yield point S_{y_u}. Yet it is most probable that the machine characteristics have the most effect.

Next the values of plastic strain observed when an increasing load pattern is used are not the same as those observed using a decreasing load pattern. It was also noted that both the cold rolled materials had a tendency to strain harden and therefore to give less plastic strain on subsequent loading to the same value of S_{max}. The hot rolled materials on the other hand had a tendency to become more compliant once they were stressed beyond S_{y_u} and showed a higher plastic deformation when

reloaded to some of the higher values of S_{max} . This phenomenon is of interest because it appears that plastic behavior of this type is intimately connected with the acoustic emission behavior of the material.

Table 3.2

PERTINENT VARIABLES DURING THE TENSILE TESTS ON VARIOUS MACHINES

Test Machine	Specimen		Surface Preparation	Surface Finish μ inches R.M.S.	Machine Characteristic
	Dia. inches	Shank length inches			
Baldwin Southwark Testing Machines	0.505	2.0	Cylindrical ground	3.5	Strain Rate .05 to .002/min.
Acoustic Test Machine	0.2	1.0	Polished with 500 grit emery cloth and electropolish	0.4	350 lb./min. constant load rate
Instron Tensile Machine	0.125	1.0	Polished with 500 grit emery cloth	4.0	constant extension rate .02 in./min.

IV. DISCUSSION

A. Significance of the Acoustic Emission That Occurs While Loading

1. High Frequency Type Emission

The high frequency type emission is probably the most frequently observed and analyzed part of the acoustic spectrum. It was first observed by Kaiser[111] and then confirmed by Schofield[110] as well as Borchers and Tensi[119]. This emission begins just before the upper yield point and continues through the period during which the specimen undergoes yield elongation. This type of emission ceases rather abruptly as soon as the specimen reaches a stress that is above the upper yield stress. This type of emission is observed in all the hot rolled specimens that show the phenomenon of upper and lower yield point. It never appears in the specimens in which the upper and lower yield has been removed by prior deformation. Thus one can conclude with certainty that this type of emission is an acoustic characteristic associated with the upper and lower yield phenomenon.

Tatro and Liptai[26] stated that this emission is caused by the disruption of the surface oxide layer that accompanies the formation of Lüders bands in most of the materials showing this type of a sudden yield drop. The two materials which showed upper and lower yield points were the 1020 and 1045 hot rolled steels. These steels behaved similarly during the abrupt yield yet showed completely dissimilar behavior on the surface. The 1020 hot rolled steels always showed the existence of Lüders bands and the 1045 steels always showed no sign of surface slip even when the surface replicas shadowed at 25° were

examined under the electron microscope. Yet as mentioned previously both the steels emitted high frequency emission. Hence a hypothesis which holds that the oxide breakage during Lüders band propagation is the source of this type of emission cannot explain the occurrence of emission in 1045 hot rolled steel. Therefore although the high frequency emission can be affected by the surface it cannot most probably be caused solely by the surface slip formation.

Figure 4.1 shows the time delay for the onset of yield as a function of stress in mild steel at 23° C. It also shows that the delay time is largest at low stresses. This is thought to be due to the fact that at low yield stresses the slip mode of deformation predominates rather than the twinning mode[124]. Such a situation in fact did exist during the acoustic tests. The strain rate used was about 3.7×10^{-4} per min. This strain rate was slow enough to start yield at low stresses as observed from Table 3.1. Under these circumstances it can be concluded that the low strain rate, the testing temperature (room temperature), the high stacking fault energy of the material, and the low yield points observed make the rapid formation of twins during the yield drop a very remote possibility. This conclusion is reinforced by the fact that the surface observations showed no evidence of twinning. Hence, it can be said that the high frequency emission (in this case) cannot be attributed to the rapid formation of twins.

It could be argued that the twins formed could have been elastic in nature and as such would disappear when the load is removed,

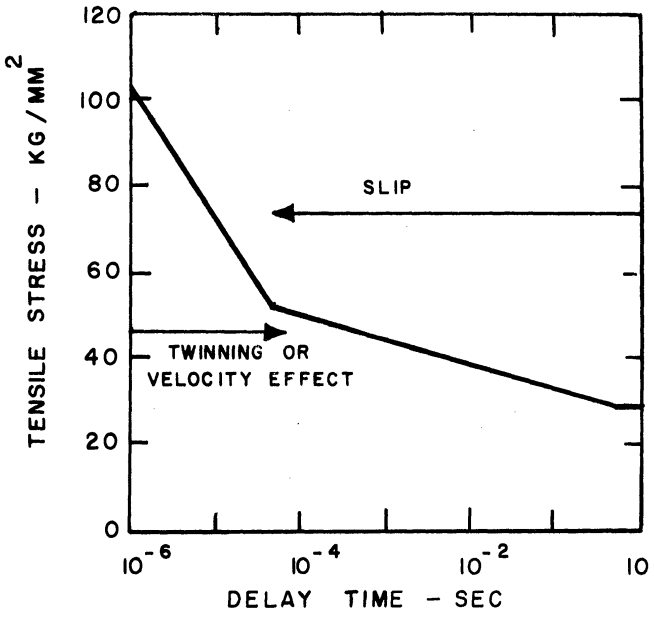

Figure 4.1. Time Dependence of Upper Yield Stress.

thus giving rise to a characteristic unload emission also. Elastic twinning can very well be the source of high frequency acoustic emission, yet this phenomenon will tend to repeat itself at every subsequent reload, thus giving rise to high frequency acoustic emission at every subsequent load. The observations show that such a repetition does not occur. Hence the possibility of elastic twinning's being the source of the high frequency emission seems quite remote.

The phenomenon of high frequency emission is connected with the upper and lower yield point phenomenon and it begins just prior to the occurrence of the upper yield point as seen in Figure 4.2. Such a phenomenon also requires a higher stress for initiation than for continuation. An explanation that is given for the upper and lower yield phenomenon in steel is that the dislocations that are pinned by solute atoms of carbon and nitrogen are suddenly unlocked by an applied stress. In such a situation a majority of the dislocations are first bowed out in kinked form between their anchoring points until the upper yield stress is reached. At this point the dislocations are detached from their anchoring points and in essence they form an avalanche and are accompanied by a sudden deformation, which is easier to continue than to initiate. It is felt that the energy released at unpinning is the most probable source of the high frequency type emission.

On careful examination of the emitted noise on the sweep of a cathode ray oscilloscope it was found that the frequency of the high frequency emission is about the same as that of the burst type emission

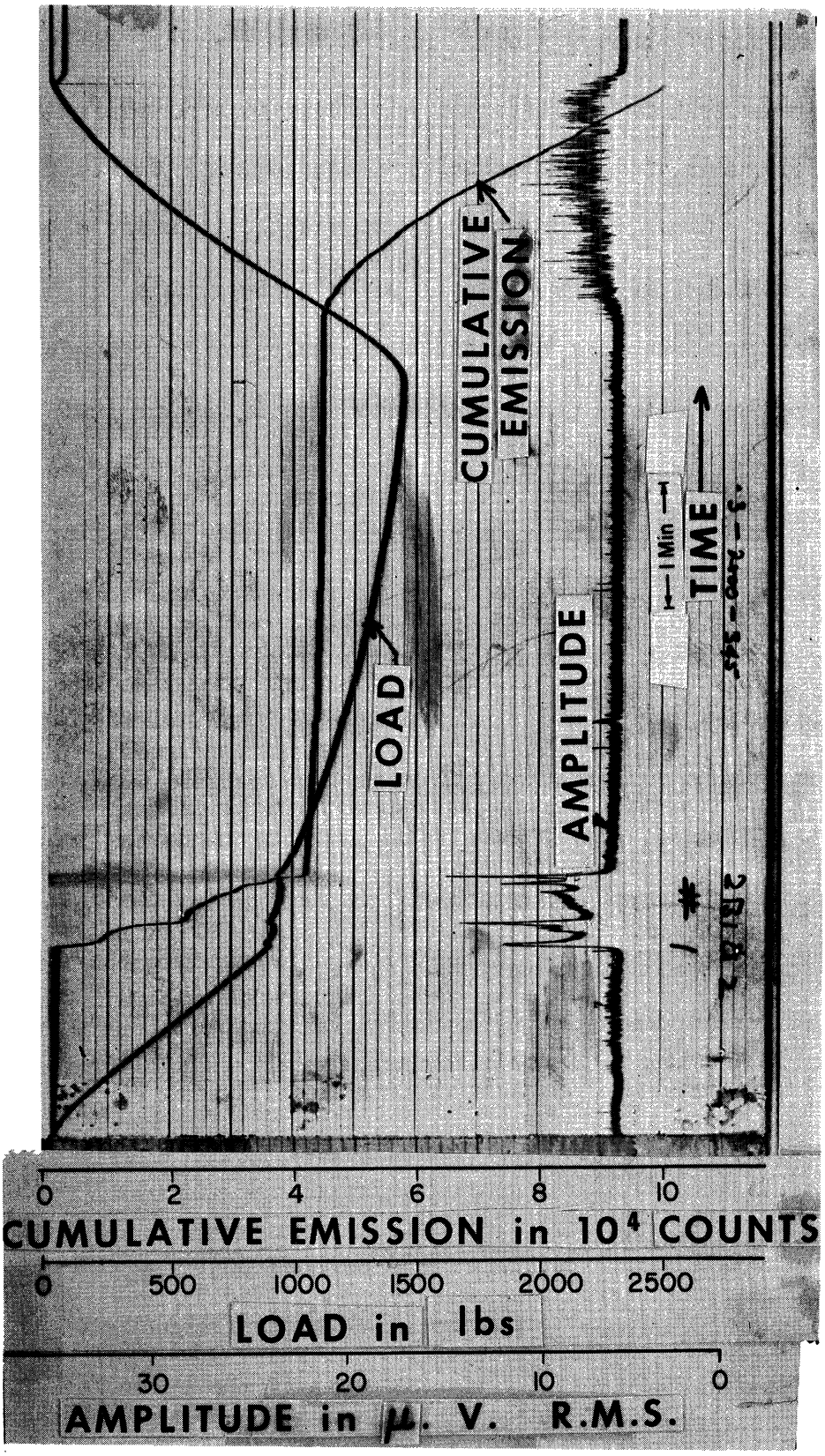

Figure 4.2. Visicorder Chart Showing the Relationship Between the Start of High Frequency Emission and the Start of the Abrupt Yielding.

(10 to 20 kcps.). Yet an observation of the same frequency using a counter could be misleading. This is because even though the frequency of these pulses is the same, the number of pulses emitted during this short span of time between a and b in Figure 3.4 may be very high. Hence more pulses will get counted during a given gating time between a and b than between o and a . Thus the words "high frequency emission" do not characterize the frequency of these pulses but they apply more to the rapid occurrence of each of these pulses.

2. Characteristics of the Burst Type of Emission

The burst type of emission appears during the first part of the loading even at very low stresses. The two distinquishing features of this emission are its sporadic appearance and its ability to reappear on subsequent loadings. This type of emission follows no definite trend from one specimen to another or one loading cycle to another, yet it persists even after long periods of aging. Fatigue below and above the fatigue limit and over extended periods of time (at 30 cps) seems to increase the rate and the amplitude of the burst type emission. Another characteristic that these bursts have is that they appear at a stress level that is too low to be conducive to the operation of a number of mechanisms that are likely to produce emission. Thus it is felt now that this type of emission is produced either by a mechanism which needs very little stress to actuate it or by mechanisms that can be present in those zones that have high internal stress. These zones of high internal stress can exist at grain boundaries, inclusions, or

twin boundaries. The high internal stress would in that case require a rather low external stress to actuate the noise producing mechanisms such as unlocking of dislocation pileups.

3. Kaiser Effect

Kaiser had concluded that when specimens loaded once were loaded precisely in the same way they would not emit acoustic pulses until the previous stress level was reached. This effect was called the Kaiser effect. One of the first tasks undertaken during these studies was to see if this effect was valid for the materials under examination. The experimental results relating to this task have been shown in Figure 3.12 and were discussed in Section III A. 5.

The results show definitely that the material used does not exhibit the Kaiser effect for loads below the upper yield point. After the upper yield stress is exceeded the high frequency type emission begins to occur. This emission continues until and as long as any part of the specimen is undergoing the yield point elongation. If this process of yield elongation is stopped abruptly by removal of the load, the emission ceases. A specimen that has under gone such a loading treatment will not show yield extension on reloading until the previous value of stress is reached. This is because all those portions that were capable of yielding suddenly during the first application of a specified maximum stress would have already done so. When that maximum stress is exceeded the specimen will start yielding in those places where the stress can now exceed the upper yield point and hence the

high frequency emission will also begin at that stress. Thus the Kaiser effect in this case is actually caused by the continuation of the yield deformation. This conclusion is in agreement with the conclusion drawn by Borchers and Tensi[119] with one reservation, i.e., the Kaiser effect does not manifest itself until the upper yield stress is reached. It would also be clearly noted that this effect is applicable only to the high frequency type of emission and not to the burst type emission which occurs on loading and unloading a specimen.

B. Significance of the Acoustic Emission That Occurs During Removal of a Load

When a specimen is unloaded from a given value of maximum stress it emits a burst type of noise whose form and pattern are discribed in Section III A. This unload emission was completely overlooked by most of the previous investigations either because most of the tests were conducted to failure or because the loading machines used could not be unloaded quickly and silently. The first observation of the phenomenon was reported by Schofield in 1964 when he was conducting acoustic tests on gold single crystals as shown in Figure 1.5, 1.6, 1.7. Yet very little attention was paid to this phenomena until the present investigation began.

This unload emission is found to be repeatable as long as $S_{max} < S^*$. Next, for a given load rate the rate of emission varies in a nonlinear manner as the unloading operation is completed. Hence, this leads one to conclude that this particular phenomenon is nonlinear and elastic.

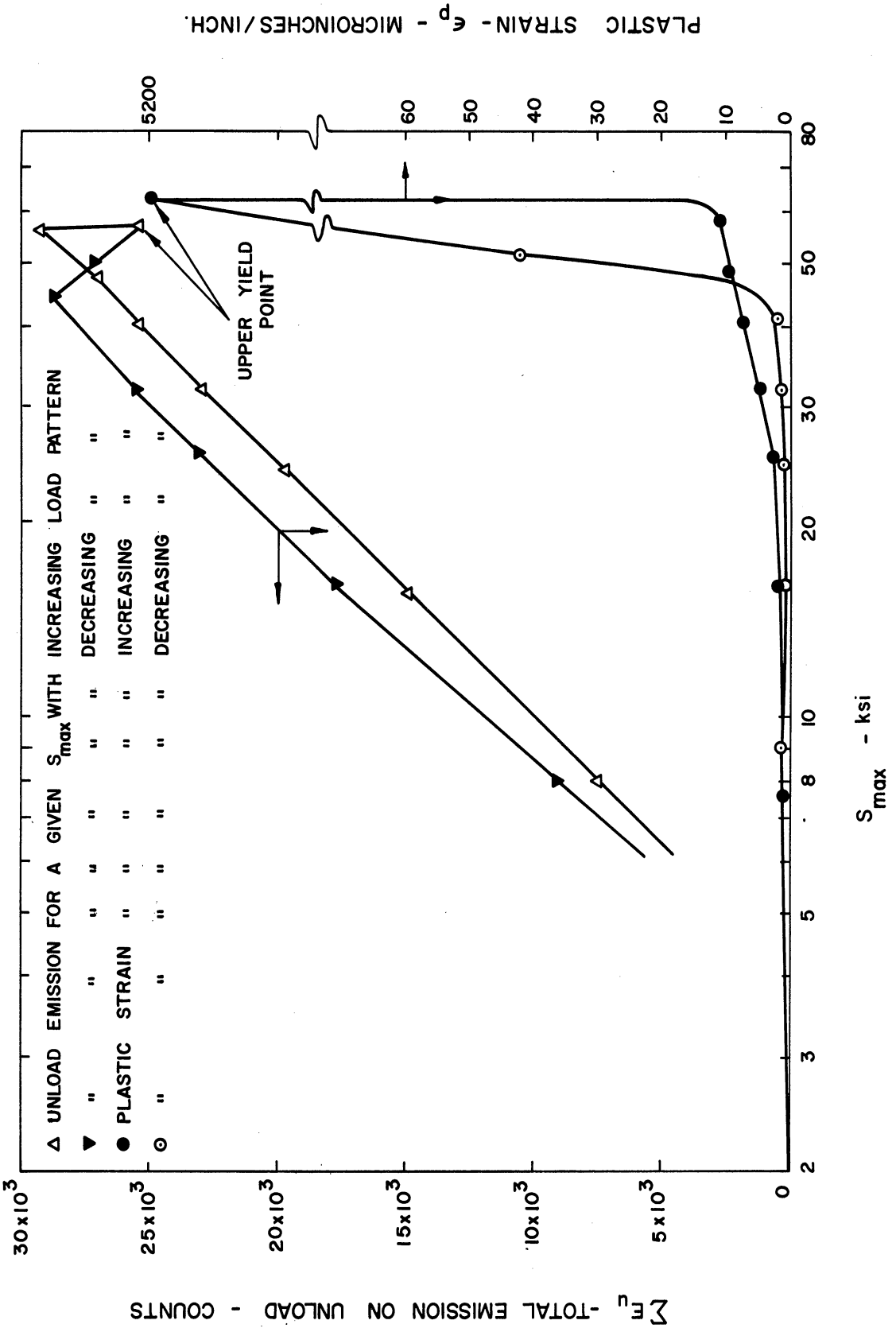

Figure 4.3. Relationship Between Plastic Strain, Unload Emission - 1045 H.R. Virgin Specimen.

1. Relationship Between the Unload Emission Behavior and Plastic Strain

The unload emission characteristic for a virgin 1045 hot rolled specimen was obtained using the acoustic test machine and the results are shown in Figure 4.3. Then using the Instron machine at the Ford Motor Company's Scientific Laboratory and a microstrain specimen the microstrain behavior of this material was observed along with the values of plastic strains at various values of S_{max}. These are also plotted in Figure 4.3. It should be noticed that these are not the usual stress-strain diagrams. Both of these curves were obtained using increasing as well as decreasing load patterns. From Figure 4.3 it is observed that the material exhibits an unload emission such as,

$$\Sigma E_u = 1.02 \times 10^4 \log S_{max} - 1.3 \times 10^4 \qquad \text{(eq. 4.1)}$$

for $S < S^*$ using an increasing load pattern

$$\text{and } \Sigma E_u = 1.1 \times 10^4 \log S_{max} - 1.5 \times 10^4 \qquad \text{(eq. 4.2)}$$

for $S < S^*$ using a decreasing load pattern

where S_{max} = maximum stress reached during the cycle, in ksi

ΣE_u = total emission on unload in counts.

It will also be noted that above 47 ksi this material became more compliant and exhibited higher plastic strain for a given load after it had been loaded beyond the upper yield point.

Next the values of plastic strain at various values of S_{max} were obtained for all the materials and (using increasing as well as decreasing load pattern), Figures 4.4(a) through (d) show the values

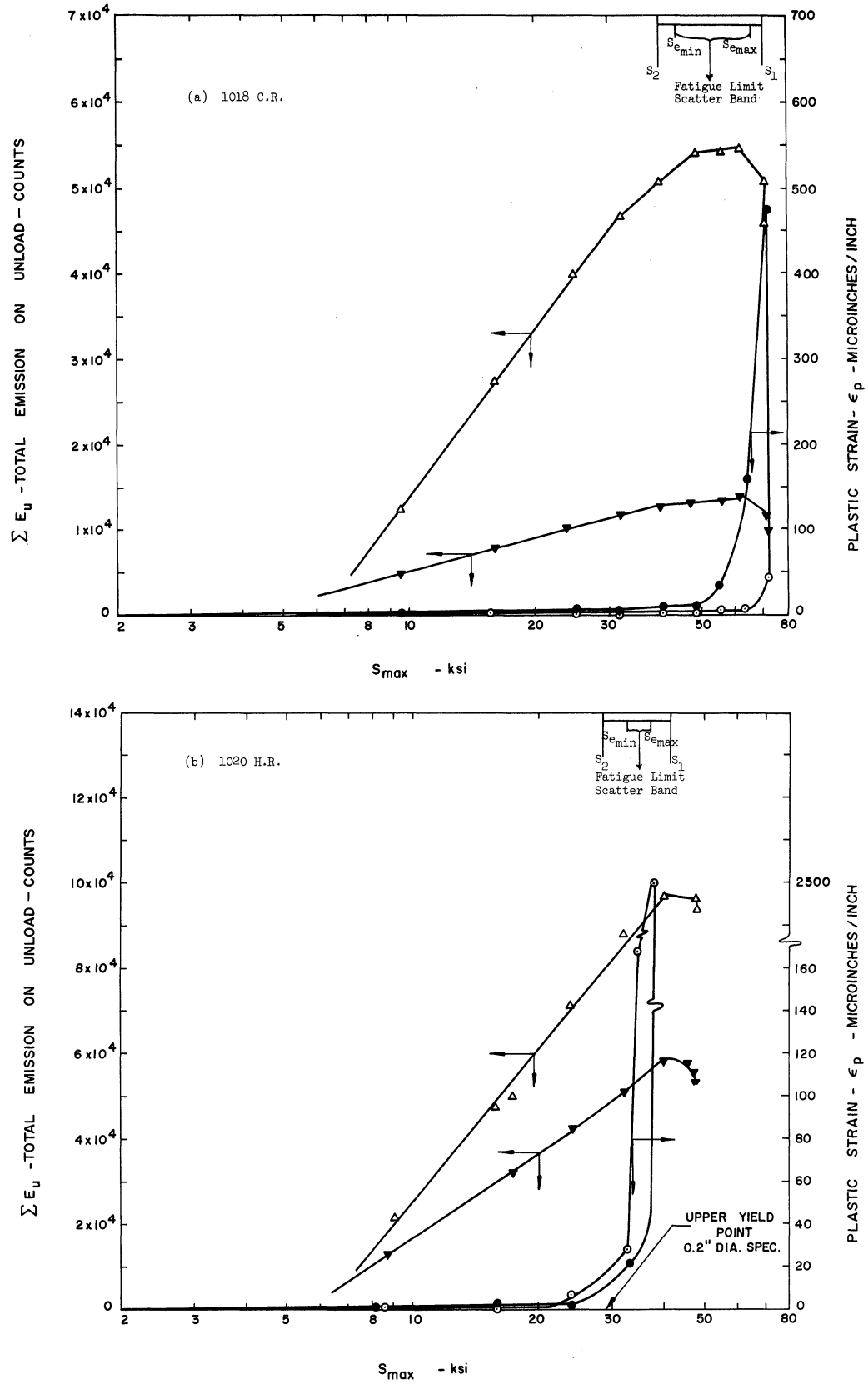

Symbol	Variables Represented			Remarks
▼	ΣE_u	v/s	S_{max}	Fatigued at S_2 Survived 10^7 cycles
△	ΣE_u	v/s	S_{max}	Fatigued at S_1 Failed between 10^6 and 10^7cycles
⊙	ϵ_p	v/s	S_{max}	Increasing Load Pattern.
●	ϵ_p	v/s	S_{max}	Decreasing Load Pattern.

Figure 4.4. Relationship Between Plastic Strain, Unload Emission and Maximum Stress in the Finite and Infinite Fatigue Life Regions.

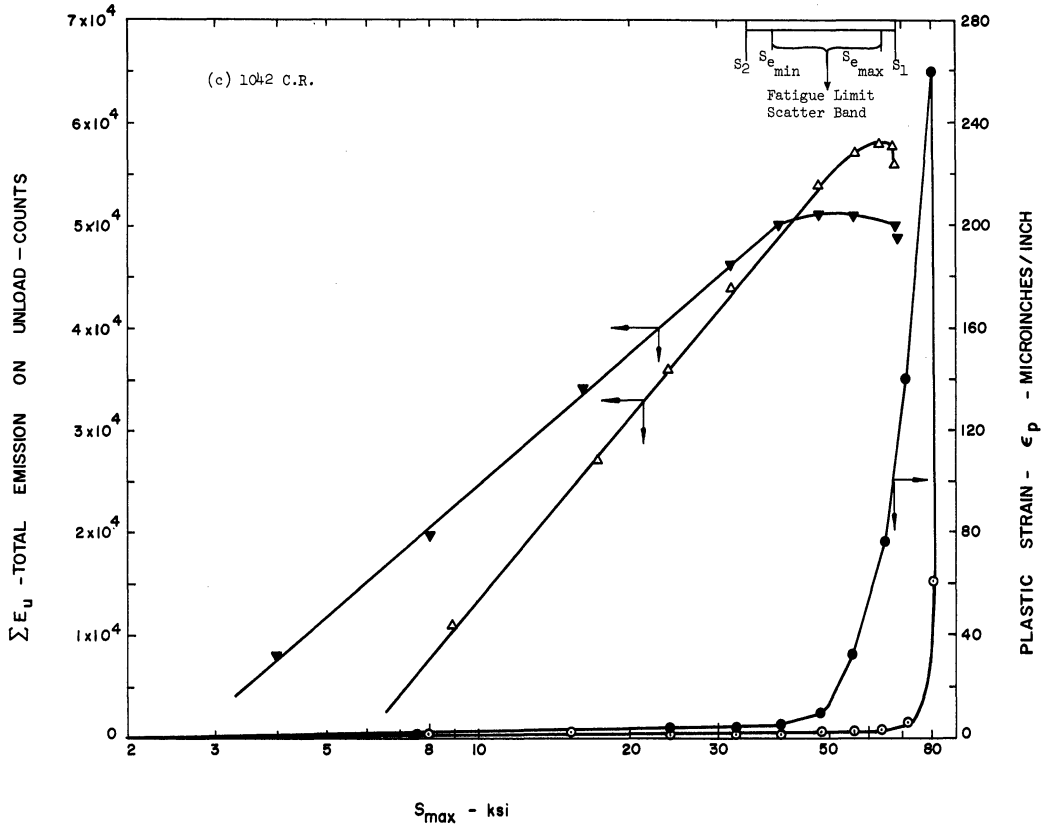

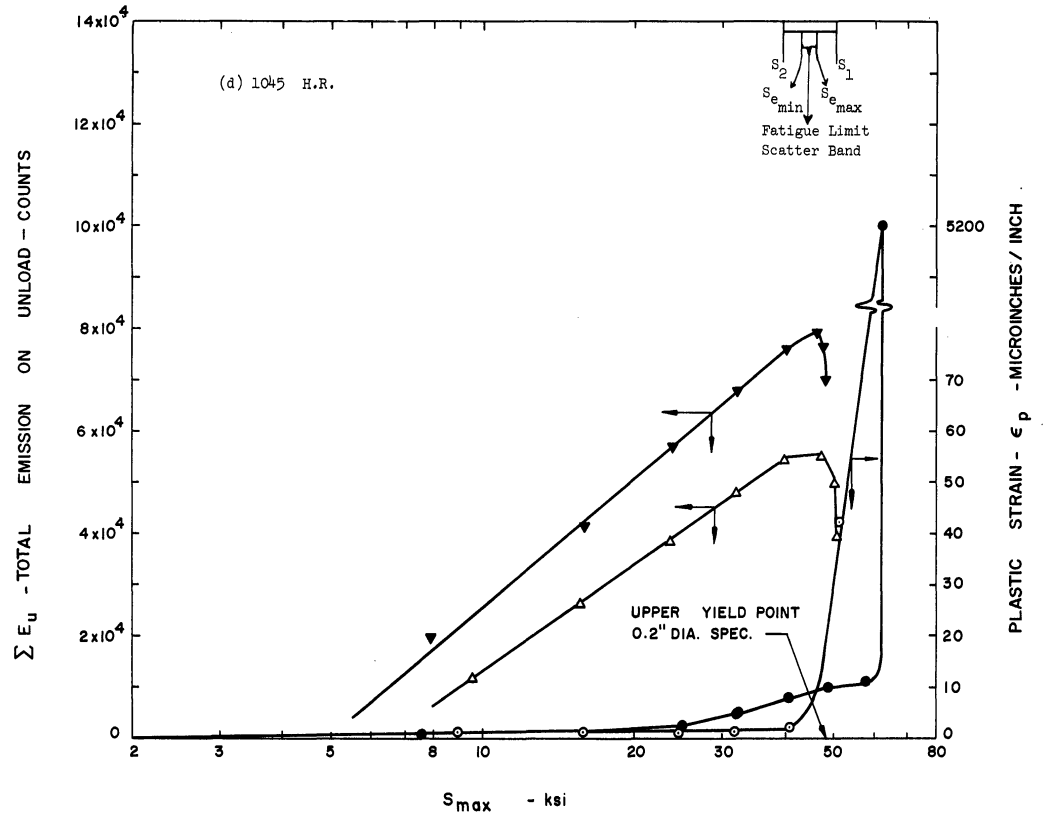

Figure 4.4. (Continued)

of ϵ_p for various values of S_{max}. In the same figures are shown the unload emission characteristics with decreasing load patterns for both the specimens of each material that were later subjected to fatigue.

It will be noted from these figures that whenever the plastic deformation is high the emission that occurs on unloading the specimens is low and vice versa.

The unload emission characteristic follows a relation such as

$$\Sigma E_u = K_1 \log S_{max} - K_2 - K(\epsilon_p) \qquad \text{(eq. 4.3)}$$

where K_1 and K_2 are constants which depend on the material, its condition, and the conditions during the test, while $K(\epsilon_p)$ is a function of the plastic strain. The present series of tests were conducted without a microstrain pickup on the acoustic test machine and the data obtained from the Instron machine were not extensive enough to obtain a good value for $K(\epsilon_p)$.

2. Relationship Between the Unload Emission, Upper Yield Stress, and Fatigue Limit

The values of the stresses S_1 and S_2 to which the fatigue specimens were loaded and the upper and lower limits $S_{e_{max}}$ and $S_{e_{min}}$ of the fatigue limit scatter band for each of the materials are given at the top of the Figures 4.4 (a) (b) (c) (d). The values of S_{yu} (in case of hot rolled materials) and the lives in cycles for each specimen at its respective fatigue stress are also given in these figures. It will be noted that the value of S*

in each case is within the scatter band of S_e , the stress for maximum unload emission. It will also be noted that in case of the 1045 hot rolled materials the value of S_{y_u} was also close to the value of S_e . All the specimens fatigued above S* failed while all those fatigued below this value of stress survived 10^7 cycles. It was also noted that in each case the value of ϵ_p as well as $K(\epsilon_p)$ is considerably higher after a stress higher than the fatigue limit was reached. S* is also the stress beyond which the plastic deformation increased rapidly. These observations are in agreement with those made by Lazan[93] on a mild steel in which the plastic strain observed during a dynamic stress strain test increased rapidly at stresses beyond the fatigue limit (Figure 1.4). Tests such as those made by Lazan and Wu indicate quite clearly that the abrupt increase in fatigue life below S_e is accompanied by the abrupt decrease in the plastic deformation ($\epsilon_p = 10^{-5}$). Plastic deformations of this magnitude are not easy to detect in many situations. However, the close relationship between unload emission and ϵ_p (as shown in Figure 4.3 and Figure 4.4) indicates that the onset of gross plastic deformation and fatigue damage can be easily detected using unload emission characteristic for a given part.

3. Explanation

At this time it is not possible to pinpoint the source of this unload emission. But the observations so far tend to indicate that the acoustic pulses observed while unloading a specimen are the

result of sudden movement of dislocation lines or tangles. These movements are accompanied by abrupt changes in line energy as well as potential energy of the dislocation as a whole as it returns to its position of minimum potential energy. Some of this energy manifests itself acoustically. The following observations reinforce this belief:

(1) Whenever the material is in its hot rolled condition the concentration of solute atoms at the dislocation is high and the motion of dislocation loops is restricted by the solute atoms. If this material undergoes yield elongation the dislocations would be moved permanently away from the concentrated zones of locking points and hence their motion would be less restricted. Hence for a given $S_{max} < S^*$ the number of dislocations moving back and forth would be higher for a material after it has been stressed beyond the S_{y_u} than before. Thus the ΣE_u would also be higher for a specimen which has been prestressed beyond the S_{y_u} than for a virgin specimen. This increase in ΣE_u was observed in Figure 4.3.

(2) If a specimen were strained plastically and then allowed to age, the emission on unload ΣE_u would tend to decrease with time because of the increased locking caused by the diffusion of interstitial solute atoms. This was observed in Figure 3.13.

(3) As the plastic strain during a load cycle increases the ΣE_u goes down. In order to get a maximum number of pulses on the unload, a maximum of the elastic energy put in during the load must be recovered during the unload. With the onset of plastic deformation the dislocations do not collapse but they come to rest at new positions of

lower potential energy and hence the energy recovered on the unload is lower, and lower emission is recorded. Hence, it is hypothesized that point S* corresponds to the stress at which a maximum of elastic dislocation motion can occur with a minimum loss of dislocation energy resulting from plastic deformation.

V. CONCLUSIONS

Several conclusions can be drawn from the results of this investigation. It should be born in mind that these conclusions apply only to the materials tested and for the specific conditions of the tests that are described. The conclusions fall into two categories, namely, those that are based on surface observations and those that have resulted from acoustic emission and microstrain studies.

A. The surface observations lead to the following conclusions:

1. Primary slip lines do not seem to be parallel to fatigue slip bands on the surface of a specimen (Figure 3.22(e)).

2. Fatigue slip bands generally develop earlier in the middle of a grain.

3. The fatigue slip bands grow in a longitudinal direction first until they encounter an inclusion crater or a grain boundary and then they begin to widen. Then cracks begin to nucleate at inclusion craters or grain boundaries where there is a conglomeration of slip bands (See Figure 3.22(a) (b) (c) (d)).

4. Cracks form within slip bands and propagate via similar cracks formed in adjacent grains. Figure 3.21.

5. The upper and lower yield phenomenon does not always result in the appearance of detectable primary slip lines at the surface. These slip lines were never observed in the pearlite grains.

6. The pearlite grains near the surface stay intact and free of slip until the specimen begins to neck down.

7. Specimens loaded below the fatigue limit do not show the intense and localized fatigue slip bands observed in those loaded above the fatigue limit.

8. Slip does occur near the surface of the specimens loaded to a stress less than the fatigue limit, but these slip lines are diffuse and can be observed by replication only after etching.

B. The acoustic emission and microstrain studies lead to the following conclusions:

1. A distinct "high frequency" type of emission occurs when the upper yield stress is exceeded. (See page 89 last paragraph.)

2. The "high frequency" type emission is not a result of the surface oxide cracking owing to the formation of slip lines. It even occurs when no primary slip lines could be detected at the surface.

3. The high frequency emission is irreversible for a given material and occurs only during the first application of stress beyond the upper yield point in the case of an annealed or hot rolled material.

4. The unload emission is totally burst type in nature and follows a relation $\Sigma E_u = K_1(\log S_{max}) - K_2 - K(\epsilon_p)$, where K_1 and K_2 are constants which depend on the material, its condition, and the conditions during the test, while $K(\epsilon_p)$ is a function of the plastic strain.

5. The total emission on unload ΣE_u is highly repeatable for $S_{max} < S^*$ for a given condition of the material.

6. The ΣE_u decreases as the amount of strain which is produced in the plastic region of the material increases.

7. The stress (S*) required to produce maximum emission on unload appears to lie within the scatter band of the fatigue limit.

8. There is always a stress delay for the start of unload emission and this stress delay is related to S_{max}, the maximum stress reached during the cycle, when $S_{max} < S^*$ (See Figure 3.6(b)).

9. Both hot rolled and cold rolled varieties of steel exhibit unload emission in their unfatigued and fatigued conditions.

10. The total emission on unload, ΣE_u, drops after strain aging.

11. There was no evidence of fatigue failure or intense slip bands occurring at stresses below S* during all the tests.

12. If the material has a tendency to work harden rapidly, the value of S* increases. In the absence of such rapid work hardening S* remains constant.

13. The Kaiser effect is not universal and is observed only after high frequency emission is observed.

14. The surface oxide layer does not seem to be the source of unload emission because for specimens fatigued below S_e the change in unload emission ΣE_u was not accompanied by changes in the surface as observed by electron microscope examination of surface replicas.

15. The emission encountered during the cracking of pearlite (while the specimen was undergoing necking) was actually lower than that encountered before the pearlite began to crack.

16. The cracking of pearlite cannot be a source of any of the acoustic emission observed in this investigation because none of the specimens used during the study were stressed sufficiently to cause any pearlite to crack.

17. The load and the unload emission are strain-rate dependent.

VI. FUTURE WORK

On the basis of the results that have been obtained so far, it appears that the following areas of investigation would be worthwhile:

1. Investigate the use of high frequency emission in obtaining the values of the yield point for mechanical components having stress concentrations or welded joints, etc.

2. Investigate the use of unload emission characteristics to determine the onset of plastic deformation in case of mechanical components that may have residual stresses or varying amounts of prior cold work.

3. The unload emission has been shown to be affected by strain aging (Figure 3.13) and strain hardening, and a quantitative relationship would be quite useful.

4. Correlate ΣE_u or ΣE_ℓ with properties such as fatigue life in the finite life region of the stress-life relationship.

5. Establish the correlation between unload emission behavior and various aspects of microstrain behavior, such as plastic strain, anelastic strain, etc.

6. Determine the unload emission characteristics of other materials with and without a fatigue limit and see if a correlation does exist between ΣE_u and ϵ_p as shown in the case of the steels used in this investigation (Figure 4.4)

7. Establish the load and unload emission under compressive loading.

8. Use the unload emission and high frequency emission to detect plastic deformation at flaws or roots of cracks.

9. Determine the actual mechanisms governing this phenomenon by using etch pit or transmission electron microscopy technique (to visually follow the dislocation processes occuring at low plastic strains of about 10^{-6} to 10^{-4}) and try to monitor the acoustic emission simultaneously or separately as may be feasible.

REFERENCES

1. Anderson, L. J., and Posakony, G. J., Investigation of Methods for Determining Actual Flaw Size in Materials by Nondestructive Ultrasonic Means, A.S.D. Technical Report 61-205.

2. Beranek, L. L., "Transmission and Radiation of Acoustic Waves by Solid Structures," from Noise Reduction, McGraw Hill, New York, 1960.

3. Beranek, L. L., "Sound Transmission Through Structures Containing Porous Materials," from Noise Reduction, McGraw Hill, New York, 1960.

4. Cottrell, A. H., Trans. of the Amer. Inst. of Min. Met. and Pet. Engrs., 212, 1958, p. 192.

5. Cottrell, A. H., "Theoretical Aspects of Fracture," Fracture, Averbach, B. L., Felbeck, D. K., Hahn, G. T., and Thomas, D. A., (eds.), Technology Press of M.I.T., and John Wiley and Sons, Inc., New York (1959).

6. Geiger, P. H., Noise-Reduction Manual, Engineering Research Institute, University of Michigan, 1953.

7. Grover, H. J., Gordon, S. A., and Jackson, L. K., Fatigue of Metals and Structures, Department of Navy, Washington, D. C., 1960.

8. Grover, H. J., Hyler, W. S., Kuhn, P., Landers, C. B., Howell, F. M.; Axial Load Fatigue Properties of 24ST and 75S-T Aluminum Alloy as Determined in Several Laboratories, NACA, TN 292, May 8, 1958.

9. Jack, W. A., Control of Sustained Noise, University of Michigan, School of Public Health and Institute of Industrial Health, 1952.

10. Kinsler, L. E., and Frey, A. R., Fundamentals of Acoustics, John Wiley, 1962.

11. Kroll, R. J., Stress Waves in Test Specimen Due to Simulated Acoustic Emissions, Doctoral Thesis, Department of Applied Mechanics, Michigan State University, 1962.

12. Lipson, C., Kerawalla, J., and Mitchell, L., Engineering Applications of Reliability, University of Michigan, 1963.

13. Liptai, R. G., and Tatro, C. A., Acoustic Emission-A Surface Phenomenon, Symposium on Nondestructive Testing of Aircraft and Missile Components, 1962.

14. Peterson, A. P., and Beranek, L. L., Handbook of Noise Measurement, General Radio Company, Mass., 1953.

15. Schofield, B. H., Bareiss, R. A., Kyrala, A. A., Acoustic Emission Under Applied Stress, Lessells and Associates, Inc., WADC Technical Report 53-194, (1958).

16. Schofield, B. H., Bareiss, R. A., Acoustic Emission Under Applied Stress, Progress Report No. 1, Contract No. AF 33(616)-5640, WADC, Ohio.

17. Schofield, B. H., Acoustic Emission Under Applied Stress, Progress Report No. 2, Contract No. AF 33(616)-5640, WADC, Ohio.

18. Schofield, B. H., Acoustic Emission Under Applied Stress, Progress Report No. 3, Contract No. AF 33(616)-5640, WADC, Ohio.

19. Schofield, B. H., Acoustic Emission Under Applied Stress, Progress Report No. 6, Contract No. AF 33(616)-5640, WADC, Ohio.

20. Acoustic Emission Under Applied Stress, Progress Report No. 7, Contract No. AF 33(616)-5640, WADC, Ohio.

21. Acoustic Emission Under Applied Stress, Progress Report No. 8, Contract No. AF 33(616)-5640, WADC, Ohio.

22. Schofield, B. H., Acoustic Emission Under Applied Stress, Progress Report No. 9, Contract No. AF 33(616)-5640, WADC, Ohio.

23. Schofield, B. H., Acoustic Emission Under Applied Stress, Progress Report No. 10, Contract No. AF 33(616)-5640, WADC, Ohio.

24. Schofield, B. H., Acoustic Emission Under Applied Stress, Progress Report No. 11, Contract No. AF 33(616)-5640, WADC, Ohio.

25. Tatro, C. A., Sonic Techniques in Detection of Crystal Slip in Metals, Division of Engineering Research, Michigan State University, Jan. 1959.

26. Tatro, C. A., and Liptai, R. G., Acoustic Emission from Crystalline Substances, Symposium on Physics and Nondestructive Testing, October 1962.

27. Weiss, V., and Sessler, J., "Low Cycle Fatigue Damage in Pressure Vessel Materials," Amer. Soc. Mech. Eng. (1962) 62-WA-233.

28. Baughman, R. A., Rolling Contract Bearing Fatigue Studies, University of Michigan Summer Conferences, 6311 No. 091, 1963.

29. Liu, S. I., Lynch, J. J., Ripling, E. J., and Sachs, G., Trans Amer. Inst. of Min. and Met. Eng., Metals Division, 175, 1948, p. 469,

30. Liu, S I., Sachs, G., Trans. Amer. Inst. of Min. and Met. Eng., Metals Division, 185, 1949, p. 293.

31. Manson, S. S., Behavior of Materials Under Conditions of Thermal Stress, Technical Note No. 2933, N.A.C.A., 1953, Report No. 1170, 1954.

32. Coffin, L. F., Jr., Trans. Amer. Soc. Mech. Eng., 76, 1954, p. 925.

33. Gough, H. J., The Fatigue of Metals, Van Nostrand Co., New York, 1926.

34. Wohler, A., Uber Die Festigkeitversuche mit Eisen und Stahl, Discription available in: Engineering (London) Vol. IV, (1867), p. 110, and Engineering (London) Vol. XI, (1871), p. 199.

35. Bauschinger, J., "Change of Position of the Elastic Limit Under Cyclical Variations in Stress," Dinglers Polytechnisches Journal, Bd. 224, Civilingenieur, (1881), Mitthlg. des Mechanisch - Technischen Laboratoriums im München, Heft XIII, XXV.

36. Basquin, H. S., Proc. Amer. Soc. For Test. Mat., Vol. X, (1910).

37. Lessels, J. M., Strength and Resistance of Metals, John Wiley and Sons, New York, Chapter 6, (1954).

38. Gerber, W., Zeitschrift für des Bayerischen, (Bavarian) Architekt und Ingenieur Vereins, (1874).

39. Goodman, J., Mechanics Applied to Engineering, Longmans Green Co., London, (1899), p. 453.

40. Orowan, E., Proc. of Roy. Soc. of London, Series A, Vol. 171, (1939), p. 79.

41. Little, R. E., Analysis of the Effect of Mean Stress on Fatigue Strength of Notched Steel Specimens, Doctoral thesis, Department of Mechanical Engineering, University of Michigan, (1963).

42. Baughman, R. A., Rolling Contact Bearing Fatigue Studies, University of Michigan Summer Conferences, 6311, No. 091 (1963).

43. Volkov, S. D., Statistical Strength Theory, Gordon and Breach, (1962).

44. Fischer, F. P., Technische Mitteilungen Krupp, Heft 3, (1933), p. 67.

45. Nishihara, T., and Sakurai, T., Trans. Soc. of Mech. Eng., Japan, 5, (1939) p. 93, English abstract on p. 3-8.

46. Soderberg, C. R., Trans. Amer. Soc. of Mech. Eng. 52, Part 1, 1930, Paper A.P.M. 52-2 -13.

47. Sines, G., Technical Note 3495, V. S. Nat. Ad. Com. for Aero., 1955.

48. Metals Handbook, 8th Edition, Amer. Soc. for Met., 1, (1961), p. 218.

49. French, H. J., Trans. Amer. Soc. for Steel Treaters (now the A.S.M.) 21, (1933).

50. Sachs, G., WADC, Technical Report, 53-254, (August 1954).

51. Frankel, H. E., Bennett, J. A., Pennington, W. A., Trans. Amer. Soc. for Met., (1960), p. 257.

52. Dieter, G. E., Mehl, R. F., Horne, G. T., Trans. Amer. Soc. for Met. 47, (1955), p. 423.

53. Boegehold, A. L., Metal Progress, March (1950).

54. Cummings, H. N., Stullen, F. B., Schulte, W. C., Trans. Amer. Soc. for Met., 49, (1957), p. 482.

55. British Iron and Steel Research Association, Research Still in Progress Reported by M. Gunton.

56. Coffin, L. F., Jr., Trans. Amer. Soc. of Mech. Eng., Vol. 76, (1954), p. 923.

57. Manson, S. S., Behavior of Materials Under Conditions of Thermal Stress, Technical Note No. 2933, N.A.C.A. (1953), Report No. 11070, (1954).

58. Bennett, J. A., Journal of Research of National Bureau of Standards, C. Eng. and Instrumentation, Vol. 68 C., No. 2, (April - June 1964).

59. Alden, T. H., and Backofen, W. A., Acta Met, 9, (1961), p. 352.

60. Hoilshousen, L., H. P. U. Tech., N. B. Standards Congress on Metal Fatigue, Iron Age, 188, No. 11, (Oct. 5, 1961).

61. Ewing, J. A. and Humpfrey, J. W. C., Phil. Trans. Roy. Soc. London, A. 200, (1903), p. 241.

62. Gough, H. J., Fatigue of Metals, Ben, London, (1924).

63. Gough, H. J., Proc. Roy. Soc., A. 118, (1928) p. 3.

64. Gough, H. J., Fatigue Phenomena, Roy. Soc. for Arts, (1928).

65. Gough, H. J., and Sopwith, D. G., Jour. of Inst. of Met., 49, (1932), p. 93.

66. Gough, H. J., and Sopwith, D. G., Jour. of Inst. of Met., 56, (1935).

67. Gough, H. J., and Sopwith, D. G., Jour. of Inst. of Met., 72, (1946), p. 415.

68. Taylor, G. I., Proc. Roy. Soc., A. 145, (1934), p. 362.

69. Seeger, Dislocations and Mechanical Properties, John Wiley and Sons, New York, 1957, p. 243.

70. Baisinski, Q. S., Phil. Mag., 4, (1959), p. 393.

71. Mott, N. F., Trans. Met. Soc. Amer. Inst. for Min. and Met. Eng., 210, (1960), p. 962.

72. Hirsch, P. B. and Warrington, D. H., Phil. Mag., 6, (1961), p. 735.

73. Kuhlmann-Wilsdorf, D., Trans. Met. Soc. Amer. Inst. for Min. and Met. Eng., 224, (1962), p. 1047.

74. Cottrell, A. H., Hull, D., Proc. Roy. Soc., 242, (1957), p. 211.

75. Mott, N. F., Acta Met., 6, (1958), p. 195.

76. Fisher, J., Acta Met., 3, (1955), p. 109.

77. Fleischer, R. L., in Discussion on "Formation of Slip bands Cracks on Fatigue," Fracture, loc. cit, p. 447.

78. Thompson, N., "Some Observations on the Early Stages of Fatigue Fracture," Fracture, loc. cit, p. 354.

79. McEvily, Jr., A. J., and Machin, E. S., "Critical Experiments on the Nature of Fatigue in Crystalline Materials," Fracture, loc. cit. p. 450.

80. Hempel, M., International Conference on Fatigue of Metals, Inst. of Mech. Eng., Amer. Soc. for Mech. Eng., London, New York, (1957), p. 543.

81. Hempel, M., Slipband formation and fatigue cracks under alternating stress ,Amer. Soc. Tes. Mat., S.T.P., 237, (1958), p. 52.

82. Hempel, M., "Performance of Steel Under Repeated Loading", Fatigue Aircraft Structures, New York, Academic Press, (1957).

83. Koehler, J. S., Phys. Rev., 60, (1940), p. 397.

84. Wood, W. A., Phil. Mag., 3, (1958), 692.

85. Wood, W. A., Jour. Inst. of Met., 86, (1955), p. 228.

86. Wood, W. A., "Some Basic Studies in Fatigue of Metals," Fracture, loc. cit, p. 412.

87. Lipson, C., Juvinall, R., Application of Stress Analysis to Design and Metallurgy, Summer 1961, University of Michigan Engineering Summer Conferences, p. 115.

88. Despres, T. A., A Study of Dislocation Distributions in Annealed 304 Stainless Steel Produced by Fatigue Loading, Thesis, Dept. of Mech. Engineering, University of Michigan, (1963), p. 55

89. Wiedersich, H., Journal of Metals, 16, May 1964, No. 5.

90. Blatherwick, A. A., Olson, B. K., Technical Report 61-451, Aeronautical Systems, Div., Office of Technical Services, U. S. Dept. of Commerce, 1961.

91. Blatherwick, A. A., Proc. Soc. for Experimental Stress Analysis, XVIII, No. 1, (1961), p. 128.

92. Lazan, B. J., Wu, T., Proc. Amer. Soc. Test. Mat., 51, 1951, p. 649.

93. Lazan, B. J., Trans. Amer. Soc. for Met., 12, (1950).

94. Lazan, B. J., Mechanical Behavior of Materials at Elevated Temperature, McGraw-Hill Book Co., New York, Chapter 15, 1961.

95. Forrest, P. G., Proceedings, International Conference on Fatigue of Metals, Inst. of Mech. Eng., Amer. Soc. for Mech. Eng., London New York, (1956), p. 171.

96. Wood, W. A., and Head, A. K., Jour. of the Inst. of Met., 79, (1951), p. 72.

97. Thomson, N. J.,and Wadsworth,N.,Advances in Physics, 7, 1958, p. 72.

98. Eshelbey, J. D., Royal Soc., 197 A., London, (1949), p. 396.

99. Zener, C., Elasticity and Inelasticity of Metals, Univ. of Chicago Press, (1948).

100. Robinson, M., and Rawlings, R., Phil. Mag., 4, (1959), 938.

101. Segall, R. L., Partridge, P. G., Phil. Mag., 4, (1959), 912.

102. Koehler, J. S., Imperfections in Nearly Perfect Crystals, John Wiley and Sons, Inc., New York, (1952), p. 197.

103. Czochralski, J., Steel and Iron, (1917), p. 502.

104. Kaiser, J., Archive fuer das Eisenhuttenivesen., 1, (1953), (also doctoral dissertation).

105. Cusick, J., N.A.S.A., Cleveland, Ohio, Personal Communication.

106. Hartauer, C., Bainbridge, D., Baker, G., Personal Communication.

107. Dunegan, H., Tatro, C., Harris, D., Technical Paper, University of California, Lawrence Radiation Laboratory, Nov. 1964.

108. Schofield, B. H., Acoustic Emission Under Applied Stress, Report No. ASD-TDR-63-509, Part I Wright Patterson Air Force Base, April 1963.

109. Schofield, B. H., Acoustic Emission Under Applied Stress, Report No. ASD-TDR-63-509, Part II Wright Patterson Air Force Base, May 1964.

110. Schofield, B. H., Proceedings of the Symposium on Physics and non-Destructive Testing, October 1963, San Antonio, Texas, Sponsored by Southwest Research Institute.

111. Kaiser, J., Forschg. Ing. Wes., 23, 1957.

112. Borchers, H., Kaiser, J., -Zeit fur Metallkunde, 49, (1958), p. 95-100.

113. Granto A., Lucke, K., Jour. of App. Phys., 27, (1956), p. 583.

114. Smith, G. C., Proc. Roy. Soc., A. 242, (1957), p. 189.

115. Thompson, N., Wadsworth, N., Louat, N., Phil. Mag., 1, (1956), p. 113.

116. Pomp, and Hempel., Mitteilungen, Kaiser-Wilhen-Institute Eisenforschung, Band XVIII, (1936), p. 205.

117. Forsythe, P. J. E., Proc. Roy. Soc., A. 242, (1957), p. 198.

118. Glenn, R. C., and Raley, J. C., An Improved Procedure for Thinning Metallic Specimens for Transmission Electron Microscopy. Amer. Soc. Test. Mat., S.T.P. No. B. 39, (1962).

119. Borchers, H., Tensi, M., Ziet fur Metallkunde, 51, No. 4, (1960) p. 212-218.

120. Polanyi, M., Zeit fuer Physik, 89, (1934), p. 660.

121. Keh, A. S., Paper intended for publication in the Phil. Mag.

122. Machlin, E. S., Trans., Amer. Inst. of Min. Met. and Pet Engineers, 206 (1939), p. 106.

123. Borchers, H., Tensi, H., Zeit fur Metallkunde, 53, No. 10, (1962), p. 692-695.

124. Kraft, J. M., Amer. Soc. Met., 48, (1956), p. 249.

APPENDIX

SPECIFICATIONS OF ELECTRONIC EQUIPMENT USED FOR SENSING AND RECORDING THE ACOUSTIC EMISSION

Crystal Transducer

Made by Clevite Corporation

Type PZT-5.

(Lead Zirconate Titanate)

Specifications:

Length = .1 in.

Diameter = .25 in.

Capacitance = 59.7×10^{-12} farads

Resistance = 12.7×10^{12} ohms

Natural frequency Radial mode= 300 kc/sec

Natural frequency Longitudnal mode = 700 kc/sec

Density = 7.7×10^{3} kg/m^3

Acoustic Impedence = 28×10^{6} $kg/m^2 sec$

Frequency thickness constant = 1800 kc/s mm

Maximum operating temperature = 290° C

Dielectric constant = 1700

Electromechanical coupling factor for thickness mode (k_{33}) = .675

Electromechanical coupling factor for radial mode (k_p) = .60

Elastic quality factor (Q) = 75

Piezoelectric modulus for thickness mode (d_{33}) = 374×10^{-12} m/v

Piezoelectric pressure constant (g_{33}) = 24.8×10^{-3} $\frac{v/m}{N/m^2}$

Volume resistivity at 25°C $> 10^{13}$

Curie temperature = 365°C

Young's Modulus = $6.75 \times 10^{10} \frac{N}{m^2}$

Rated dynamic tensile strength = 4000 psi

Preamplifier

Hushed transistor amplifier

Made by Millivac Instruments Inc.

Type VS - 68B

Specifications:

Gain: 10 - 80 db ± 1 db, in 10 db steps

Input impedance: Either 10K, 100K, or 50 meg

Frequency Response: -3 db 2 cps and 180 kc

Band pass: between 2 and 180 kc

Output Impedence: less than 2 K

Maximum Output: 1 V R.M.S.

Power Supply: two Burgess F4P1, 6V Batteries

Band Pass Filter

Made by Krohn Hite Corporation

Type-310 AB

Specifications:

Type: Band Pass

Band Width:

Continuously variable up to the maximum width covering the entire frequency range from 20 cps to 200 kc.

Frequency Range:

Continuous coverage from 20 cps to 200 kc for both high cut-off and low cut-off frequencies independently; frequency range is covered by separate calibrated dials and four-decade band switches; center frequency and width of pass band continuously adjustable within the above frequency range.

Band	Multiplier	Frequency (cps)
1	1	20 - 200
2	10	200 - 2,000
3	100	2,000 - 20,000
4	1,000	20,000 - 200,000

Frequency dials:

Each dial is engraved and individually hand calibrated with a single logarithmic scale reading directly in cycles per second from 19 to 210; dials are 4 inches in diameter with an effective scale length of approximately 8 inches per band giving a total effective scale length of approximately 32 inches for the range of 20 cps to 200 kc.

Accuracy of cut-off frequency calibration:

± 10% (± 5% available on special order).

Insertion loss:

Zero db ± db in pass band

Atenuation slope:

Nominal 24 db per octave each side of pass band with peaking factor to reduce attenuation at the cut-off frequencies.

Maximum Attenuation:

Greater than 60 db

Input Characteristics:

Impedance: Approximately 6 megohms in parallel with 50 uuf.

Maximum Input Amplitude: 5 volts rms.

Maximum dc Component: 400 volts.

Output Characteristics:

Impedance: Approximately 500 ohms.

Maximum Power: 2.5 volts rms across 500 ohms or 12 milliwatts.

Internally Generated Hum and Noise: Less than 0.2 millivolt.

Vacuum Tube Volt Meter

Made by Electronics Instruments Company, Incorporated

Type 250

Specifications:

Voltmeter

Voltage Ranges: 1, 3, 10, 30, 100, 300 RMS millivolts

1, 3, 10, 30, 100, 300 RMS volts

Decibel Range: -80 to +52 db, in 12 ranges

Frequency Response: ± 0 db 10c to 600 kc

Input Impedance: 10 megohms shunted by 15 m mf

Accuracy: ± 3% of full scale

Digital Counter

Made by Hewlett-Packard Company

Model 5233 L

Specifications:

Input Channels (A and B)

Range: DC coupled: 0 to more than 2 Mc. AC coupled: 10 cps to more than 2 Mc.

Impedance: Approximately 1 megohm, 80 pf shunt.

Sensitivity: 0.1 volt rms sine wave; 1 volt pulse, 0.2 μsec minimum width.

Trigger Level: -100 to +100 volts, adjustable, either positive or negative slope; independent controls on each channel.

Channel Inputs: Common, Separate, Check.

Marker Output: Available at rear panel for oscilloscope intensity modulation to mark trigger points on input waveforms; 1 μsec duration and -15 volts peak.

BCD Output: 4-line 1-2-2-4 BCD; 1-2-4-8 optional.

Impedance: 100 K each line.

"0" State Level: approximately -8 volts

"1" State Level: approximately +18 volts

Reference Levels: Approx +17 volts, 350-ohm source impedance: and approx -6 volts, 1000-ohm source impedance.

Print Command: Step from -9 volts to +19 volts from 2700-ohm source coupled through 1000 pf capacitor.

Hold-off Requirements: Anywhere from +2 volts to -20 volts.

Manual

Input: Channel A.

Multiplier: Prescales input of Channel A in decades, 1 to 107.

Totalize: Periodic events at rates to more than 2 x 10^6/sec.

Random events with pulse spacing to 0.5 μs or less.

Digital-Analog Converter

Made by Hewlett-Packard Company

Type 580 A

Specifications:

Accuracy: 0.5% of full scale or better

Potentiometer output: 100 mv full scale. Minimum load resistance 20K. Calibrate control. Dual binding posts front and rear.

Galvanometer Output: 1 ma full scale into 1500 ohms or less. Zero and calibrate controls. Phone jack front and rear.

Reference voltages: Reference voltages required for both the "0" and "1" state. Reference voltages not to exceed ±150 volts to chassis.

Command pulse: Positive or negative pulse, 20 μsec or greater in width, 6 to 20 volts amplitude, rise time greater than 1 V/μsec into 1500 ohms.

Transfer time: 1 millisecond.

Driving source: Parallel entry 4-line BCD, 1-2-2-4 (9 digits maximum). "1" state +4 to +75 volts with reference to "0" state.

Visicorder

Made by Minneapolis Honeywell Regulation Company

Type 906 C

Specifications:

Record width: 6 inches

Recording speed used for this investigation: 1 in/min

Recording made by: Ultra-violet light beam on a photosensitive chart.

No. of channels used: 3

galvanometers: Type M40-120A

Frequency response: flat between 0-24cps.

x-y Recorder

Made by F. L. Moseley Company

Model 3

Specifications:

Accuracy and Resolution:	.25% of full scale
Response speeds:	.5 seconds for full scale defl.
Damping:	adjusted manually
Calibration stability:	.25% drift in 6 months
Range:	5 mv to 500 v.
Input Impedance:	1000 Ω at 5 mv sens.